Tribochemistry of the Decomposition Mechanisms of Perfluoropolyether Lubricants at the Head-Disk Interface of Hard Disk Drives in UHV

by

Chao-Yuan Chen

B.S. (National Taiwan University) 1991
M.S. (University of California at Los Angeles) 1995

A dissertation submitted in partial satisfaction of the

requirements for the degree of

Doctor of Philosophy

in

Engineering – Mechanical Engineering

in the

GRADUATE DIVISION

of the

UNIVERSITY of CALIFORNIA at BERKELEY

Committee in charge:

Professor David B. Bogy, chair
Professor Kyriakos K. Komvopoulos
Professor Tim Sands

Fall 1999

Tribochemistry of the Decomposition Mechanisms of Perfluoropolyether Lubricants at the Head-Disk Interface of Hard Disk Drives in UHV

by

Chao-Yuan Chen

Abstract

Tribochemistry of the Decomposition Mechanisms of Perfluoropolyether Lubricants at the Head-Disk Interface of Hard Disk Drives in UHV

by

Chao-Yuan Chen

Doctor of Philosophy in Mechanical Engineering

University of California at Berkeley

Professor David B. Bogy, Chair

The successful operation of a hard disk drive requires the presence of a monolayer Perfluoropolyether (PFPE) film at the head-disk interface. The adhesion, mobility, and physical properties of this lubricant can significantly affect the tribological reliability of the hard-disk drive. The physical properties of this PFPE film, and hence its lubricity, are dictated by the interplay of the intramolecular cohesive interactions between PFPE molecules, and by the adhesive interactions between the PFPE lubricant and the underlying surface.

The mechanical properties of the contacting materials are important parameters to study in order to understand the friction and wear at the head-disk interface. The tribochemistry of the involved contacting surfaces is another important issue.

This dissertation focuses on the study of the tribochemistry at the head-disk interface in a computer hard disk drive. An effort is made to understand the lube decomposition mechanisms and the wear and friction mechanisms at the interface in order to enhance the wear durability.

Drag tests and thermal desorption tests were conducted in an ultra-high vacuum (UHV) tribochamber equipped with a mass spectrometer. The tribochemical tester can be used to monitor the tribochemistry at the head-disk interface in real time along with friction and temperature measurements. An optical surface analysis (OSA) system was also used to observe the lube migration behavior.

The results show that the deposited carbon films on the Al_2O_3/TiC sliders' air bearing surfaces can significantly improve the wear durability at the interface. Different lube decomposition mechanisms are found for the coated and uncoated sliders.

The hydrogen evolution from the CH_x carbon overcoat initiates lube catalytic decomposition with an Al_2O_3/TiC slider. But for CN_x films, catalytic reactions are prevented due to less hydrogen evolution from the CN_x overcoat, resulting in a better wear durability as compared to the CH_x films.

The studies also demonstrate that the catalytic degradation process of ZDOL in the presence of Lewis acid occurs most readily at the acetal units (-O-CF_2-O-) within the internal backbones of the lubricant.

In addition, this catalytic reaction is also shown to be prevented by using X-1P as an additive in ZDOL, thereby passivating the activity centers (Lewis acid) of Al_2O_3. The X-1P additive also increases the mobility of PFPE lubricants because X-1P molecules preferably occupy the bonding sites on the carbon surface.

The effect of the lube molecular weight is studied by testing fractionated ZDOL. With higher molecular weight, the poorer mobility causes higher viscosity and higher friction. However, the degradation rate is slower with the higher molecular weight.

Lubricant interaction with the carbon overcoat varies as a function of lubricant thickness. In the sub-monolayer regime, adhesion of the lubricant to the carbon surface is much stronger. When the lubricant thickness is above a monolayer, cohesion among the lube molecules plays a greater role.

The lubricant performance is also a function of the bonded fraction. The wear durability of disks improves with increased mobile lube fraction up to a point because the mobile layers provide a reservoir to constantly replenish the ZDOL displaced in the test track.

Professor David B. Bogy

Dissertation Chair

To my parents

Acknowledgments

I would like to express my sincere gratitude to my research advisor, Professor David B. Bogy, for his academic guidance, research advice, and financial support throughout my career at UC-Berkeley. Working with Professor David B. Bogy has been an invaluable and honorable experience.

Thanks also belong to Dr. C. Singh Bhatia of IBM. His encouragement and enthusiasm for my research have been invaluable for my progress, and in particular during the later stages of my research as I was led away from more familiar aspects of mechanical engineering to chemistry subjects.

I would like to thank Dr. Tai Cheng of HMT and also Dr. Robert Waltman, and Dr. Paul Kasai of IBM. Without their patient knowledge transfer in tribochemistry and continuous material supplies, this research would not have been possible. I appreciate their aid, and I value our friendship. Appreciation also goes to Dr. Bruno Marchon of IBM, Dr. Jing Gui of Seagate, Dr. Don J. Perettie of Dow Chemical, Professor Steven Hsu of NIST, and Professor Andrew J. Gellman of Carnegie-Mellon University for their many helpful discussions and advice in the NSIC meetings.

Appreciation also goes to Professor Kyriakos Komvopoulos and Professor Tim Sands for their sitting in my dissertation committee. I would like to thank Professor Panayiotis Papadopoulos for his assist on my academic progress and qualifying exam.

Thanks also belong to my fellow graduate students at the Computer Mechanics Laboratory, many of whom have helped me in my course work and in the laboratory. Dr. Xiao-Han Yun and Dr. Brian Strom were especially helpful during my first year in the laboratory, when help was most needed. I particularly appreciate Walton Fong for many thoughtful discussions regarding the finer points of tribochemistry, and as a team partner on many occasions. Thanks also go to Joy Jiang, Weidong Huang, Liangshen Chen, and Wei Lu because they made my graduate life even more enjoyable and colorful.

This research was supported by the Computer Mechanics Laboratory (CML) at the University of California at Berkeley (UCB). Portions were also supported by the National Storage Industry Consortium (NSIC) Grant with CML, the Shared University Research Grant with CML from IBM, Seagate, and HMT.

In the end, it is my pleasure to thank my parents and sisters in Taiwan for their encouragement and support. And last but not the least, my deepest appreciation goes to my girlfriend Chia-Huei Lin for her incredible dedication, patience and endless love, I know she always takes my struggles and successes as her own. I would not have been able to accomplish my goals without her love and support.

Berkeley, December 1999

TABLE OF CONTENTS

Abstract

Dedication ……..…… iv

Acknowledgments ……..... v

Table of Contents …..……..…….……...… vii

List of Figures ……. xi

Chapter 1 Introduction …….. 1

1.1 Tribology ……. 1

1.2 Lubricant History ……. 2

1.3 Tribology at the Head-Disk Interface of a Hard Disk Drive ……... 5

1.4 Thin Film Disk Design Issues ……. 6

1.5 Tribochemical Characterization Techniques ……... 9

1.6 Objectives ……... 11

1.7 Dissertation Organization ……...… 12

Chapter 2 Experimental Set-up …….. 15

2.1 Ultra-High Vacuum (UHV) Tribochamber Tests ……...…… 15

2.1.1 Drag Tests ……...…. 16

2.1.2 Thermal Desorption Tests …… 16

2.2 Optical Surface Analysis (OSA) Measurements …….. 17

2.3 Thermogravimetric Analysis (TGA) Measurements ……...…… 18

Chapter 3 The Decomposition Mechanisms of PFPE Lubricants ….. 20

3.1 Introduction …….. 20

3.2 Experimental Procedure and Set-up ……. 21

3.3 Results and Discussions ……...… 21

3.4 Conclusions …….. 27

Chapter 4 The Thermal Stability of PFPE Lubricants ……..... 32

4.1 Introduction …….. 32

4.2 Experimental Procedure and Set-up ……. 33

4.3 Results and Discussions ……... 34

4.4 Conclusions …….. 38

Chapter 5 Hydrogen Evolution Initiates Lubricant Catalytic Decomposition ……...……..… 42

5.1 Introduction ……. 42

5.2 Experimental Procedure and Set-up ……..… 43

5.3 Results and Discussions ……...… 44

5.3.1 Study of Thermal Desorption Data ……..…. 44

5.3.2 UHV Drag Tests – Comparison of the CH_x and CN_x Films ...… 45

5.4 Conclusions ……...… 47

Chapter 6 Effect of Backbone and Endgroup on the Lube Decomposition Mechanisms …...…… 52

6.1 Introduction ……...… 52

6.2 Experimental Procedure and Set-up ……. 52

6.3 Results and Discussions ……... 53

6.4 Conclusions …….. 58

Chapter 7 Effect of the Additive X-1P in PFPE Lubricants …… 63

7.1 Introduction ……..… 63

7.2 Experimental Procedure and Set-up ……..… 65

7.3 Results and Discussions ……...… 65

7.3.1 Results from the AM3001/CNx samples ……..… 65

7.3.2 Results from the ZDOL2000/CHx samples ……..… 68

7.4 Conclusions ……...… 70

Chapter 8 Effect of Lubricant Molecular Weight ……..… 76

8.1 Introduction ……..… 76

8.2 Experimental Procedure and Set-up ……..… 77

8.2.1 UHV Drag Tests ……...… 77

8.2.2 Optical Surface Analysis (OSA) ……...… 78

8.2.3 Thermogravimetric Analysis (TGA) …… 79

8.3 Results and Discussions ……...… 79

8.3.1 Results from the UHV Drag Tests ……...… 79

8.3.2 Results from the OSA Measurements ……...… 83

8.3.3 Results from the TGA Measurements ……...… 85

8.4 Conclusions ……...… 86

Chapter 9 Lubricant Thickness Study ……...… 96

9.1 Introduction ……..… 96

9.2 Experimental Procedure and Set-up ……..… 97

9.3 Results and Discussions ……...… 98

9.3.1 Results from the UHV Drag Tests ……...… 98

9.3.2 Results from the UHV Thermal Desorption Tests ……..….. 102

9.4 Conclusions …….. 107

Chapter 10 Effect of Lubricant Bonding Fractions ……..…. 116

10.1 Introduction ……...… 116

10.2 Experimental Procedure and Set-up ……..… 117

10.3 Results and Discussions ……..….. 118

10.3.1 Results from the UHV Drag Tests ……...… 118

10.3.2 Results from the UHV Thermal Desorption Tests ……...… 120

10.4 Conclusions ……...… 122

Chapter 11 Conclusions …… 127

References …….. 132

Appendix I ……...… 140

LIST OF FIGURES

Chapter 1

Figure 1.1 The Stribeck curve.

Figure 1.2 (a) Boundary lubrication.
(b) Hydrodynamic lubrication.

Figure 1.3 Typical thin film disk.

Chapter 2

Figure 2.1 Ultra-High Vacuum (UHV) tribochemical chamber.

Figure 2.2 Optical Surface Analyzer (OSA).

Chapter 3

Figure 3.1 The friction coefficient curves of ZDOL lubricated CH_x disks with uncoated Al_2O_3/TiC slider and carbon coated slider.

Figure 3.2 The integrated mass spectra (the first 30 seconds before wear) of ZDOL decomposition products generated at the carbon-coated slider/CH_x disk interface.

Figure 3.3 The integrated mass spectra (the first 30 seconds before wear) of ZDOL decomposition products generated at the uncoated slider/CH_x disk interface.

Chapter 4

Figure 4.1 The thermal desorption profile of four primary decomposed fragments of ZDOL.

Figure 4.2 The thermal desorption profile of fragments CFO (47) during two different heating rates: one at 0.2 K/sec and the other is 1.6 K/sec.

Figure 4.3 The desorbed mass spectra of mobile ZDOL fragments produced from the ZDOL/CH_x disk at 352 K.

Figure 4.4 The desorption mass spectra of bonded ZDOL fragments produced from the ZDOL/CH_x disk at 429 K.

Figure 4.5 The thermal desorption profile of ZDOL fragments F (19) and HF (20).

Chapter 5

Figure 5.1 The thermal desorption profile of H_2 (2) evolution from both CH_x and CN_x coated disks in UHV.

Figure 5.2 The thermal desorption profile of HF (20) formation from both CH_x and CN_x coated disks in UHV.

Figure 5.3 The thermal desorption profile of ZDOL fragment CFO (47) from both CH_x and CN_x coated disks in UHV.

Figure 5.4 The friction coefficient curves of ZDOL lubricated CH_x disks on uncoated Al_2O_3/TiC slider and carbon coated slider.

Figure 5.5 The friction coefficient curves of ZDOL lubricated CN_x disks on uncoated Al_2O_3/TiC slider and carbon coated slider.

Figure 5.6 The normalized mass spectra of four major ZDOL decomposition products generated at the ZDOL/CH_x and ZDOL/CN_x disk interface during UHV drag tests.

Chapter 6

Figure 6.1 Friction coefficient of UHV drag tests on 12 Å ZDOL 4200 lubricated CH_x disk.

Figure 6.2 Friction coefficient of UHV drag tests on 12 Å Demnum SA 5500 lubricated CH_x disk.

Figure 6.3 Friction coefficient of UHV drag tests on 12 Å AM 3001 lubricated CH_x disk.

Figure 6.4 Integrated degradation intensities of four major PFPE fragments during UHV drag tests on CH_x disks lubricated with different lubricants.
(a) with DLC coated slider.
(b) with uncoated slider.

Figure 6.5 Wear durability of CH_x disks lubricated with different lubricants during UHV drag tests.

Figure 6.6 Weight loss observed on PFPEs when heated in contact with Al_2O_3 (1 wt. %) at 200 ^oC.

Chapter 7

Figure 7.1 Friction coefficient of 12 Å pure AM 3001 lubricated CN_x disk in UHV drag tests.

Figure 7.2 Friction coefficient of 12 Å AM 3001 with 2% X-1P lubricated CN_x disk in UHV drag tests.

Figure 7.3 Friction coefficient of 12 Å AM 3001 with 4% X-1P lubricated CN_x disk in UHV drag test.

Figure 7.4 (a) Lubricant thickness versus time graphs from OSA data.
(b) The AM 3001 lube migration rate versus X-1P additive %.

Figure 7.5 Wear durability of CN_x disks with different X-1P additive % in AM 3001 in UHV drag tests.

Figure 7.6 Integrated degradation intensities of four major AM fragments during UHV drag tests on CN_x disks with different X-1P additive %.

Figure 7.7 Wear durability of ZDOL/CH_x disks with X-1P additive in UHV drag tests.

Figure 7.8 Integrated degradation intensities of four major ZDOL fragments generated during UHV drag tests of CH_x disks with X-1P additive.

Chapter 8

Figure 8.1 (a) Friction coefficient of UHV drag test on 24 Å mono-dispersed ZDOL MW 4200 lubricated disk.

(b) Mass spectra of the major ZDOL MW 4200 decomposition fragments.

Figure 8.2 (a) Friction coefficient of UHV drag test on 24 Å mono-dispersed ZDOL MW 7600 lubricated disk.
(b) Mass spectra of the major ZDOL MW 7600 decomposition fragments.

Figure 8.3 (a) Friction coefficient of UHV drag test on 24 Å mono-dispersed ZDOL MW 8500 lubricated disk.
(b) Mass spectra of the major ZDOL MW 8500 decomposition fragments.

Figure 8.4 Integrated degradation intensity of ZDOL during UHV drag tests on CH_x disks with different ZDOL molecular weight.
(a) Mass 47 (CFO) under frictional action.
(b) Mass 69 (CF_3) under catalytic reaction.

Figure 8.5 UHV drag tests on CHx disks with different ZDOL molecular weight with DLC coated or uncoated Al_2O_3/TiC sliders.
(a) Wear durability.
(b) Friction coefficient.

Figure 8.6 (a) The OSA data on the lubricant thickness versus time.
(b) The ZDOL lube migration rate versus molecular weight.

Figure 8.7 (a) The TGA data on the lube weight loss versus temperature.
(b) The TGA data on the desorption temperature versus molecular weight.

Chapter 9

Figure 9.1 (a) Friction coefficient of UHV drag test on 4.5 Å ZDOL lubricated disk.
(b) Mass spectrum of four major ZDOL decomposed fragments.

Figure 9.2 Integrated degradation intensity of ZDOL during UHV drag tests on CH_x disks with different ZDOL thickness. Two major decomposition fragments occur under frictional action:
(a) Mass 47 (CFO).
(b) Mass 66 (CF_2O).

Figure 9.3 Integrated degradation intensity of ZDOL during UHV drag tests on CH_x disks with different ZDOL thickness. Two major decomposition fragments occur under catalytic reaction:
(a) Mass 69 (CF_3)
(b) Mass 119 (C_2F_5).

Figure 9.4 Wear durability of CH_x disks with different ZDOL thickness during UHV drag tests with DLC coated or uncoated Al_2O_3/TiC sliders.

Figure 9.5 Wear durability of CH_x disks with different mobile ZDOL thickness during UHV drag tests with DLC coated or uncoated Al_2O_3/TiC sliders.

Figure 9.6 History profiles of mass 47 (CFO), and mass 66 (CF_2O) during the thermal desorption tests of CHx disks with ZDOL thickness ranging from 4.5 Å to 15.4 Å.

Figure 9.7 History profiles of mass 69 (CF_3), and mass 119 (C_2F_5) during the thermal desorption tests of CH_x disks with ZDOL thickness ranging from 4.5 Å to 15.4 Å.

Figure 9.8 Thermal desorption peak temperatures of ZDOL for CH_x disks with ZDOL thickness ranging from 4.5 Å to 15.4 Å.

Figure 9.9 (a) Integrated thermal desorption intensity of CFO (47) versus mobile ZDOL thickness during the first desorption peak.
(b) Integrated thermal desorption intensity of CFO (47) versus bonded ZDOL thickness during the second desorption peak.

Chapter 10

Figure 10.1 (a) Friction coefficient of UHV drag test with 12 Å pure bonded ZDOL lubricated disk.
(b) Mass spectrum of four major ZDOL decomposition fragments.

Figure 10.2 Integrated degradation intensity of ZDOL fragment CFO (47) during UHV drag tests on CH_x disks with different ZDOL bonded fractions.

Figure 10.3 Wear durability of CH_x disks with different ZDOL bonded fractions during UHV drag tests against coated and uncoated Al_2O_3/TiC sliders.

Figure 10.4 Thermal desorption history profiles of mass 47 (CFO) during thermal desorption tests on CH_x disks with different ZDOL bonded fractions.

Figure 10.5 Thermal desorption peak temperatures of ZDOL for CH_x disks with different ZDOL bonded fractions.

Chapter 1

INTRODUCTION

1.1 Tribology

Tribology is the science and technology that deals with the friction, wear and lubrication of interacting surfaces in relative motion. The word tribology has originated from the Greek word “tribos”, which means rubbing of two surfaces, and was introduced in the English language about thirty years ago. The nature and the consequence of the interactions that take place at the interface control the friction and wear behavior of the materials involved. During these interactions, forces are induced; energy is consumed; physical and chemical natures of the materials are changed; the surface topography is altered; and sometimes loose wear particles are generated. All these seemingly random and complex surface phenomena follow a certain order and satisfy the laws of nature. Understanding the nature of these interactions and solving the technological problems associated with the interfacial phenomena constitute the essence of tribology.

The implications of the various tribological phenomena in the design of mechanical systems, such as bearings, gears, cams, flexible couplings, slides, guides, etc., have attracted the attention for investigation especially during the last thirty years due to economic situation and the demand for material and energy conservation. It is estimated that the damage done by wear in the recent U.S. economy is about 6 percent of the Gross National Product. It has been well emphasized that the main causes of energy dissipation and material wastage are due to friction and wear at the contact interfaces.

Since sliding between the components of most machine elements cannot be avoided, the design of antifriction and high wear resistance surfaces is vital. Considerable savings can be made if the predominant friction and wear mechanisms are identified and minimized sufficiently. The failure of various machines, however, can be due to different mechanisms depending on the application and the operating conditions. It is imperative, therefore, that the rate controlling friction and wear mechanisms are successfully analyzed.

1.2 Lubrication History

One of the most effective means of controlling friction and wear is by proper lubrication of the sliding interfaces. A lubricant is any substance that is used to reduce friction and wear, increase the operation life, and provide smooth and quiet running. Machine elements are lubricated by interposing and maintaining between moving surfaces easily shearable films that minimize the solid-to-solid contacts and reduce the frictional power losses. With inadequate lubrication, excessive wear is the most serious consequence which often leads to unexpected catastrophic failures. Consequently, properly designed lubricated surfaces can last significantly longer resulting, thus, in low cost and high production rates.

About the history of lubrication theory, Petroff (1883) [1], a 19th century Russian researcher, first presented that the important fluid property is viscosity instead of density. In addition, he also presented that frictional force is proportional to velocity, contact area and viscosity and inversely proportional to spacing. Tower (1883) [2] extended Petroff's work and applied frictional concepts on the practical issue of bearing load-carrying capacity.

Later, Reynolds (1886) [3] contributed a theory to previous experimental work. He built up a fundamental equation of lubrication theory and important theoretical relationships between viscosity and temperature. He also analyzed the "wedge effect" required for load-carrying capacity. Kingsbury (1897) [4] extended hydrodynamic lubrication theory to compressible fluids and noted that lubricating medium could be gas or liquid. Harrison (1913) [5] made use of perfect gas relation under isothermal conditions and wrote compressible Reynolds equation in form most widely used today. Later, Reyleigh (1918) [6] added some notes on the theory of lubrication. Most theory of lubrication was accomplished during that period (between 1883 and 1918).

The most widely understood relationship in tribology was introduced by Stribeck and is shown in Fig. 1.1 below:

Fig. 1.1 The Stribeck Curve

Figure 1.1 describes the effect of viscosity, velocity, and the normal load on the friction coefficient and the lubricant thickness. It is seen that at low velocities/load ratios, the film thickness is reduced, the friction force is increased and solid interactions occur. As the velocity/load increases, the film thickness increases to a lowest value of friction and, subsequently, it increases gradually. There are two distinct regions of interest as regards to film thickness: the "boundary lubrication" region and the "hydrodynamic lubrication" region. In the boundary lubrication region, contact between materials is present. The emphasis is on the surface and bulk properties of the contact materials, aspects of solid mechanics and surface chemistry. In the hydrodynamic lubrication region, no material contact is possible and the fluid mechanics of the lubricants and elastic deformation of the solid surfaces are important. Figures 1.2 (a) & (b) show the scheme of these two regions.

Fig. 1.2 (a) Boundary Lubrication, and (b) Hydrodynamic Lubrication

1.3 Tribology in Hard Disk Drive

The ongoing growth of the computer industry and the advent of the information superhighway, high definition television, digital images, etc. generates an enormous demand for data storage capacity. To supply such increasing data storage capacity, several competing technologies are available. Some of these are magnetic hard disk, optical disk, and magnetic flexible tape. However, magnetic hard disk technology continues to be the primary choice for high performance storage. In the past five years, the areal density of disk drive storage has grown 60% annually. Areal density of 10 Gb/in^2 at a head/disk spacing of 25 nm is currently in production for laptop drives. Recently, Read-Rite Corporation demonstrated a record areal density of 26.5 Gb/in^2, and this device is capable of achieving 40 Gb/in^2. With optimum material selection for recording media and transducer, reduction of written magnetic bit aspect ratio to roughly four, and process equipment enhancement to fabricate ultra narrow track width and achieve uniform recording media grain size, it is believed that the current longitudinal recording systems can be extended 100 Gb/in^2 areal density.

The reliable implementation of 100 Gb/in^2 recording systems will depend on the head/disk interface design and testing at narometer scales. Recording performance modeling indicates that 10 nm magnetic spacing is required to achieve this areal density. Allowing for sufficient wear and corrosion protection, overcoats on media and head would permit only a sub 6 nm physical head disk separation. The decreases in the head-disk spacing, coupled with desire to minimize the thickness of the protective carbon layers on both the head and the disk, have forced the magnetic recording industry to investigate alternative overcoat and lubricant materials, and the materials methodologies required for their production. Due to high data rate demand, these interfaces have to operate reliably (1 million hours life time) at

ever increasing speeds. Therefore, the lubrication efficiency to reduce friction and wear becomes more and more important in hard drive performance.

Interface tribology design for 100 Gb/in^2 requires in-depth understanding of tribomechanics, tribochemistry, tribomaterials, and tribotesting. Intricate trade-offs are often made to achieve optimum interface performance for reliability vs. magnetic recording system.

1.4 Thin Film Disk Design Issues

The distinction between thin-film and thick film technology is that the former involves deposition of individual molecules, while the latter involves deposition of particles. Thin films are deposited onto bulk materials (substrates) to achieve properties unattainable or not easily attainable in the substrates alone. A typical thin film disk is composed of multilayers as shown in Fig. 1.3 below:

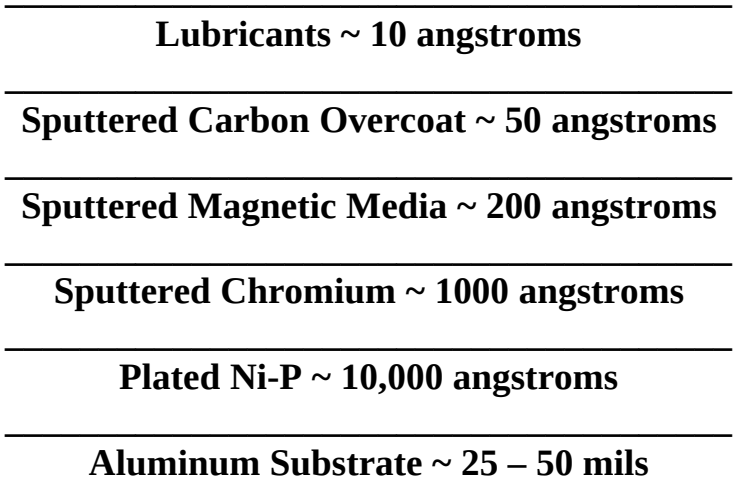

Fig. 1.3 Typical Thin Film Disk

The top layer is lubricant which provides lubrication for head/disk contact to reduce friction. The sputtered carbon overcoat protects media from corrosion and wear. The sputtered magnetic media is composed of alloys of cobalt. The sputtered chromium is to orient the magnetic layer. The plated Ni-P is hardener for polishing. The substrate, in general, is Aluminum or glass. As the head-disk spacing (flying height) is still decreasing, some disk design issues are becoming more imperative.

First, the Fluorocarbon lubricant has become the universally accepted choice for creating a chemically inert layer which will decrease the surface friction of a disk and reduce drive failure. A good lubricant should exhibit: (1) good affinity for the carbon surface; (2) good viscosity characteristics; (3) low volatility (low vapor pressure); (4) low surface tension; (5) good thermal stability; and (6) minimum chemical reactions.

Recently, how lubricant molecules move around on disk surface plays a key role in how well a lubricant film protects against slider contacts. Two contradictory properties are desired from the mobility of the lubricant molecules: (1) low mobility during slider-disk contacts, so that lubricant will not be displaced from the contact zone, and (2) high mobility after the slider-disk contacts, so that those molecules displaced during the contacts can be quickly replenished with molecules from surrounding areas. Various driving forces could cause movement of lubricant molecules on disk surfaces. The forces can be divided in three general categories, plus sub-categories [7]:

1. Molecular forces
    a. Diffusion of lubricant towards areas of thinner lubricant.
    b. Evaporation of lubricant in one area followed by redeposition in another.
2. Forces deriving from disk rotation

a. Centrifugal driven flow of lubricant toward OD.

b. Air shear generated by the air flow toward the OD that pushes lubricant toward the OD. At typical disk drive rotation speeds (7200 RPM), the air shear force can be several orders of magnitude greater than the centrifugal force.

3. Slider forces

a. Air pressure gradients generated underneath the slider rails during flying that push lubricant away from rails.

b. The air shear force generated by the shearing the air film between the slider and the disk that pushes the lubricant ahead of and to the side of the slider rails.

c. Gigantic shear stresses are generated when the slider physically contacts the disk surface, at high speeds that will not only displace unbonded lubricant molecules from the contact zone, but can potentially break internal chemical bonds of those molecules remaining in the zone.

More understanding of the mechanisms of these driving forces help predict and improve the tribological performance at the head-disk interface.

Secondly, Silicone contamination on the disk surface can cause uneven application of topical fluorocarbon lubricant. This is compounded by the fact that under certain drive conditions friction can cause polymerization of the silicone and even conversion to an oxide form which balls up and eventually produces head crashes. It has become vital to detect and characterize silicones and other microcontaminants, even though they may be present only in quantities as small as tenths of monolayer.

Thirdly, the ability of a thin film disk to resist corrosion can be correlated with the presence and/or absence of oxygen within its amorphous carbon layer overcoat. Recently,

ultra thin films (2 nm) of carbon nitride were grown using dc magnetron sputtering [8]. A pulsed bias was applied to both the target and the substrate during deposition to help sustain a stable plasma and enhance ion bombardment of the growing film. These films exhibit excellent corrosion resistance at film thickness around 2 nm. The role of pulsed bias and bombardment by ionized species is to obtain low defect-density overcoats.

1.5 Tribochemical Characterization Techniques

The ongoing development of disk drive materials technology has relied on concurrent advancements in materials characterization techniques. Two of the most significant advances, the practical application of surface analysis and the ability to analyze organic microcontamination, have generated a growing requirement for material analysis within the head/disk assembly industry. The following techniques are representative:

Fourier Transform Infrared Spectroscopy (FTIR) measures the infrared absorption spectra of materials and provides a unique "fingerprint" of organic and some inorganic compounds. The ability of FTIR to identify specific molecules is useful for verifying composition as well as characterizing and tracing sources of organic contamination.

Electron Spectroscopy for Chemical Analysis (ESCA) is a surface sensitive technique providing elemental and chemical information from the top 40 to 50 Å of both conductive and insulating materials. ESCA's surface sensitivity enables it to characterize thin film contamination and measure disk lubricant thickness, Surface derivatization is a special application of ESCA involving the tagging of specific surface functional endgroups (-OH, -COOH) with fluorocarbon reagents.

Auger Electron Spectroscopy (AES) is a spatially resolved electron beam technique which provides elemental composition of surfaces (20 to 30 Å depth). Combined with ion etching, AES yields rapid depth profiles of thin films. Spot sizes of less than one micrometer enable AES to analyze microcontamination and corrosion.

Scanning Electron Microscopy (SEM) is a technique which is capable of magnifying sample surface features up to 200,000 times or more. When equipped with an Energy **Dispersive X-Ray (EDX)** detector, substrate elemental composition information can readily obtained from very small areas. SEM is useful in characterizing the morphology of critical surfaces and in measuring particle size and distribution. EDX helps identify inorganic composition and other features of particles.

Gas Chromatography (GC) and High Performance Liquid Chromatography (HPLC) are methods used for separating organic mixtures. They are useful for fingerprinting complex organic mixtures and also detecting contaminants in solvents.

Recently, **Optical Surface Analyzer (OSA)** system is used to measure carbon wear, lubricant depletion/accumulation, surface roughness, corrosive wear, and lubricant alternation on carbon coated thin film disks. More information is given in chapter 2.

The use of materials analysis in the disk drive industry has grown significantly. Development of new head and disk materials and a great need for microcontamination control have spurred this growth. Various techniques are now utilized in R&D, production, and failure analysis to better understand and control the surface and bulk chemistry of drive materials.

1.6 Objectives

The successful operation of a hard disk drive requires the presence of a monolayer PFPE film at the head-disk interface. The adhesion, mobility, and physical properties of this lubricant can significantly affect the tribological reliability of the hard-disk drive. The physical properties of this PFPE film, and hence its lubricity, are dictated by the interplay of the intramolecular cohesive interactions between PFPE molecules, and by the adhesive interactions between the PFPE lubricant and the underlying surface.

Mechanical properties of the contacting materials are important parameters to study in order to understand the friction and wear at the head-disk interface. Tribochemistry of the involved contacting objects is another important issue. In this dissertation, the research focus is on the decomposition mechanisms of the PFPE lubricants in order to improve the wear durability of disks and sliders during their contact. The interactions of the PFPE lubricant with the carbon overcoats are investigated in terms of overcoat content, lube backbone, lube endgroup, lube additive, lube molecular weight, lube thickness, and lube bonded fraction. The ultimate goal is to find an optimized thin film design which performs excellent tribological property.

1.7 Dissertation Organization

The dissertation is divided in to 10 chapters. In the first chapter, the term “tribology” and lubrication history are introduced. From the development history of the hard drives, the challenge of increasing areal density is presented. To face this challenge, important Tribochemical concerns invalid in the thin film disk designs are reviewed. Some

characterization techniques are also introduced to better understand the surface and bulk chemistry of drive materials. After these background descriptions, the objectives and configuration of this dissertation are outlined.

In Chapter 2, experimental procedure and set-up of the research work is presented. The experiments include drag tests and thermal desorption tests in the ultra high vacuum (UHV) tribochamber, optical surface analysis (OSA) measurements, and thermogravimetric analysis (TGA) measurements.

In Chapter 3, two decomposition mechanisms of PFPE lubricants are studied: one is frictional scission/thermal action, and the other is the catalytic reaction. Chemical bonding theory is used to analyze the lube decomposition process.

In Chapter 4, the thermal stability of PFPE lubricants and their thermal desorption mechanisms are studied. The results illustrate that frictional heating is the primary decomposition mechanism of ZDOL in the carbon-coated slider/CHx disk case.

In Chapter 5, we study the ZDOL decomposition mechanisms on hydrogenated carbon films (CHx) and nitrogenated carbon films (CNx). The results show that for CNx films the catalytic reactions were less than for CHx films, presumably due to less hydrogen evolution from the CNx overcoat.

In Chapter 6, the studies demonstrate the backbone and endgroup effect on the catalytic reactions of PFPE lubricants. The catalytic degradation in the presence of Lewis acid occurs most readily at acetal units within the internal lube backbones.

In Chapter 7, the effect of adding X-1P in PFPE lubricant is studied. X-1P passivates the head and prevents catalytic reaction of the PFPE when used as an additive. In addition,

X-1P also increases the PFPE's mobility and, hence, improves PFPE's tribological performance.

In Chapter 8, studies are carried out to investigate the lubricant molecular weight effect on the tribological performance. The lube mobility decreases with increasing molecular weight. In addition, the thermal desorption temperatures increases with increasing molecular weight.

In Chapter 9, lubricant thickness effect are studied. Lube wear durability improves considerably when the carbon overcoat surface is fully covered by one layer of ZDOL. Moreover, the ZDOL desorbed peak temperatures shifts to lower temperatures with increasing lubricant thickness.

In Chapter 10, we study the effect of ZDOL bonding fraction. Wear durability improves with an increase in the mobile portion.

Chapter 2

EXPERIMENTAL SET-UP

2.1 Ultra-High Vacuum (UHV) Tribochamber Tests

In order to study the tribochemistry of the decomposition mechanisms of the PFPE lubricants, the ultra-high vacuum (UHV) tribochamber is developed in our laboratory. The UHV tribochamber consists of a disk spindle, a slider actuator, a substrate heater, and a Balzers QMG 420 high-resolution quadrupole mass spectrometer (QMS) in a stainless-steel vacuum chamber. A base pressure of less than 2×10^{-8} Torr is achieved through the use of a Balzers TPU 330 turbo-molecular pump that is backed by a Balzers DUO 016B mechanical pump. The chamber pressure is monitored with two Varian gauges: 1 524-2 cold cathode ionization gauge and a UHV-24 Bayard-Alpert type ionization gauge. The disk spindle is driven by a DC motor at rotational speeds of 50 to 64 rpm through a UHV-compatible feedthrough. A slider may be mounted on the slider actuator, which has a strain arm instrumented with semiconductor strain gauges to measure forces in the vertical and horizontal directions, and its XYZ position is controlled via linear stages. A picture of the chamber is shown in Fig. 2.1.

The QMS provides *in situ* detection of the gaseous products generated at the HDI during drag tests and thermal desorption studies. The QMS can monitor simultaneously 15 different atomic mass units (AMUs) ranging from 1 to 500 along with friction or temperature data from strain gauge transducers or a thermocouple, respectively. It is noted that all AMUs

from 1 to 192 of ZDOL decomposition products generated at the Al_2O_3/TiC slider/CHx disk interface were previously investigated under the same test conditions and only the most pertinent AMUs were monitored in this study.

2.1.1 Drag Tests

Drag tests in the UHV tribochamber were conducted as follows. Initially, the tribochamber was baked out at 500 K at high vacuum for 24 hours. The chamber was then backfilled with Argon gas as the disk and slider samples were mounted inside. Next, the chamber was pumped down to a base pressure of 2×10^{-8} Torr and the channels of the QMS were assigned to selected AMUs. Background intensities were recorded before the drag tests were initiated with the following parameters: 0.2 m/s drag speed, a load of 2.5 grams, and a sliding time of 20 minutes. The mass spectrum and friction data is collected every 2 seconds by a computer connected to the QMS via a serial connection.

2.1.2 UHV Thermal Desorption Tests

Prior to conducting thermal desorption tests in the UHV tribochamber, the substrate heater is baked at 600 K in high vacuum for 4 hours to remove any residual contaminants on the heater surface after each thermal desorption test. A test sample is cut from each disk into 2 cm x 2 cm squares. Each sample is mounted on the heater where a thermocouple in contact with the heater is used to monitor the temperature during testing sample. As with the drag tests, the chamber was pumped down to a base pressure of 2×10^{-8} Torr and the channels of the QMS were assigned to the selected AMUs. The sample is heated at a rate of 0.3 K/sec from room temperature to 550 K while the mass spectrum and temperature data is collected every two seconds by a computer connected to the QMS via a serial connection.

Afterwards, the spectra were analyzed in order to obtain the thermal desorption profile for each mass as a function of sample temperature.

2.2 Optical Surface Analysis (OSA) Measurements

The optical surface analysis (OSA) system was also used to observe the lube migration behavior. The OSA is an *in situ* device, which has approximately 5 micron resolution and 2 MHz of bandwidth. This device can be used to measure less than one Angstrom of carbon wear or lubricant depletion/accumulation. The OSA can also measure index of refraction changes caused by lubricant degradation or lubricant migration. The OSA is essentially a quantitative robot reflectometer microscope for imaging and analyzing the surface of a thin film disk. It operates by illuminating the surface of a carbon-coated disk with a highly stabilized laser diode beam at a wavelength of 780 nm. A wavelength of 780nm is chosen since carbon is reasonably absorptive at this wavelength. Also, off-the-shelf optical components are available at this wavelength. The OSA is designed so that it allows a choice of either P or S polarized light, and the scattered or specular component of light coming from the surface can be measured. Fig. 2.2 shows a schematic diagram of the OSA, and more information about the principle of operation can be found in Meeks's paper [9].

2.3 Thermogravimetric Analysis (TGA) Measurements

The thermogravimetric analysis (TGA) is a sensitive measurement to observe the weight change of a sample as a function of temperature. Typical applications include the

assessment of thermal stability and decomposition temperature in polymers [10-13]. The TGA experiments were carried out in a TGA model 2050 manufactured by TA Instruments Inc., which has a temperature range from liquid nitrogen temperatures to 650^{o}C, and was operated at a mass resolution of 0.3 μg. A typical sample size is on the order of 8 mg. Evaporation rate data was collected during a linear temperature ramp-up, usually 10^{o}C/min, under a dry nitrogen purge. The samples were contained in aluminum pans.

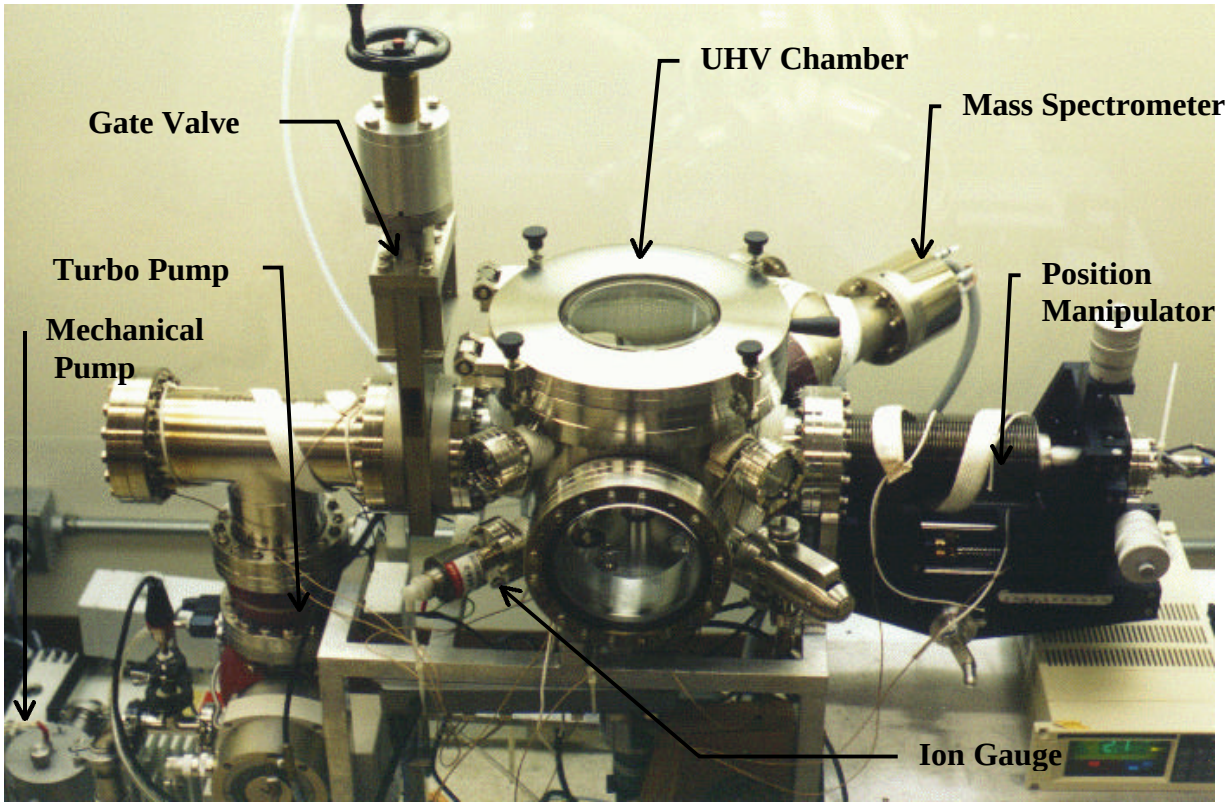

Fig. 2.1 Ultra High Vacuum (UHV) Tribochemical Chamber

Fig. 2.2 Optical Surface Analyzer

Chapter 3

THE DECOMPOSITION MECHANISMS OF PFPE LUBRICANTS

3.1 Introduction

To reduce friction and wear, magnetic recording thin-film disks have a hard overcoat lubricated with a thin layer of a liquid lubricant. Because of the superior properties, such as low vapor pressure, good viscosity, high thermal stability and chemical inertness, perfluoroether (PFPEs) have been extensively used as the lubricants of magnetic media in hard disk drives. The molecular structure, containing only carbon, fluorine and oxygen atoms, gives PFPEs this set of properties. Many experiments demonstrate that PFPEs, subjected to electron irradiation, are easily decomposed into smaller fragments [14]. Vurens et al. [15] used low energy electrons to bombard PFPEs and observed that the electron decomposition of PFPEs occurs at an energy below their ionization potential (about 14 eV). It is reported that the decomposition rates of PFPEs are much higher in the presence of Lewis acid forming materials, such as Fe_2O_3 [16], Al_2O_3 and $AlCl_3$ [17], than their intrinsic decomposition rate.

In this paper, we study the ZDOL decomposition mechanisms on hydrogenated carbon films (CHx) using an ultra-high vacuum (UHV) tribochamber equipped with a mass spectrometer. The studies consist of drag tests in the UHV tribochamber. Two decomposition processes of ZDOL under sliding friction conditions are studied. One is with

---

∗ Parts of this chapter are to be appeared in J. Tribology, 2000 [40].

a carbon film coated slider/CHx coated disk system, and another is with an uncoated Al_2O_3-TiC slider/CHx coated disk system. Chemical bonding theory is used to analyze the decomposition process of ZDOL. The decomposition mechanisms caused by friction, electron bombardment and catalysis are proposed.

3.2 Experimental Procedure and Set-up

Drag tests were conducted in the UHV chamber. The sliders were 50% (2mm x 1.6mm) taper-flat Al_2O_3/TiC sliders with and without amorphous carbon films on the air bearing surfaces. The disks were commercial 95mm smooth thin film disks with 75Å amorphous hydrogenated carbon overcoat (CHx). The hydrogen content in the CHx film was 30 atomic percent. The disks were lubricated with ZDOL by a dipping process. The chemical structure of ZDOL is shown in Appendix I. The resulting thickness of ZDOL on the disks was 9Å as measured by the Fourier Transform Infrared Spectroscopy (FTIR).

3.3 Results and Discussions

In this section, we present and discuss the results from the UHV drag tests. Figure 3.1 shows the friction coefficient curves for the ZDOL lubricated CHx disks against an uncoated Al_2O_3/TiC slider and a carbon coated slider. Before the friction tests started, the background intensities were recorded for 80 seconds by the mass spectrometer. For the uncoated Al_2O_3/TiC slider, the friction coefficient increased to a peak value of 1.6 within 40 seconds and dropped to 0.4 after reaching its peak value. A wear track was observed on the disk after the friction coefficient had dropped. The friction variation, as shown as in Fig. 3.1, is most likely due to three body contact resulting from small wear particles that were

generated at the head-disk interface. For the carbon-coated slider, the friction coefficient started at 0.3 and increased steadily to 0.8 within 400 seconds before wear occurred. The above results indicate that ZDOL has little lubricating action against the uncoated slider, but it has good lubricating action against the carbon-coated slider.

Figure 3.2 shows the integrated mass spectra of ZDOL fragments produced from the carbon-coated slider/CHx disk. The mass spectra signals were integrated over the first 30 seconds (before wear occurred) of the sliding time during the UHV drag tests. The five primary peaks in Fig. 3.2, in decreasing intensity order, belong to mass fragments F (19), CFO (47), CO_2 (44), CF_2O (66), and HF (20). No H_2 (2) is released in this case. Because no contact with Lewis acid is possible in this case, the ZDOL decomposition should be caused by friction/thermal actions only, and therefore it should be directly related to the molecular bond energies. The relevant bond dissociation energies (shown in Table 3.1) are used to judge the bond strength and possible decomposition trends [18]. Because the weakest bonds in ZDOL are C-O-C (3.5 eV), and C-C (3.8 eV), the molecule is expected to cleave preferentially at these locations. A radical mechanism proposed by Sianesi et al. [19] postulates that PFPEs dissociate by breaking the weaker C-C bonds followed by β scission to form perfluorinated aldehyde and alkene.

The following decomposition mechanism is proposed for this case: (1) the ZDOL molecule decomposes under frictional action and then (2) the gaseous by-products are further cleaved by electron bombardment in the QMS. In other words, the following processes occur:

$$\text{-O-/CF}_2\text{-O/-CF}_2\text{-CF}_2\text{-O-/-CF}_2\text{-} \rightarrow \text{CF}_2\text{=O (66)} + \text{-CF}_2\text{-CF}_2\text{-O- (116)} \qquad (3\text{-}1)$$

$$-CF_2-CF_2-O- \rightarrow -CF_2\ (50) + CF_2=O\ (66) \quad (3\text{-}2)$$

$$-CF_2 \rightarrow -CF\ (31) + F\ (19) \quad (3\text{-}3)$$

$$CF_2=O \rightarrow CFO\ (47) + F\ (19) \quad (3\text{-}4)$$

$$CFO \rightarrow CO\ (28) + F\ (19) \quad (3\text{-}5)$$

Therefore, F (19), CFO (47), CO_2 (44), CF_2O (66), and CO (28) are the primary decomposition fragments according to reactions (3-1) through (3-5). In reactions (3-4) and (3-5), oxygen is not a decomposition product because the C=O bond is stronger than the C-F bond within the CF_2=O and CFO molecules. The occurrence of HF may result from the formation of F and subsequent attack of F on surface adsorbates [20] such as hydroxyl groups (-OH) or surface CH groups. In the same way, CF_2H is from the formation of CF_2 and the hydroxyl group (-OH); CO_2 is from the formation of CO and the hydroxyl group (-OH). Moreover, the intensity of CO_2 is stronger than that of CO since the CO_2 molecule (two C=O bonds) is more stable than the CO molecule (one C=O bond). The maximum degradation intensity is from the F (19) component because F (19) is the final decomposition product of ZDOL. No larger groups than CF_2O appear in the mass spectrum; the reason is that the groups larger than CF_2O may contain weaker single bonds (e.g., C-O-C and C-C), that are easily cleaved by frictional shear and electron bombardment.

For the uncoated slider case, the integrated mass spectra (the first 30 seconds before wear) of ZDOL fragments are shown in Fig. 3.3. Note that the mass intensity scale is one order of magnitude higher than that in Fig 3.2. Besides the peaks associated with the frictional decomposition of the ZDOL molecule, new peaks appear at CF_3 (69), C_2F_5 (119), and H_2 (2) which are due to the catalytic effect of the Al_2O_3-TiC slider material. Moreover,

the major five peaks in descending order are CO_2 (44), F (19), CF_3 (69), C_2F_5 (119), and CFO (47) which is a little different from those of Fig. 3.2.

The following catalytic decomposition mechanism of ZDOL on an AL_2O_3-TiC surface is proposed, based on our results and those in literature:

1. ZDOL decomposes and forms CF_2=O from friction stimulation, while the CH_x film degrades and produces H_2.

$$\text{-O-/-}CF_2\text{-O-/}CF_2\text{-}CF_2\text{-O-/-}CF_2\text{-} \rightarrow CF_2{=}O\ (66) + \text{-}CF_2\text{-}CF_2\text{-O-}\ (116) \qquad (3\text{-}1)$$

2. Complex chemical reactions of ZDOL decomposition products occur with H_2 and produce HF [20].

3. CF_2=O and HF react with Al_2O_3 to produce a strong Lewis acid, AlF_3.

$$Al_2O_3 + 6HF \rightarrow AlF_3 + 3H_2O \qquad (3\text{-}6)$$

$$Al_2O_3 + 3CF_2O \rightarrow 2\ AlF_3 + 3CO_2 \qquad (3\text{-}7)$$

4. Finally, rapid decomposition reactions along the main ZDOL chain take place on the AlF_3 surface to form methoxy (CF_3-O-), ethoxy (CF_3CF_2-O-) compounds, and acyl fluoride (R-CF=O).

$$R\text{-}CF_2\text{-}O\text{-}CF_2\text{-}R \rightarrow R\text{-}\overset{\overset{F}{|}}{C}=O + CF_3\text{-}R$$

(CF_3-R: CF_3-O-, CF_3CF_2-O-) (3-8)

Subsequent electron impact fragmentation of the products from (8) then leads to the CF_3 (69) and CF_3CF_2 (119) fragments observed in the mass spectrum. It is noted that reaction (3-1) is demonstrated by our test results. Reaction (3-6) is often used to etch alumina surfaces (Al_2O_3 films are etchable in HF) [21], and reaction (3-7) is supported by the occurrence of significant amounts of CO_2 and the results of John et al. [22], where acyl fluoride (R-CF=O) reacts with alumina and forms AlF_3. Catalytic reaction (3-8) was obtained by Kasai et al. [17].

Berry et al. [23] also investigated the decomposition of perfluorodimethyl ether, PFDME, to CF_2O and CF_4. They observed that, in the absence of a Lewis acid catalyst, disproportionation via a transition state proceeds (TS1) with a reaction barrier of 374 kJ/mole, while the AlF_3 Lewis acid assisted disproportionation via another transition state (TS2) and reduced the reaction barrier to 165 kJ/mole, reflecting a more than 50% lowering of the barrier due to the Lewis acid catalyst. Pacansky and Waltman [24, 25] also proposed a model for the Lewis acid interaction and the origin for the catalytic degradation. From the optimized geometry, they identified a strong electrostatic interaction between the aluminum surface and the lubricant ether oxygen atom, which stabilizes the transition structure during the catalytic reaction. At the transition geometry, the Al-O interaction develops some covalent character. The effect of the Lewis acid catalyst is to reduce the activation energy for decomposition from 431 to 197 kJ/mole. These results provide a fundamental

understanding of why catalytic surfaces must be avoided to ensure the integrity of polyperfluorinated ether lubricants.

The mass spectrum in Fig. 3.3 can be explained according to the above. The decomposed products of ZDOL contain both frictional products and catalytic products. The occurrence of the CF_2O (66) and CFO (47) peaks is a result of friction and electron decomposition as shown in Fig. 3.2. Meanwhile, the catalytic process may also produce these fragments. One of the catalytic products, R-CF=O, may decompose into two fragments (CF_2=O and CF=O) under electron impact as shown in reaction (3-9). This explains why the intensities of CF_2=O and CF=O are stronger in figure 3 (uncoated slider case) than in Fig. 3.2 (carbon-coated slider case).

$$\text{R-CF=O} \rightarrow \text{CF}_2\text{=O or CF=O} \qquad (3\text{-}9)$$

The CF_3 peak is due to the cleavage of the catalytic products with methoxy end groups (CF_3-O-) as shown in reaction (3-10). The C_2F_5 peak is due to the cleavage of the catalytic products with ethoxy end groups (CF_3CF_2-O-) as shown in reaction (3-11).

$$\text{CF}_3\text{-O-R} \rightarrow \text{CF}_3 \qquad (3\text{-}10)$$

$$\text{CF}_3\text{CF}_2\text{-O-R} \rightarrow \text{CF}_3\text{CF}_2 \qquad (3\text{-}11)$$

Strom and Bogy [26] also observed that CF_3, CF, CF_2, and CF_2H are the primary ZDOL decomposition fragments against an uncoated Al_2O_3/TiC slider. They suggested that the degradation reaction is activated by low energy electrons produced at the tribological

interface. Vurens et al. [15] used the electron stimulation method and mass spectrometer to observe the ZDOL desorption behavior. They observed that HF, CO_2, CO, CF_2O are the primary fragments, but no CF_3 peak was observed. From our data and Vurens's data, the fragment CF_3 is mostly from the catalytic reaction at the Al_2O_3/ZDOL interface. The occurrence of the HF and CF_2H fragments is due to the H_2 evolution of the worn CHx surface and subsequent complicated reactions of H_2 with ZDOL decomposition products (CFx). The formation of HF involves a basic radical reaction of the H and F radicals as shown in reaction (3-12). The formation of CF_2H may involve more complicated radical reactions.

$$H^{\cdot} + F^{\cdot} \rightarrow HF \qquad (3\text{-}12)$$

The strongest intensity peak is from CO_2 which is due to reaction (3-7) and is not from the formation of CO and the hydroxyl end group as mentioned before. The evidence is that the CO intensity is not very strong in Fig. 3.3 as compared to the CO_2 intensity since CO is the source of the formation of CO_2 by that mechanism.

Based on the above results, it is found that the decomposition mechanisms of ZDOL in the case of the uncoated Al_2O_3/TiC slider are much more complicated than those with the carbon coated slider. For the carbon-coated slider, ZDOL decomposition is caused by frictional actions, which include frictional heat , triboelectrons, and mechanical shear actions. For the uncoated slider, ZDOL decomposition is controlled by tribochemical and catalytic reactions. Tribochemistry involves three aspects. The first part is the tribochemical decomposition of ZDOL and the tribochemical degradation of the CHx overcoats, producing

significant amounts of gaseous products such as CFO, CF_2O and H_2. The second part is the tribochemical reactions of ZDOL decomposition products with H_2, forming HF and CF_2H. The third part is the tribochemical reactions of the Al_2O_3 surface with HF and ZDOL decomposition products, forming a strong Lewis acid AlF_3. Once AlF_3 is formed, the catalytic decomposition reactions dominate the decomposition process of ZDOL, forming CF_3 and C_2F_5, which are responsible for the high decomposition rate of ZDOL.

3.4 Conclusions

The experiments presented here illustrate the complex chemical relationships that occur at the head/disk interface during drag tests. The UHV tribochamber was used to monitor *in situ* gaseous wear products generated at the HDI during dragging. In studies of CH_x carbon overcoats paired with carbon-coated sliders, the primary decomposition mechanism of ZDOL was due to frictional effects, and it was characterized by the generation of F (19), HF (20), CO_2 (44), CFO (47), and CF_2O (66) fragments. The absence of a carbon coating on the slider led to a more complex catalytic decomposition mechanism of ZDOL during drag tests: (1) initial friction decomposition of ZDOL and degradation of CH_x to form gaseous products such as CF_2O and H_2; (2) reaction of these products with H_2 to produce HF and CF_2H; (3) production of AlF_3 when CF_2O and HF react with Al_2O_3, followed by rapidly decomposition of ZDOL.

Bond	[kcal/mol]	[eV]
C-F	116	5.0
C-O-C	81	3.5
C-C	88	3.8
C-H	98	4.2
C-OH	91	3.9
O-H	103	4.5
C=C	146	6.3
C=O	179	7.8

TABLE 3.1 BOND DISSOCIATION ENERGIES

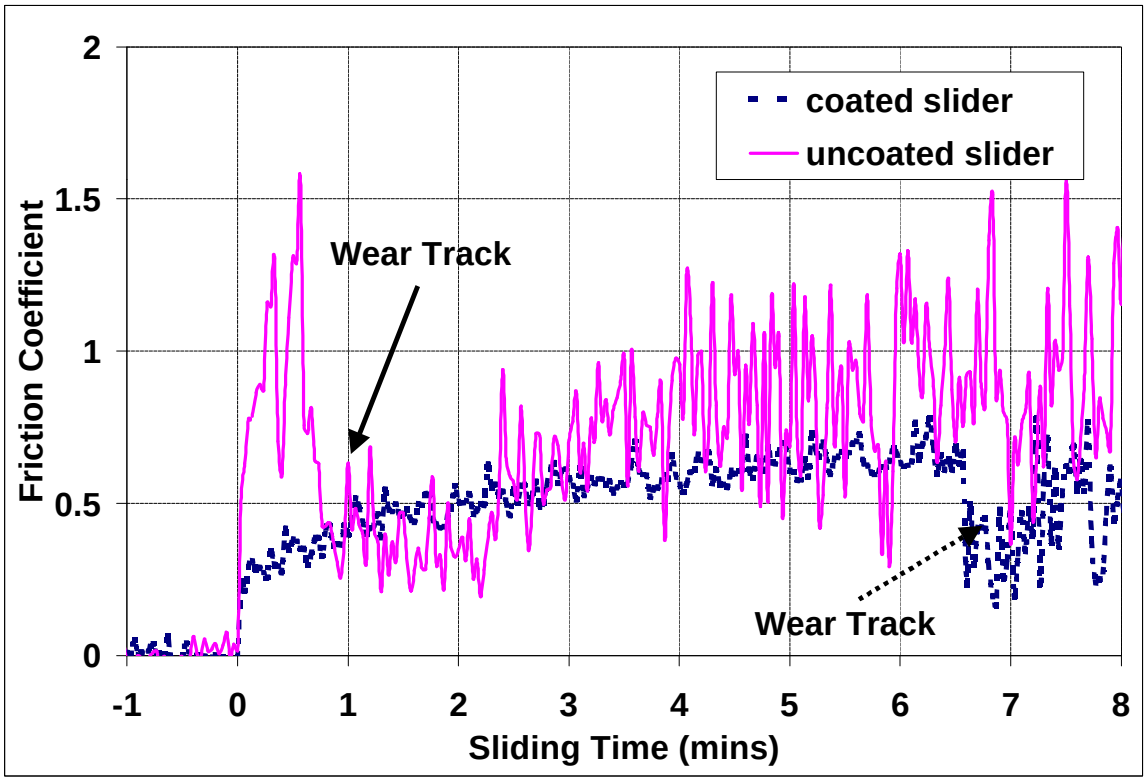

Figure 3.1 The friction coefficient curves of ZDOL lubricated CHx disks on uncoated Al_2O_3/TiC slider and carbon coated slider.

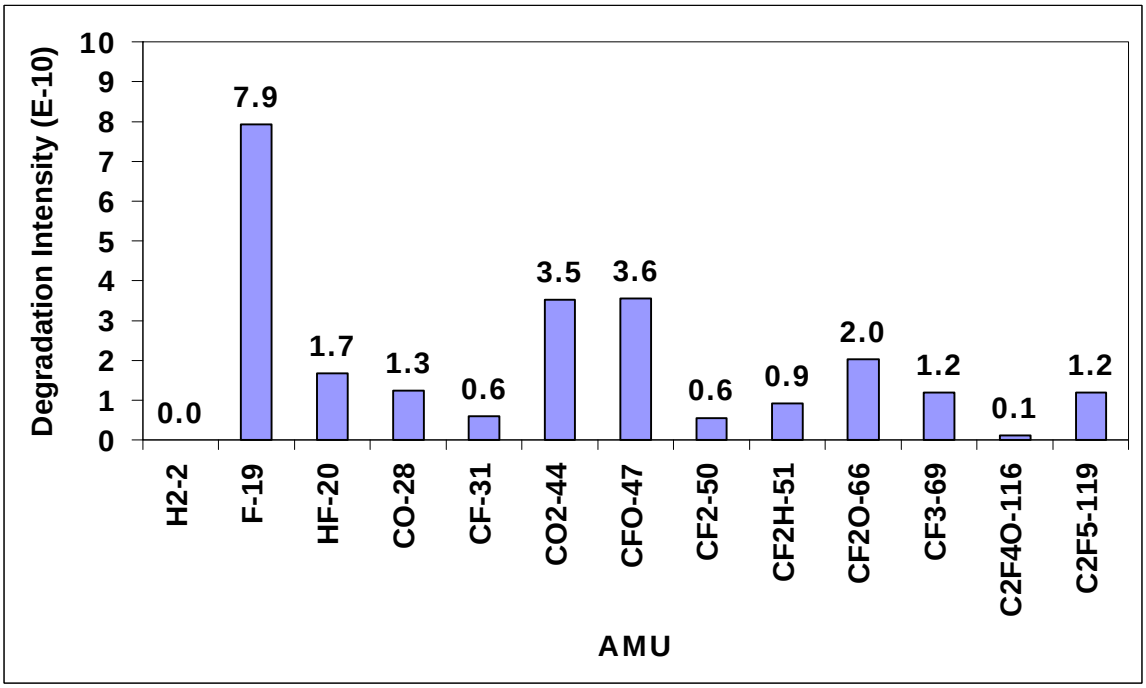

Figure 3.2 The integrated mass spectra (the first 30 seconds before wear) of ZDOL decomposition products generated at the carbon-coated slider/CHx disk interface.

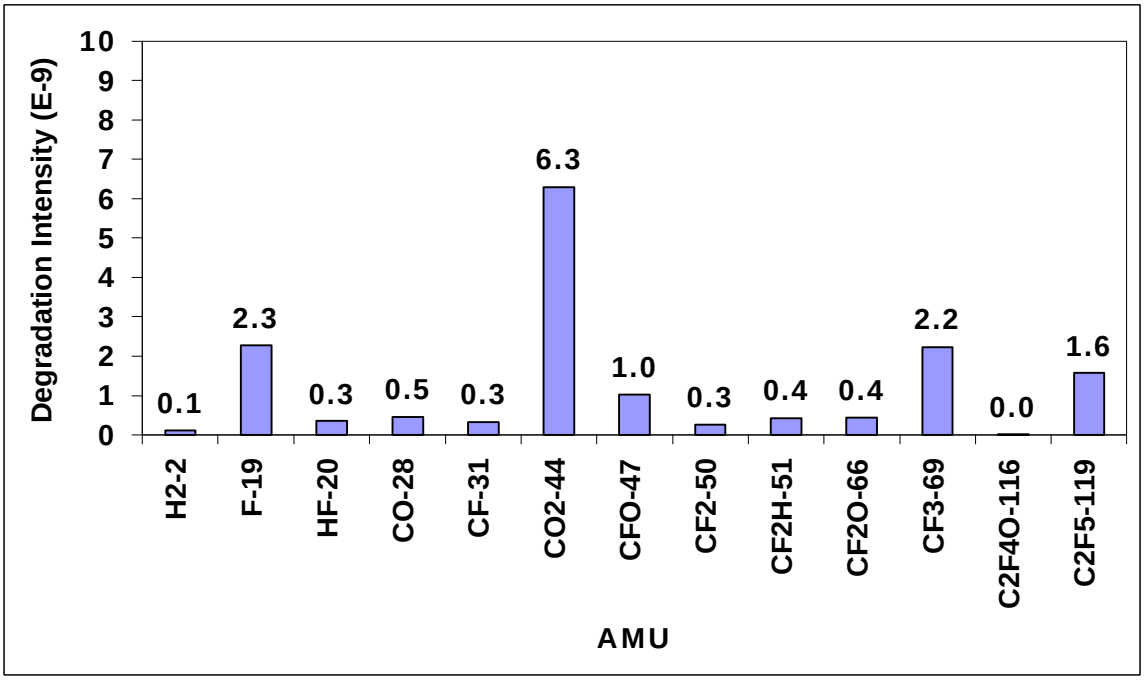

Figure 3.3 The integrated mass spectra (the first 30 seconds before wear) of ZDOL decomposition products generated at the uncoated slider/CHx disk interface.

Chapter 4

THE THERMAL STABILITY OF PFPE LUBRICANTS

4.1 Introduction

The thermal stability of PFPE molecules has also been studied extensively. PFPE is intrinsically stable below ~570K, even in an oxygen atmosphere [27, 28]. However, Fomblin-Z dissociates in the presence of Lewis acid sites on Fe_2O_3 at 450K [29], and on Al_2O_3 at 470K [30]. Lin et al. [20] used temperature-programmed reaction/desorption (TRP/D) and electron simulated desorption (ESD) to study the roles of temperature and triboelectric charges in the decomposition of Fomblin-ZDOL lubricant molecules. They showed that the threshold temperature for dissociation of the Fomblin-ZDOL molecule is at 500-550K in accordance with the known thermal stability of the free ZDOL molecule. Vurens [31] also showed that molecules having a CF_2-CF_3 endgroup (Demnum S65) display enhanced thermal stability compared to molecules with the CF_2-CF_2-CH_2-CH_2O-phenyl endgroup (Demnum SP). Gellman [32] showed that the heat of adsorption of the hydrocarbon ether was greater than that of the corresponding fluorocarbon ether, suggesting that the ethers are bonded to the films through the donation of the electron pair on the oxygen atom. Gellman also proposed a model in which the electropositive nature of the hydrogen in the a-CH films weakens the extent of electron donation from the ether lone pairs and, hence, weakens the bonding of the ethers to the a-CH films.

∗ Parts of this material are to be appeared in J. Tribology, 2000 [40].

Furthermore, Perry [33] used temperature-programmed desorption and scanning force microscopy to probe the interaction of ZDOL with both hydrogenated carbon overcoats and nitrogenated carbon overcoats. The data showed that the nitride surfaces are more reactive toward the ZDOL lubricant and, as a result, the thin lubricant film is more tightly bound to the overcoats. As the flying height of sliders approaches zero and near contact, the chances of contact between the head and the disk are greater. Ettles [34] used a numerical solution in two dimensions to predict the thermal effects of the asperity contact between sliders and magnetic recording disks. He showed that temperatures exceeding several hundred degrees centigrade are quite possible. Suzuki et al. [35] estimated that the contact temperature in the MnZn ferrite slider/thin film disk case may be up to 550K. The temperature rise and signal loss were especially significant when crash of the slider occurred, resulting in large-scale wear of the disk surface. Therefore, understanding the thermal response of the materials used in the hard drive becomes imperative.

In this paper, we study the ZDOL thermal stability on hydrogenated carbon films (CHx) using an ultra-high vacuum (UHV) tribochamber equipped with a mass spectrometer. The studies consist of thermal desorption experiments in the UHV tribochamber. The desorption mechanisms of ZDOL lube are discussed.

4.2 Experimental Procedure and Set-up

Thermal desorption experiments were conducted in the UHV chamber. A CHx/ZDOL disk was cut into square pieces of roughly 2 x 2 cm^2. The disks were commercial 95mm smooth thin film disks with 75Å amorphous hydrogenated carbon overcoat (CHx). The hydrogen content in the CHx film was 30 atomic %. The disks were

lubricated with ZDOL by a dipping process. The resulting thickness of ZDOL on the disks was 9Å as measured by FTIR. The lubricated samples were mounted onto a heater and the sample temperature measured by a thermocouple in contact with the heater near the heating sample. A typical experiment consisted of heating a sample at a rate of 0.2 K/s starting at room temperature and stopping before 550K. A mass spectrum was collected on a computer every two seconds (i.e., every 0.4K) during the heating of the samples.

4.3 Results and Discussions

In this section, we show and discuss the results from UHV thermal desorption experiments. Before starting the thermal desorption tests, the background intensities were recorded for 80 seconds. The data presented in this study have subtracted the background intensity from the mass spectrometer signals. Figure 4.1 shows thermal desorption profiles for four primary ZDOL desorbed fragments CFO (47), CF_2O (66), CF_3 (69), and C_2F_5 (119). The first two fragments are under friction/mechanical shear actions and electron bombardment as discussed in Chap 3. The last two fragments are due to catalytic reactions in the presence of Al_2O_3 also as discussed in Chap 3.

Two desorption features peaked at 352K and 429K at the heating rate of 0.2K/sec. The desorption peak temperatures are much lower than those in the literature [27~32]. The peak temperatures are highly dependent on the heating rate. Figure 4.2 shows thermal desorption profiles of fragment CFO (47) using two different heating rates: one is 0.2K/sec, and the other is 1.6K/sec. For the 1.6K/sec case, the first desorption peak temperature of ZDOL was at 405K, and the second peak temperature was at 541K. The lower heating rate (0.2K/sec) is much lower than usual, which accounts for the lower peak temperatures.

During the first thermal desorption period (between 300K and 400K), mobile ZDOL lubricants were desorbed and friction/electron bombardment associated fragments (CFO and CF_2O) are observed. However, no catalytic related fragments (CF_3, and C_2F_5) are observed. These results illustrate that CFO (47) and CF_2O (66) are the primary thermal desorption fragments of mobile ZDOL in addition to the primary decomposed fragments of ZDOL under friction/mechanical shear and electron bombardment actions. These results are consistent with Lin and Kasai's results [30, 20]. During the second thermal desorption period (between 400K and 500K), bonded ZDOL lubricants were desorbed and all four primary fragments are observed. But the friction heat/electron bombardment associated fragments (CFO and CF_2O) are much stronger than the catalytic related fragments (CF_3, and C_2F_5) which may be due to the complicated reactions between the bonded lubricants and the CHx surface as a consequence of desorption of bonded ZDOL from the CHx surface.

Figure 4.3 presents the desorbed mass spectra of ZDOL fragments produced from the ZDOL/CHx disk during the thermal desorption experiments at the first peak (352K). The five primary peaks in descending order belong to mass fragments F (19), CFO (47), CO_2 (44), CF_2O (66), and HF (20) which is the same order as in Fig. 3.2. Furthermore, the ratios between these five peaks in Fig. 4.3 are close to those in Fig. 3.2. Karis et al. [36] also observed that the thermally degraded polymer fragments are almost the same as the mechanically degraded polymer fragments. These results further prove that frictional heating is the dominant decomposition mechanism of ZDOL in the carbon-coated slider/CHx disk case.

Lin et al. [20] observed that CF_2O and CFO are the main thermal desorption fragments at 640K, probably originating from desorbing CF_2O fragments. Vurens et al. [31]

found that the intensity of mass fragment CFO (47) is greater than that of mass fragment CF (31) in the thermal desorption profiles of ZDOL, while for the Demnum compounds the converse is true. This indicates that the desorption products for ZDOL are substantially more oxygen rich (CFO, and CF_2O) compared to those from the Demnum compounds, which should be expected since the ZDOL backbone has an O/C ratio twice that of the Demnum backbone. These results are consistent with those in this chapter.

Figure 4.4 presents the desorbed mass spectra of ZDOL fragments produced from the ZDOL/CHx disk during the thermal desorption experiments at the second peak (452K). The spectrum is very similar to the one in Fig. 4.3, except for fragment H_2 (2). H_2 is the highest desorbed peak in Fig. 4.4 due to the H_2 evolution from the CHx surface as a consequence of the desorption of bonded ZDOL during this period (between 400K and 500K). The H_2 evolution from the CHx surface initiated more lube complicated desorption actions (e.g., stronger desorbed fragments CF_3, and C_2F_5). During the first desorption period (between 300K and 400K), little desorbed H_2 fragment is observed since only mobile ZDOL is desorbed during this period, and less desorbed reactions at the ZDOL lubricants/CHx disk interface are involved. Gellman [32] found that heating a-CH films to temperatures above 500K results in dehydrogenation of the films. It is reported [37, 38] that the strength of the interaction at the head-disk interface is influenced by the hydrogen content of the CHx films.

Figure 4.5 presents the thermal desorption profile of fragments F (19) and HF (20). The first peak of HF was found at 323K corresponding to the drop of F at the same time. The negative intensity of F means that the intensity during this period (300-350K) is below the background intensity. This data is the evidence for reaction (3-12), where the occurrence of HF is due to a basic radical reaction of H and F radicals. However, the increased amount

in HF is less than the decreased amount in F. One possible explanation is that F radicals may react with other radicals instead of H radicals only. Lin et al. [20] observed that HF evolved at 500-550K, and which is probably due to reactions with surface OH groups and surface CH groups present at the ZDOL/hard carbon interface. In Fig. 4.5, we did see another HF peak in the temperature range of 400-500K. HF is responsible for the AlF_3 formation which is the necessary component for the occurrence of the catalytic process as shown in reactions (3-6) and (3-7). More information in details will be shown in chapter 5.

The first thermal desorption peak of F was found at 374K which was 22K higher than the peak desorption temperatures of CFO and CF_2O. The delay of the F peak supports the assertion that F is the final decomposed product of ZDOL as shown previously in reactions (3-3) to (3-5). Another evidence is that the second desorption peak of F was found at 445K, which was 16K higher than those of CFO and CF_2O. These thermal desorption results further support our previous bonding energy theory in reactions (3-1) to (3-5).

4.4 Conclusions

Based on the above thermal desorption mass spectra, it is found that the mass spectrum of mobile ZDOL is very similar to the mass spectrum obtained from sliding at the carbon-coated slider/CHx disk interface. These results illustrate that frictional heating is the primary decomposition mechanism of ZDOL in the carbon-coated slider/CHx disk case. At higher temperatures (above 400K), bonded ZDOL is decomposed and there is H_2 evolution from the worn CHx surface. The H_2 evolution from the CHx surface initiates more complicated desorption actions, forming CF_3 and C_2F_5. The generation of HF during the thermal desorption experiments provides the formation mechanism of HF, which is the

necessary component for catalytic reactions. The delay of the F peak in the thermal desorption profile indicates that F is the final decomposition product of ZDOL.

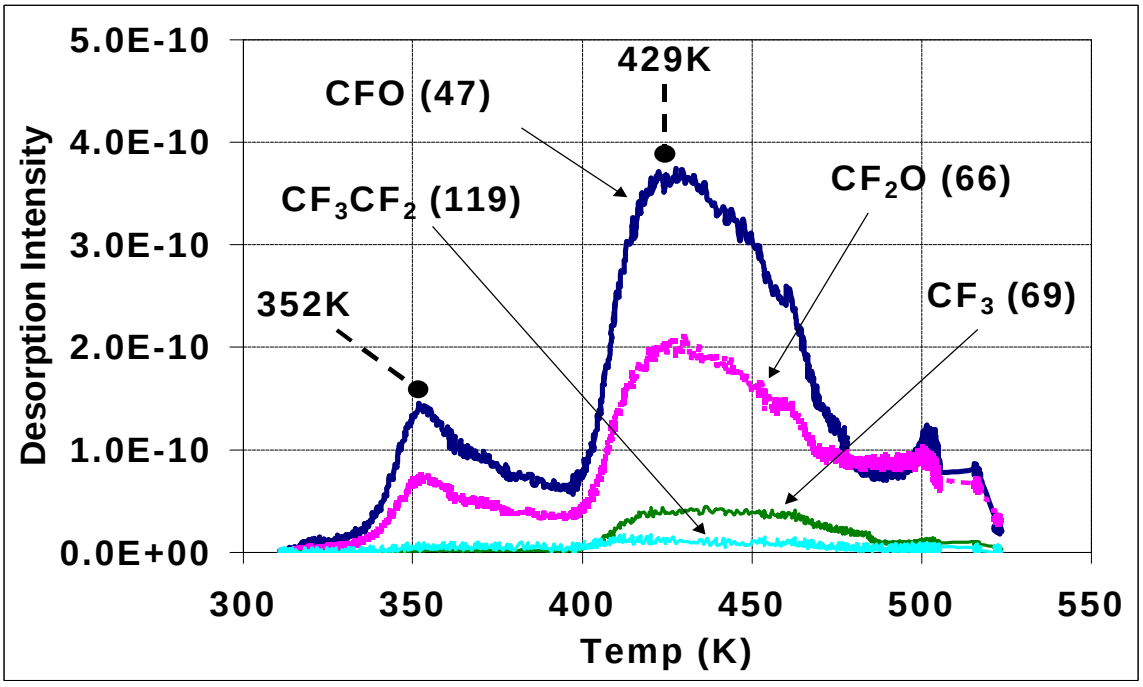

Figure 4.1. The thermal desorption profile of four primary decomposed fragments of ZDOL.

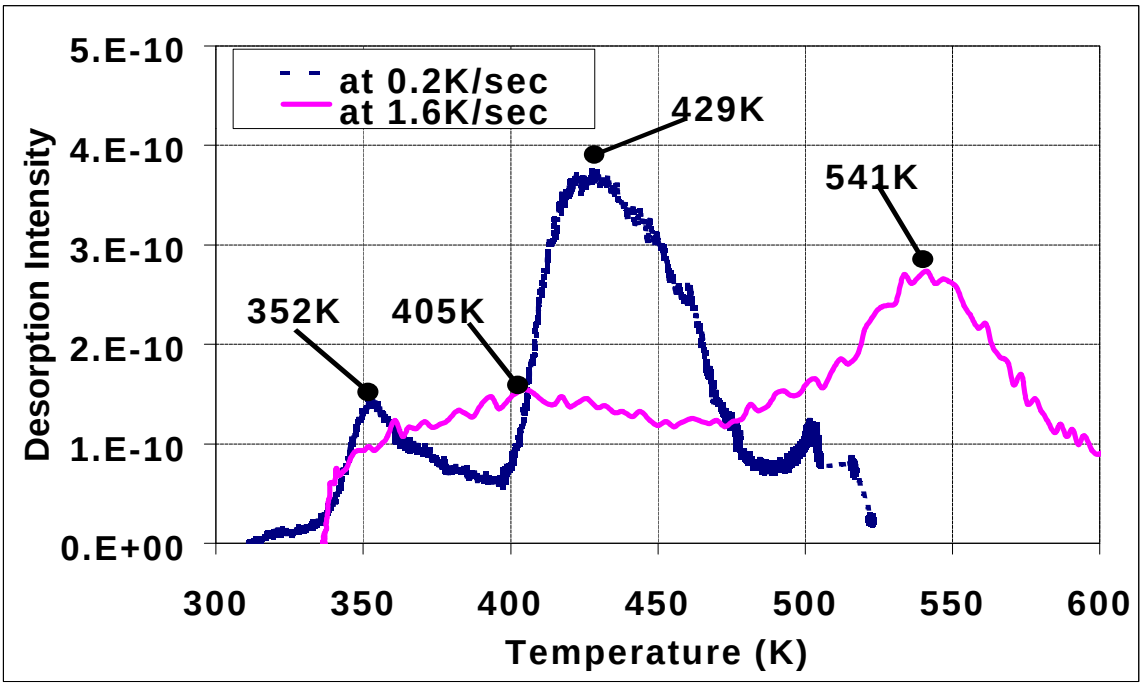

Figure 4.2. The thermal desorption profile of fragment CFO (47) using two different heating rate: one at 0.2K/sec and the other at 1.6K/sec.

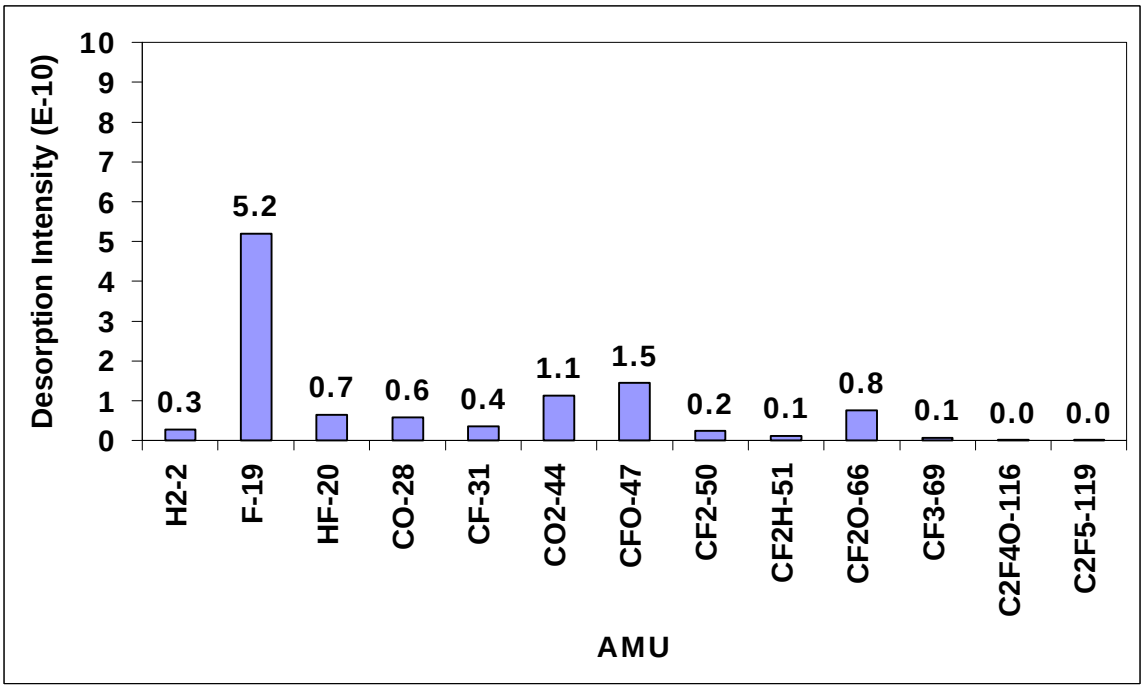

Figure 4.3. The desorbed mass spectrum of **mobile ZDOL** fragments produced from the ZDOL/CHx disk at 352K.

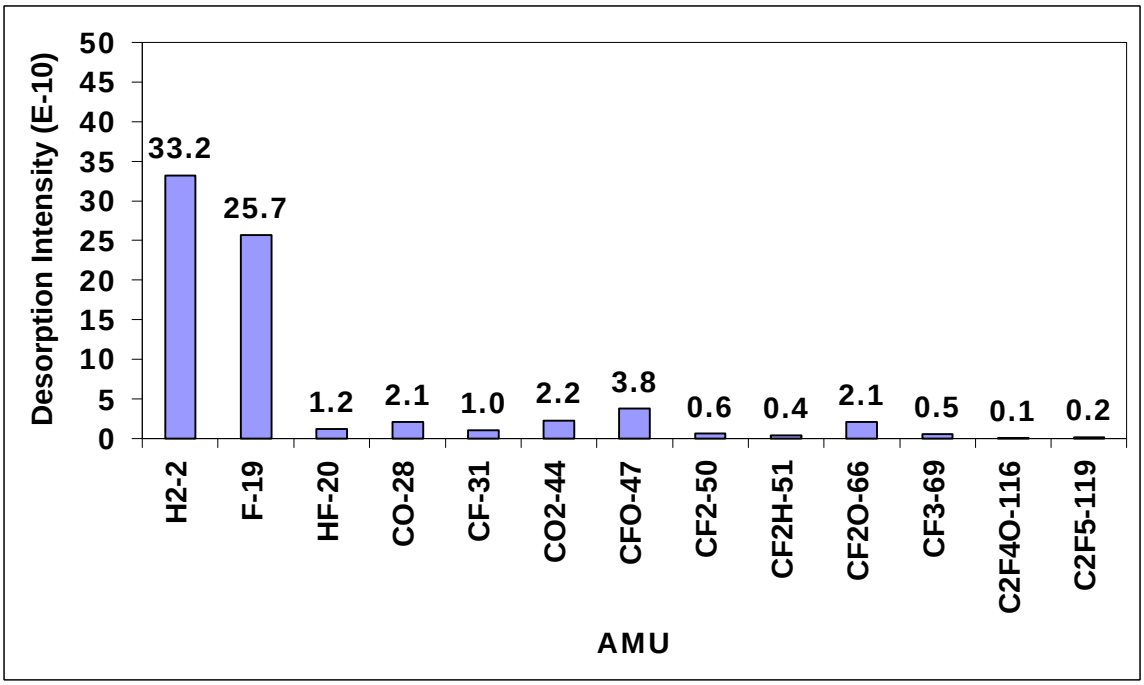

Figure 4.4. The desorption mass spectra of **bonded ZDOL** fragments produced from the ZDOL/CHx disk at 429K.

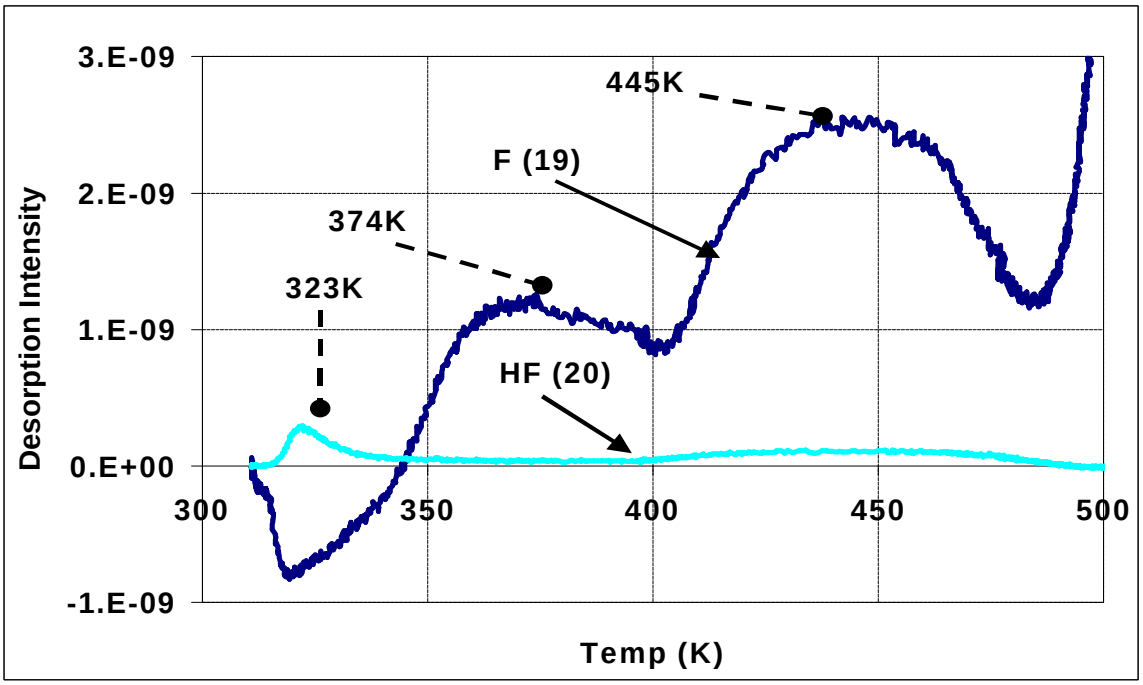

Figure 4.5 The thermal desorption profile of ZDOL fragments F (19) and HF (20).

Chapter 5

HYDROGEN EVOLUTION INITIATES LUBRICANT CATALYTIC DECOMPOSITION

5.1 Introduction

In chapter 3, our studies of the decomposition of ZDOL lubricant on hydrogenated carbon overcoats (CHx) [39, 40] indicate that the decomposition rate is significantly affected by the slider materials. The use of uncoated Al_2O_3-TiC sliders leads to the rapid decomposition of ZDOL due to catalytic reactions, while carbon coated sliders produce less intense decomposition due primarily to frictional actions [42]. Recently, a number of manufacturers of magnetic recording media have replaced the CHx overcoat with an amorphous nitrogenated carbon (a-CNx) overcoat. Most reports have attributed the tribological benefits of CNx overcoats relative CHx overcoats to the increased hardness of the CNx film [43-45]. The hardness of CHx films first increases, then decreses sharply with hydrogen doping, while the hardness of the CNx films decrease linearly with nitrogen doping. However, altering the nature of the carbon surface could also strongly influence the PFPE lubricant by modifying the adhesive strength, bonding kinetics, lubricant orientation, and lubricant mobility [46]. A change in any of these properties could easily manifest itself

∗ Materials from this chapter are submitted to Tribology Letters [41].

in substantially different tribological properties of the computer hard disk. It is also reported that CHx systems fail due to lubricant degradation, while CNx systems fail due to gradual overcoat wear [47].

In this paper, we study the ZDOL decomposition mechanisms on hydrogenated carbon films (CHx) and nitrogenated carbon films (CNx) using an ultra-high vacuum (UHV) tribochamber equipped with a mass spectrometer. The studies consist of UHV drag tests and thermal desorption experiments. The results show that for CNx films the catalytic reactions were less than for CHx films, presumably due to less hydrogen evolution from the CNx overcoat.

5.2 Experimental Procedure and Set-up

Drag tests in the tribochamber were conducted in the UHV with the following parameters: 0.2 m/s drag speed, a load of 30 mN, and a sliding time of 20 minutes. The sliders were 30% (1.2mm x 1mm) negative pressure Al_2O_3/TiC sliders with and without amorphous carbon films on the air bear surfaces. The disks were commercial 95mm thin film disks with 105Å amorphous hydrogenated carbon overcoat (CHx) or 105Å amorphous nitrogenated carbon overcoat (CNx). The hydrogen content in the CHx film was 30 atomic %, and it was 5 atomic % in the CNx film. The disks were lubricated with ZDOL by a dipping process. The resulting thickness of ZDOL on the disks was 12Å, measured by FTIR.

For the thermal desorption tests in the tribochamber, disks were cut into square pieces of roughly 2 x 2 cm^2. The lubricated samples were mounted onto a heater and the temperatures of the samples were measured by a thermocouple in contact with the heater

near the testing samples. A typical experiment consisted of heating a sample at a rate of 0.2K/s starting at room temperature and stopping before 550K. A mass spectrum was collected on a computer every two seconds (i.e., every 0.4K) during the heating of the samples.

5.3 Results and Discussions

5.3.1 Study of Thermal Desorption Data

In this section, we show and discuss the results from UHV thermal desorption experiments. Figure 5.1 shows the thermal desorption profiles of the hydrogen (H_2) evolution from a CHx film and a CNx film, respectively. Figure 5.2 shows the thermal desorption profile of HF. More hydrogen evolution at higher temperatures (above 400K) was observed from the CHx (30% hydrogen content) film than from the CNx (5% hydrogen content) film due to their intrinsic hydrogen content. At the same time, HF was formed as the hydrogen evolution occurred. These data provide the evidence of reaction (3-11), where the occurrence of HF is due to a basic radical reaction of the H and F radicals. Lin et al. [20] observed that HF is evolved starting at 500-550K, which is probably due to reactions with surface OH groups and surface CH groups present at the ZDOL/hard carbon interface. HF is responsible for the AlF_3 formation, which is the necessary component for the occurrence of the catalytic process as shown in reactions (3-6) and (3-7).

Figure 5.3 shows the thermal desorption profile of the ZDOL fragment CFO (47). The peak desorption temperature of ZDOL from the a-CNx surface is 32K lower than the peak temperature from the a-CHx surface. Perry et al. [33] also observed that the peak temperature of ZDOL from the a-CNx surface is 60K lower than the peak temperature from

the a-CHx surface. Vurens and Mate [48] attributed the lower peak temperatures to a more reactive amorphous carbon surface to Fomblin ZDOL decomposition. These results indicate that the carbon films become more reactive with the incorporation of nitrogen. Waltman et al. [49-51] also used the *ab initio* calculations to simulate the van der Waals interactions between the ZDOL chain segments and the surface to strongly impact the lowest energy polymer conformations on the surface. In their work, the nitrogen functional moieties present on the CNx surface were found to be basic (electron-rich) in the Lewis sense and interacted repulsively with the basic ZDOL backbone. This repulsion resulted in a distance of closest approach between the ZDOL backbone and the CNx surface that was larger than that found for the less repulsive CHx surface. The results of the *ab initio* calculations are consistent with the present experimental results since the peak desorption temperature of ZDOL from the CNx surface is 32K lower than the peak temperature from the CHx surface. These repulsive interactions between the ZDOL backbone and the CNx surface result in the lower peak desorption temperature of ZDOL from the CNx surface. They also concluded that, on the CHx surface, ZDOL preferentially lies more parallel to the surface, whereas on the CNx surface, ZDOL is oriented more perpendicular to the surface.

5.3.2 UHV Drag Test - Comparison of the CHx and CNx Films

In this section, we present and discuss the results from the UHV drag tests to compare the tribological performance of the ZDOL/CHx film with the ZDOL/CNx film. Figure 5.4 shows the friction coefficient curves for the ZDOL lubricated **CHx** disks against an uncoated Al_2O_3/TiC slider and a carbon coated Al_2O_3/TiC slider. For the uncoated Al_2O_3/TiC slider, the friction coefficient increased to a peak value of 1.7 within 10 cycles

and dropped to 1 after reaching its peak value. One wear track was observed on the disk just after the friction coefficient had dropped. For the carbon coated slider, the friction coefficient started at 1.3 and increased steadily to 1.8 within 220 cycles before wear occurred.

Figure 5.5 shows the friction coefficient curves for the ZDOL lubricated **CNx** disks against an uncoated Al_2O_3/TiC slider and a carbon coated Al_2O_3/TiC slider. For the uncoated Al_2O_3/TiC slider, the friction coefficient increased to a peak value of 1.7 within 20 cycles and dropped to 1 after reaching its peak value. One wear track was observed on the disk just after the friction coefficient had dropped. For the carbon coated slider, the friction coefficient started at 1.3 and increased steadily to 1.5 within 290 cycles before wear occurred. The above results further support the claim that ZDOL has little lubricating action against the uncoated slider but it has good lubricating action against the carbon-coated slider. In addition, the wear durability of ZDOL/CNx film is better than ZDOL/CHx film.

Figure 5.6 shows the normalized mass spectra of four ZDOL major fragments produced from the ZDOL/CHx and ZDOL/CNx disks. The first two fragments CFO (47) and CF_2O (66) are related with the mechanical shear/friction action, while the last two CF_3 (69) and C_2F_5 (119) are due to catalytic decomposition. The mass spectra signals were integrated over the first 10 cycles (before wear occurred) of the sliding time during the UHV drag tests. For the CHx film, the intensities of catalytic fragments (CF_3 and C_2F_5) increased when using an uncoated slider as compared to a coated slider, although the increase was not very large. These results, together with the thermal desorption data in Figs. 5.1 and 5.2, indicate that less hydrogen evolution from CNx film prevents the forming of HF. HF is the

necessary component for the lubricant catalytic reaction, resulting in a better tirbological performance of the CNx film as compared to the CHx film.

5.4 Conclusions

The hydrogen evolution from the CHx overcoat initiates lubricant catalytic decomposition with an uncoated Al_2O_3/TiC slider, forming CF_3 (69) and C_2F_5 (119). The generation of Hydroflouric acid (HF) during the thermal desorption experiments provides the formation mechanism of Lewis acid, which is the necessary component for catalytic reaction causing ZDOL lube degradation. On the other hand, for CNx films, catalytic reactions were prevented with an uncoated slider due to less hydrogen evolution from the CNx overcoat, resulting in a better tirbological performance for the CNx film as compared to the CHx film.

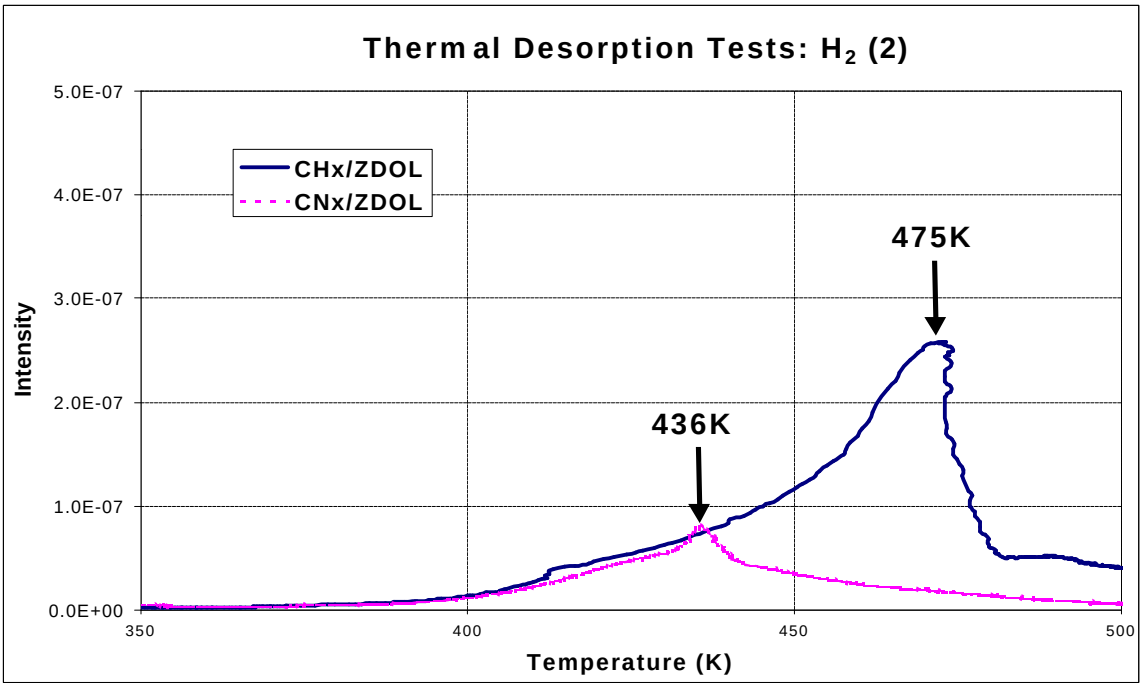

Figure 5.1 The thermal desorption profile of H_2 (2) evolution from both CHx and CNx coated disks in UHV.

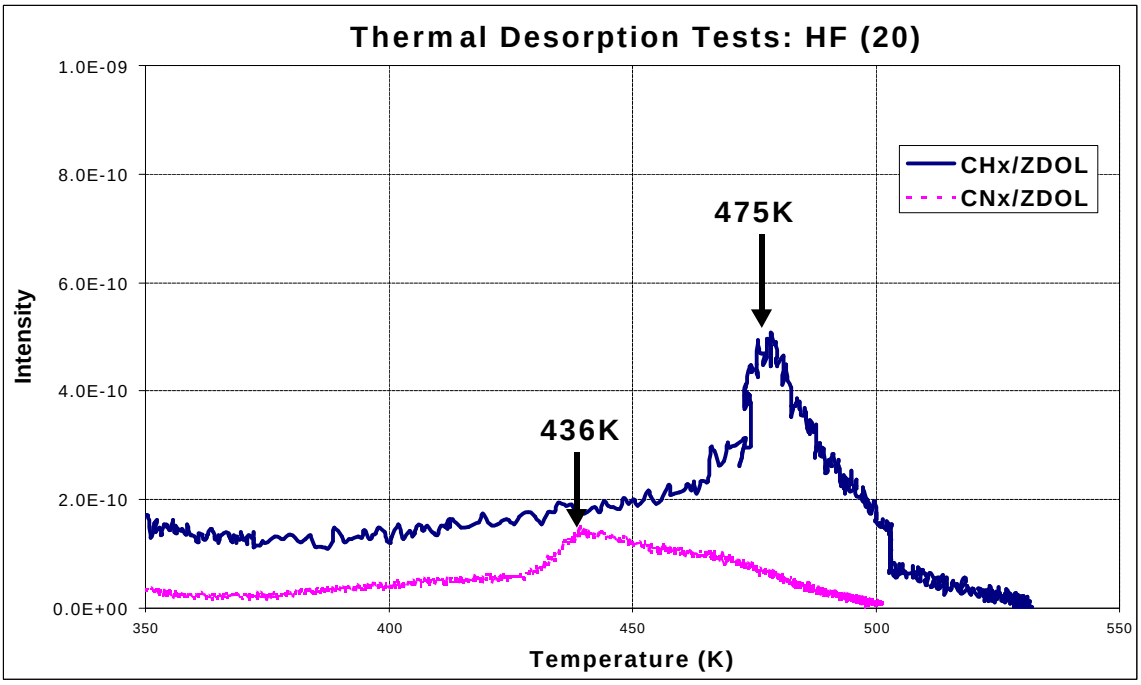

Figure 5.2 The thermal desorption profile of HF (20) formation from both CHx and CNx coated disks in UHV.

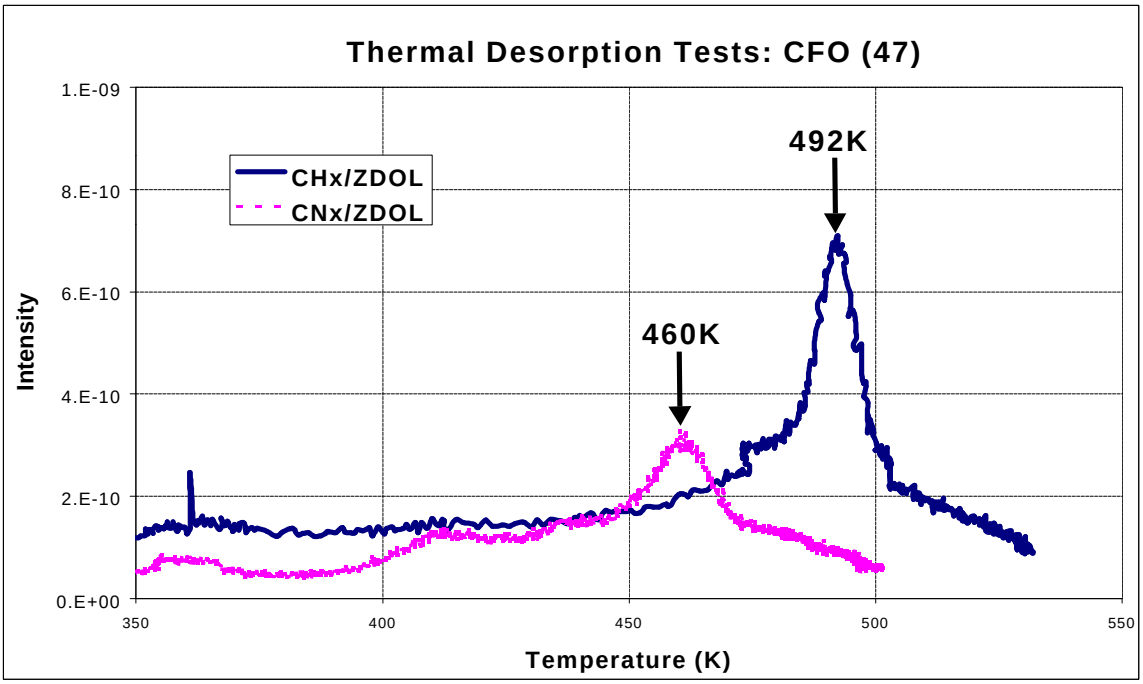

Figure 5.3 The thermal desorption profile of ZDOL fragment CFO (47) from both CHx and CNx coated disks in UHV.

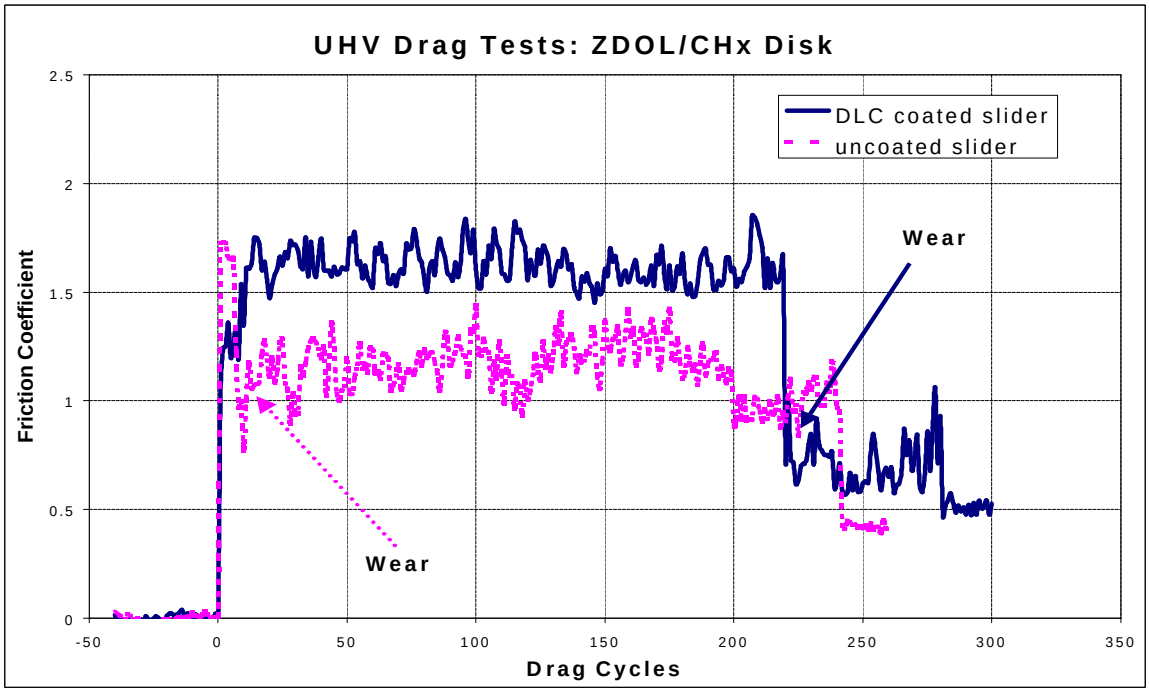

Figure 5.4 The friction coefficient curves of ZDOL lubricated CHx disks on uncoated Al_2O_3/TiC slider and carbon coated slider.

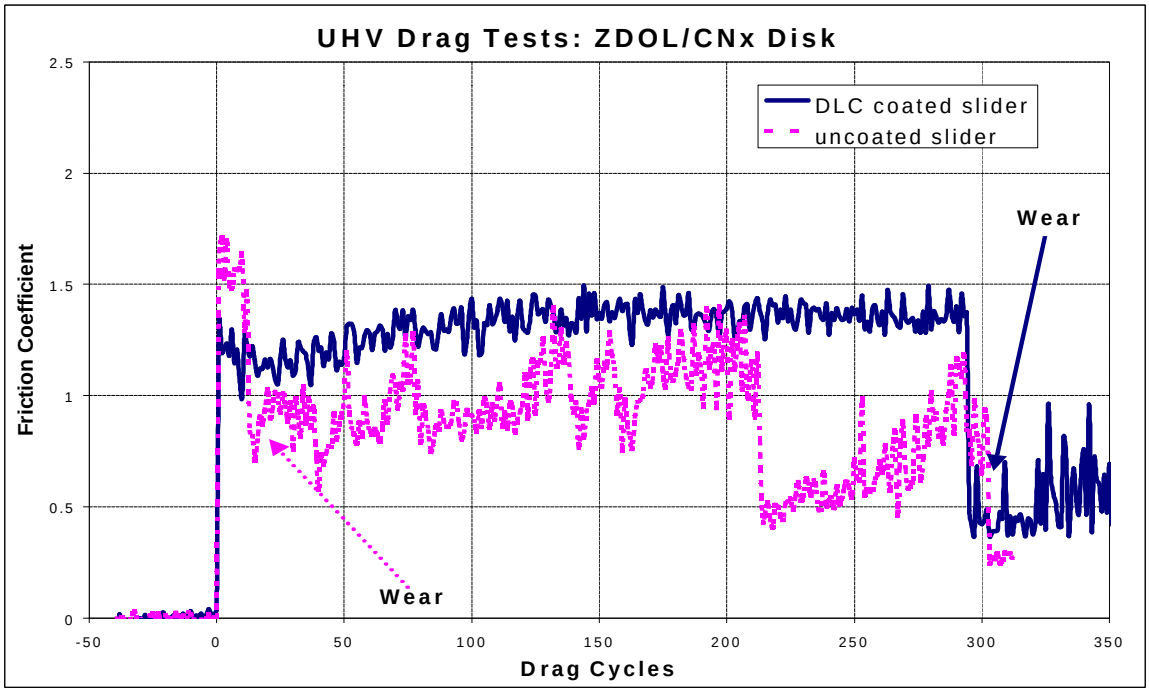

Figure 5.5 The friction coefficient curves of ZDOL lubricated CNx disks on uncoated Al_2O_3/TiC slider and carbon coated slider.

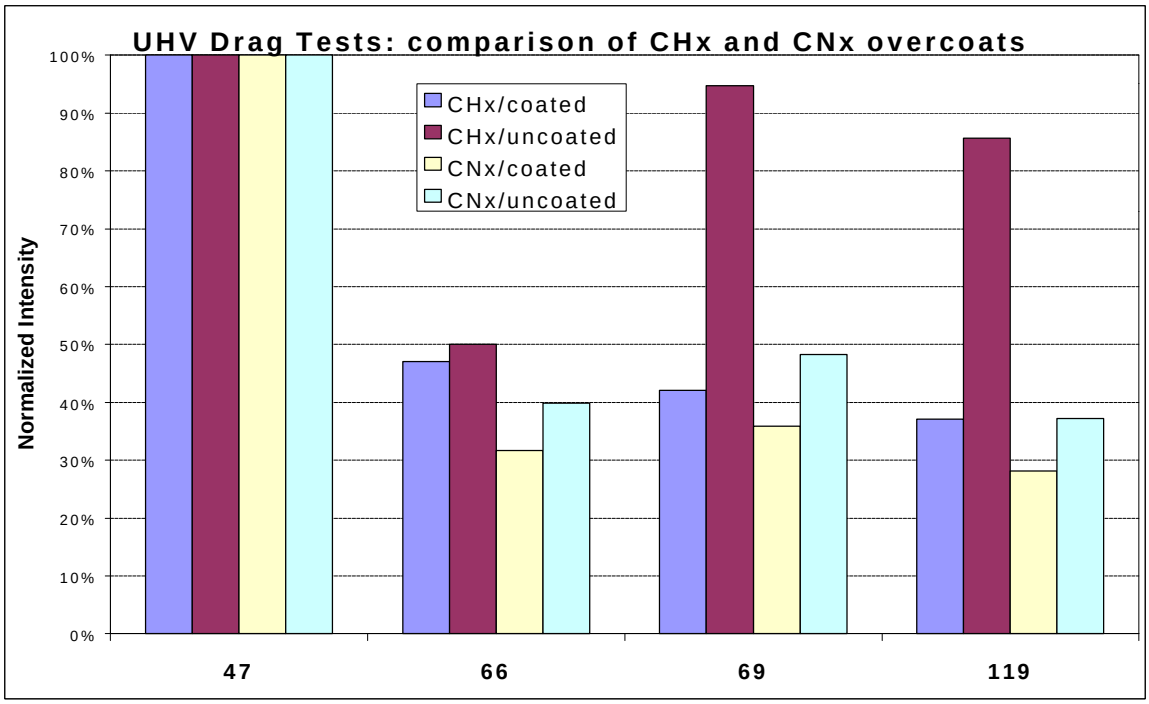

Figure 5.6 The normalized mass spectrum of four major ZDOL decomposition products generated at the ZDOL/CHx and ZDOL/CNx disk interface during UHV drag tests.

Chapter 6

EFFECT OF BACKBONE AND ENDGROUP ON THE LUBE DECOMPOSITION MECHANISMS

6.1 Introduction

In Chap 3~5, we study the decomposition mechanisms and thermal stability of PFPE lubricants during contact sliding at the head-disk interface. We observed that catalytic reactions occur at the endgroup functionals in the presence of an Al_2O_3 surface, where the fluorine atom transfer is from the endgroup to the internal sector [53]. In this chapter, we study the backbone and endgroup effect on the catalytic reactions of PFPE lubricant. The studies demonstrate that the catalytic degradation process of ZDOL in the presence of Lewis acid occurs most readily at acetal units (-O-CF_2-O) within the internal backbones (CF_2O and CF_2CF_2O) instead of the endgroup functionals. Thus, Demnum, with no acetal units, performs less catalytic degradation with the uncoated Al_2O_3/TiC sliders as compared to ZDOL.

6.2 Experimental Procedure and Set-up

Drag tests in the tribochamber were conducted with the following parameters: 0.2 m/s drag speed, a load of 25 mN, and a sliding time of 20 minutes. The sliders were 30% (1.2mm by 1mm) negative-pressure Al_2O_3/TiC sliders with and without amorphous carbon

∗ Material from this chapter are ready for submission [52].

films on the air bearing surfaces. The disks were commercial 95mm thin film disks with a 105Å amorphous carbon overcoat. The disks were lubricated by a dipping process. The resulting thickness of lubricant on the disks in this study was 12Å. Three different PFPE lubricants were tested: ZDOL, Demnum SA, and AM. The representation formulas of such PFPE's are given in Appendix I.

Fomblin ZDOL is synthesized by photo-oxidation of hexafluoropropylene, and consists of linear and random copolymers of two backbones: perfluoromethylene oxide (C_1) and perfluoroethylene oxide (C_2) [54]. Both C_1 and C_2 backbones have acetal units (-O-CF_2-O). In addition, ZDOL has two active OH endgroups on each chain end. Demnum is made similarly but starts with 2,2,3,3-tetrafluoro-oxetane; the hydrogen atoms in the resulting polymers are replaced by fluorine atoms by subsequent contact with F_2 [55]. There are no acetal units within Demnum's chemical structure. Demnum SA has only one active OH endgroup and the other is a non-active CF_3 endgroup. AM has the same backbones (C_1 and C_2) as ZDOL. However, AM has two piperonyl endgroups (-CH_2-phenyl=O_2=CH_2) which are not as active as the OH endgroup. The molecular weights of the polydisperse lubricants in our study are 4200, 5500, and 3001, respectively.

6.3 Results and Discussions

Figure 6.1 shows the friction coefficient curves for the 12Å ZDOL 4200 lubricated hydrogenated carbon overcoated (CH_X) disks. For the 70Å DLC-coated Al_2O_3/TiC slider, the friction coefficient started at 0.9 and increased steadily to 1.3 within 650 drag cycles. No wear track was observed after 650 drag cycles. For the uncoated Al_2O_3/TiC slider, the friction coefficient increased to a peak value of 6 immediately and dropped to 0.3 after

reaching its peak value. A wear track was observed on the disk just after the friction coefficient dropped. The above results indicate that 12Å ZDOL 4200 has good lubricating action against the 70Å DLC-coated Al_2O_3/TiC sliders, but little lubricating action against uncoated Al_2O_3/TiC sliders. Figures 6.2 and 6.3 show the friction coefficient curves for the 12Å Demnum SA 5500 and AM 3001 lubricants**,** respectively.

Figure 6.4 shows the integrated mass spectra of the degradation fragments produced at the head-disk interface. The four primary peaks are from the mass fragments CFO (47), CF_2O (66), CF_3 (69), and C_2F_5 (119). In our previous studies of CHx carbon overcoats paired with carbon-coated sliders [40], the primary decomposition mechanism of PFPEs was due to frictional effects, and it was characterized by the generation of CFO (47), and CF_2O (66). The absence of a carbon-coating led to a more complex catalytic decomposition mechanism of PFPEs, and it was characterized by the generation of CF_3 (69) and C_2F_5 (119).

In Fig. 6.4 (a) for the DLC coated slider case, more of the AM lubricant was decomposed than ZDOL or Demnum under the same UHV drag condition. One possible explanation is that, without any active OH endgroup bonded strongly to the carbon overcoats, the AM lube experiences a much faster removal rate than ZDOL (two active OH endgroups) or Demnum SA (one active OH endgroup) during the contact sliding. The active OH endgroups of ZDOL or Demnum SA “attach” themselves to active sites on the carbon surface and mitigate the “spin-off” rate during the drag tests. These results indicate that a good lubricant should have at least one very active OH endgroup that provides enough adsorption energy with the disk carbon surface.

The decomposition mechanisms of PFPEs in the case of the uncoated Al_2O_3/TiC slider are much more complicated than those with the DLC coated slider. For the uncoated

slider, catalytic reactions control the PFPE decomposition and the catalytic reactions lead to the generation of masses 69 (CF_3) and 119 (C_2F_5). In Fig. 6.4 (b) for the uncoated slider, the degradation intensities of the catalytic associated fragments CF_3 and C_2F_5 of the ZDOL lube are much greater than those for the Demnum SA or AM lubes. In our previous paper [53] we observed that the catalytic reactions occur at the OH endgroup functionals, where the fluorine atom transfer is from the OH endgroup to the internal sector in the presence of an Al_2O_3 surface. These results indicate that with a non-active endgroup that acts loosely with the Al_2O_3 surface of the uncoated slider, Demnum SA experiences a much reduced rate of catalytic decomposition - the non-active CF_3 endgroup of the Demnum SA prevents the catalytic decomposition. Li et al. [56] also observed that the presence of Lewis acids sites and reactive OH species are both necessary for the catalytic decomposition of PFPE lubricants. It is believed that the role of the active OH endgroup is to “anchor” the PFPE molecules to the Al_2O_3 surface for further decomposition.

However, according to Kasai [57, 58], less catalytic degradation in the presence of the Al_2O_3 surface (Lewis acid) in Demnum is due to the effect of the acetal units. He found that the catalytic degradation of ZDOL occurs most readily at the acetal units within the internal backbones with the following intramolecular disproportionation reaction:

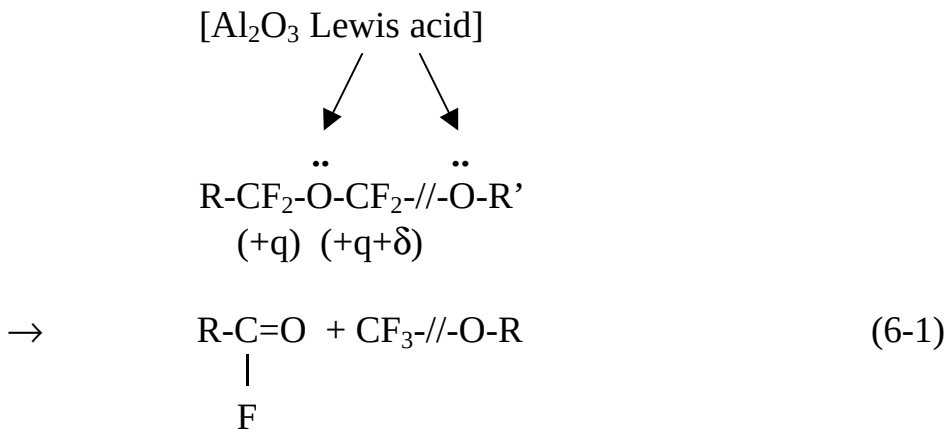

(6-1)

The reaction (6-1) occurs when differential charges are induced on the two carbon atoms of an ether linkage by the simultaneous interaction of two successive ether oxygens with Lewis acid sites present at the Al_2O_3 surface [59, 60]. The susceptibility of the various PFPE to this reaction is hence determined by the disposition of the two oxygens flanking the monomer unit, and the net atomic charges of the carbons involved in the fluorine transfer. Therefore, ZDOL performs more catalytic degradation with the uncoated Al_2O_3/TiC sliders than Demnum. The greater vulnerability of ZDOL toward catalytic degradation is due to the presence of acetal units, -O-CF_2-O-, in the polymeric chains. More information about this mechanism could be found in Kasai [60].

Figure 6.5 shows the wear durability of these disks lubricated with different lubricants. For the DLC coated slider case AM has a poor wear durability, since AM has a faster removal rate because of its very weak adsorption with the disk carbon surface. However, both ZDOL and Demnum SA pass 700 drag cycles without wear. For the uncoated slider case, only Demunm SA shows very good wear durability. Again, the non-

acetal backbones and the non-active endgroup of Demnum SA prevents the catalytic decomposition in the presence of the Al_2O_3 surface, resulting in a much better wear performance than ZDOL.

Figure 6.6 shows the weight loss observed on the Z-lube and D-lube when heated in contact with Al_2O_3 (1 wt. %) at 200^{o}C. In the actual experiment the degradation was induced by placing a given amount (5 g) of lubricant and 1 wt. % of Al_2O_3 in a test lube, and immersing the tube in an oil bath maintained at a desired temperature (200^{o}C). For each lubricant, the weight loss was measured after the heat treatment for a given period of time, and the remaining fluid was analyzed by F-19 NMR. In Fig. 6.6, the weight loss of D-lube is only 0.4% after four hours heating at 200^{o}C, however, the weight loss of Z-lube is 96% after 2 hours heating at the same temperature. These results further support our data from the UHV drag tests that ZDOL lube experiences a much stronger catalytic decomposition than Demnum lube in the presence of the Al_2O_3 surface.

However, Demnum performs very poorly during CSS tests due to its high viscosity. Waltman et al. [61] used quantum chemical modeling calculations to understand how the –CF_2O- (C_1) and -CF_2CF_2O- (C_2) structural units in the ZDOL backbone can influence the bonding kinetics. They observed that the barrier for internal rotation about the C-O bonds in ZDOL will be significantly smaller than those rotation about the C-C bonds. Also, rotations about the C-O bond in the –CF_2O- (C_1) units are more facile than either rotations about the C-C or C-O bonds in the -CF_2CF_2O- (C_2) units, increasing the C_1/C_2 ratio in the ZDOL backbone will increase the relative flexibility of the ZDOL polymer. The rotations about either the C-O or C-C bonds in the Demnum -$CF_2CF_2CF_2O$- units are even more difficult

than those within ZDOL's backbones. Therefore, Demnum's mobility is poor as compared to ZDOL, resulting in the higher viscosity and higher stiction in CSS tests.

6.4 Conclusions

The UHV drag tests show that a good lubricant should have one active endgroup and one non-active endgroup. The active one helps lubricants to be adsorbed very well onto the carbon surface and reduce the removal rate of the lubricants during the contact sliding. In the other hand, the non-active one prevents the catalytic decomposition in the presence of the Al_2O_3 surface of the uncoated slider.

The studies also demonstrate that the catalytic degradation process of ZDOL in the presence of Lewis acid occurs most readily at the acetal units (-O-CF_2-O) within the internal backbones (CF_2O and CF_2CF_2O) instead of the endgroup functionals. Therefore, Demnum, without any acetal units, performs less catalytic degradation with the uncoated Al_2O_3/TiC sliders as compared to ZDOL. However, Demnum performs high stiction during CSS tests due to their higher intrinsic viscosity.

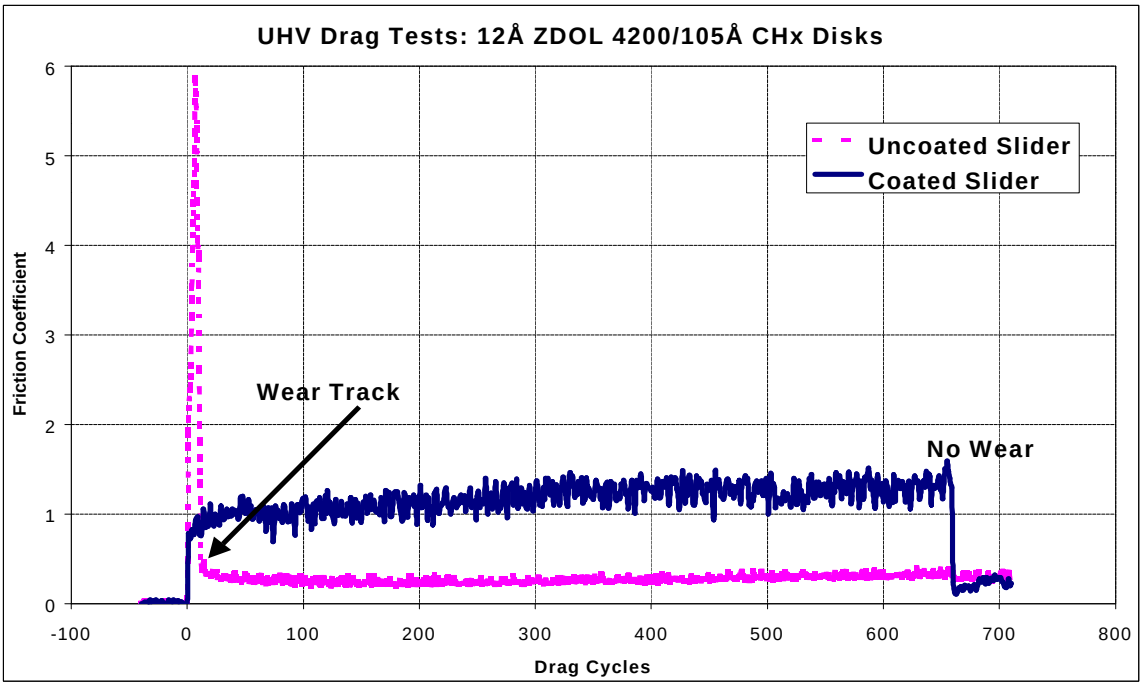

Figure 6.1 Friction coefficient of UHV drag test on 12Å ZDOL 4200 lubricated CHx disk.

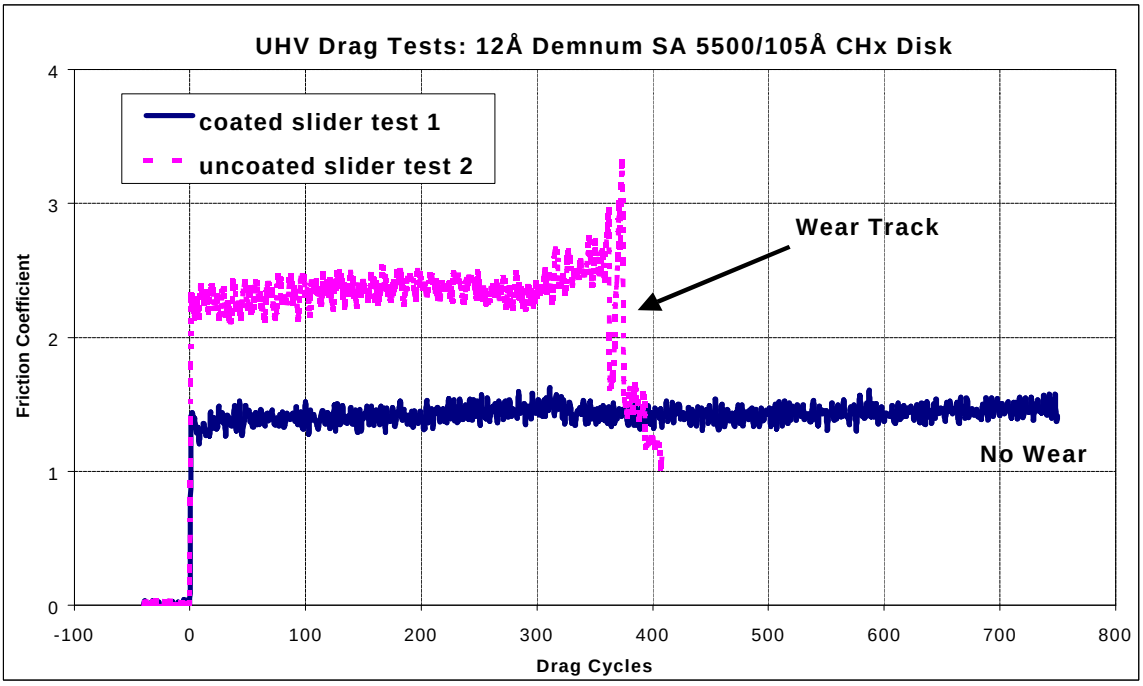

Figure 6.2 Friction coefficient of UHV drag tests on 12Å Demnum SA 5500 lubricated CHx disk.

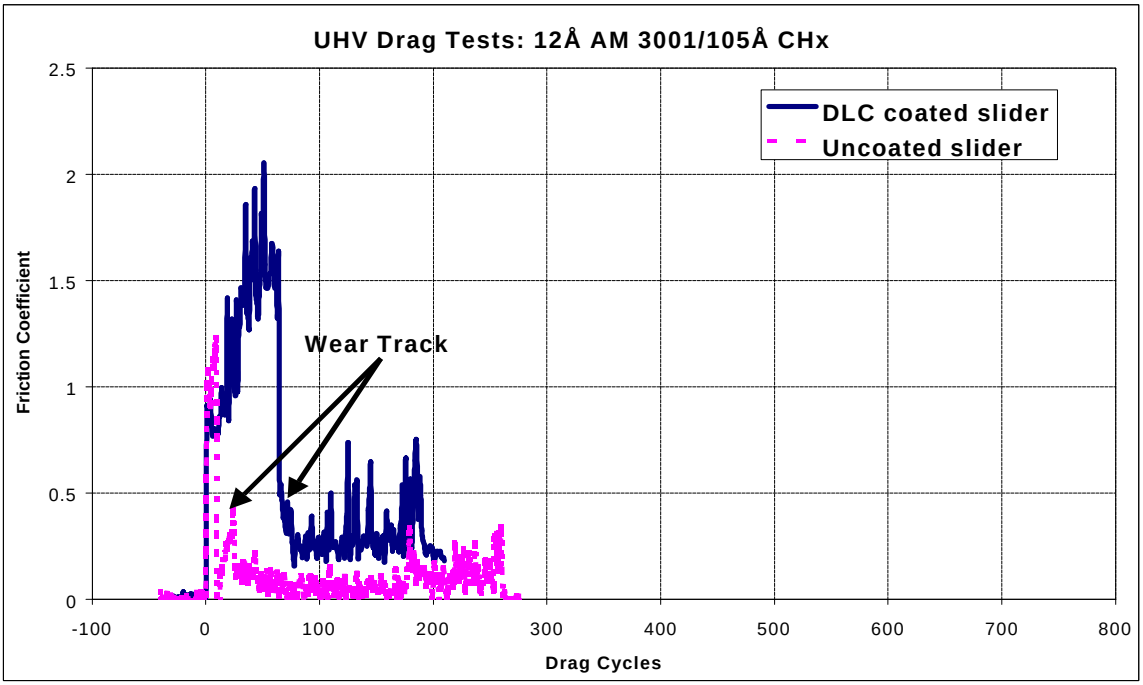

Figure 6.3 Friction coefficient of UHV drag test on 12Å AM 3001 lubricated CHx disk

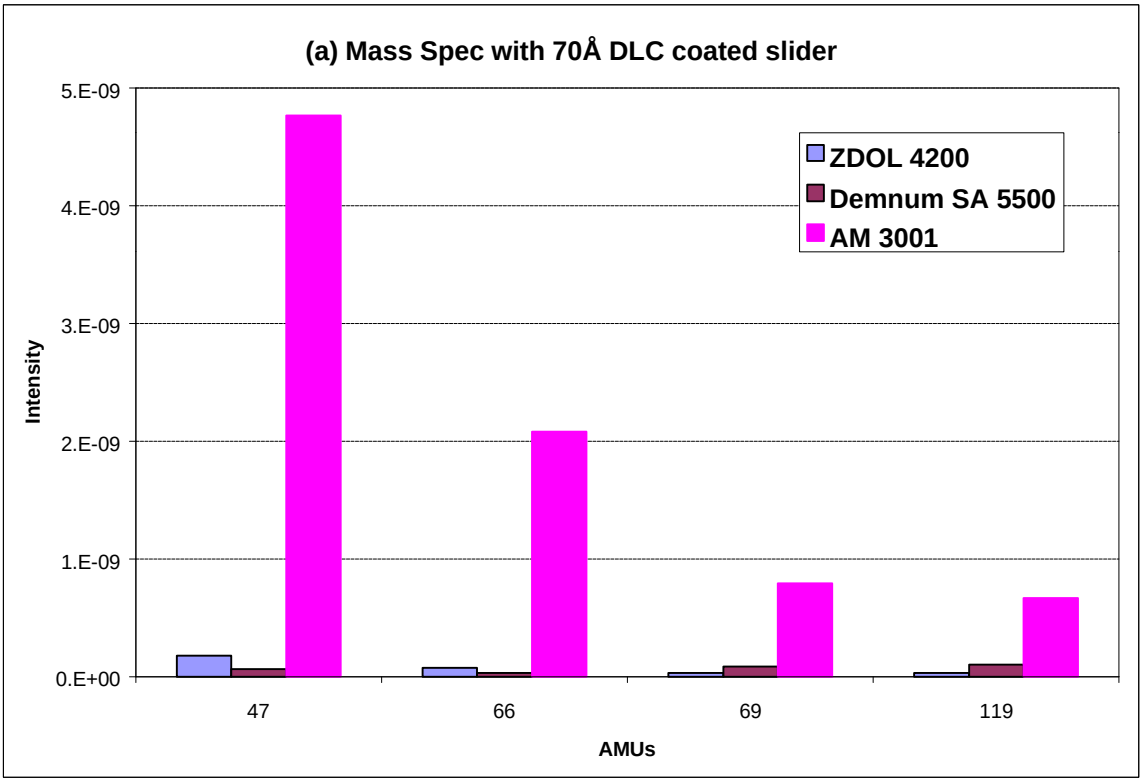

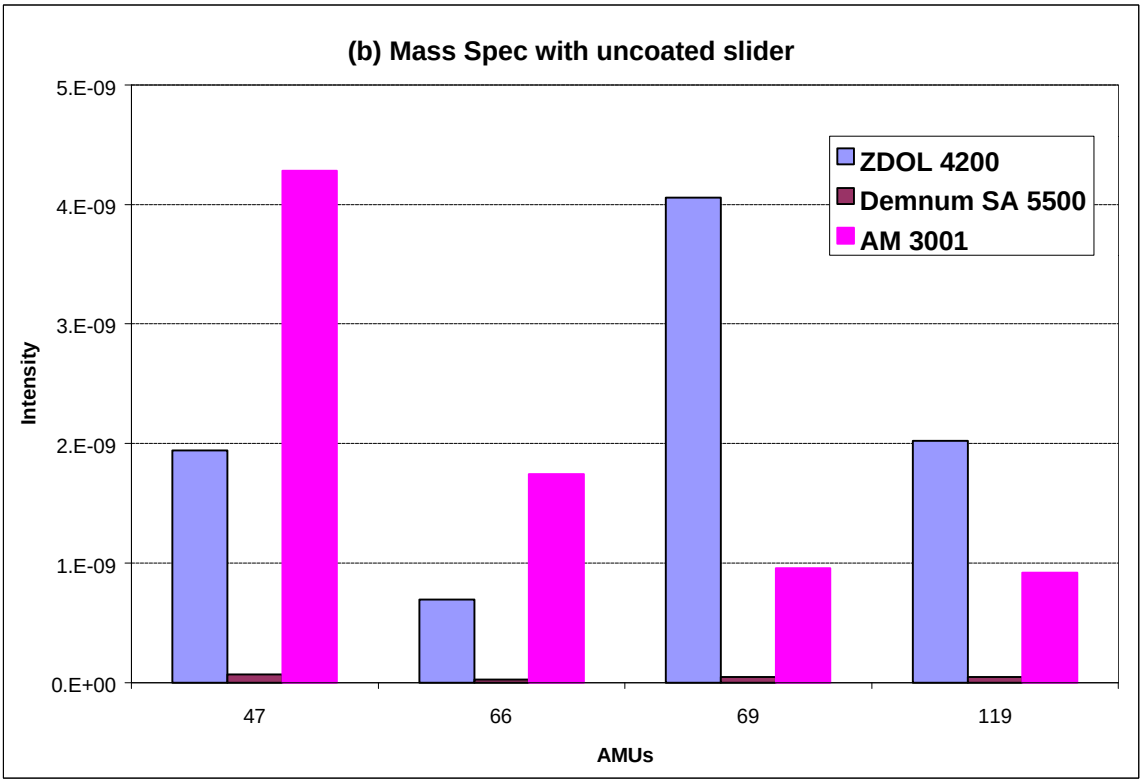

Figure 6.4 Integrated degradation intensities of four major AM fragments during UHV drag tests on CHx disks lubricated with different lubricants: (a) with DLC coated slider; (b) with uncoated slider.

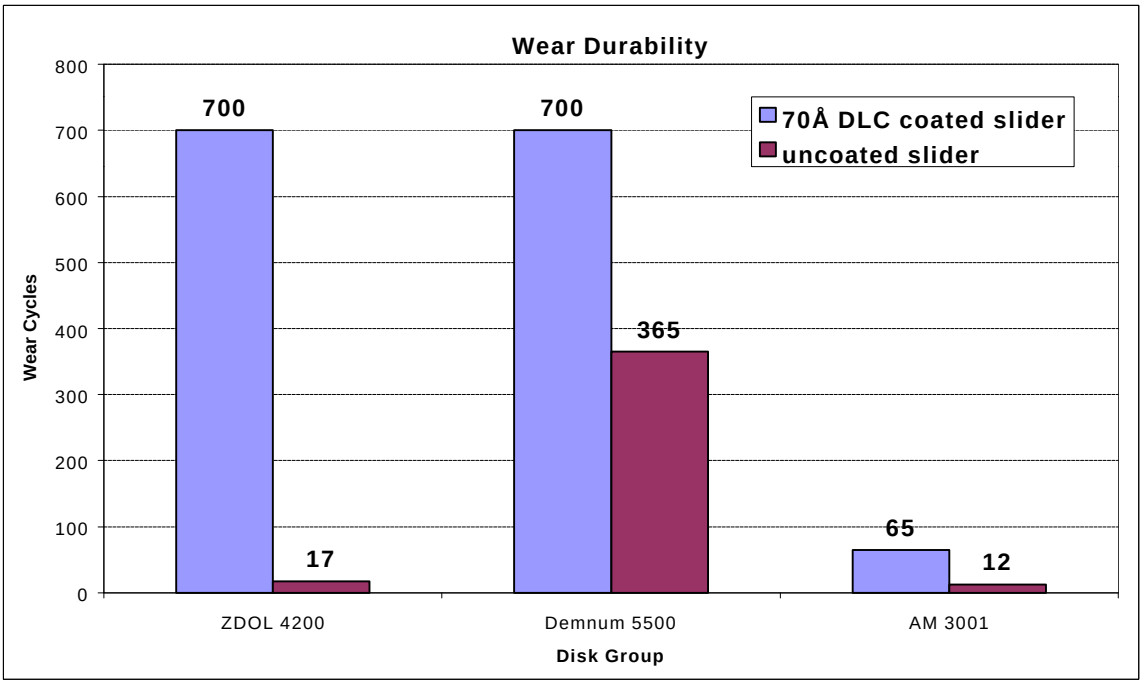

Figure 6.5 Wear durability of CHx disks lubricated with different lubricants during UHV drag tests.

Figure 6.6 Weight loss observed on PFPE's when heated in contact with Al_2O_3 (1 wt. %) at 200^{o}C. (reproduced from Kasai, 1999, with permission).

Chapter 7

EFFECT OF THE ADDITIVE X-1P INTO PFPE LUBRICANTS

7.1 Introduction

X-1P, a cyclic phosphazene lubricant, is a new non-polymer lubricant being developed for the disk drive industry [63]. X-1P compounds possess excellent lubricity with optimal reduction in friction and wear achieved when a combination of CF_3 and F substitution is employed. Consideration of pour point, oxidative stability, and lubricity data, as well as economical factors, led to X-1P, a derivative containing four meta-CF_3 and two para-F substituents, as the leading fluid candidate. Much of the early work with X-1P involved its use as a pure fluid coated by dip or gravity/drain coating processes, resulting in a thickness less than 1 nm. The advantage of X-1P in lubricant applications is its low vapor pressure, high thermal stability, and good solubility in non-CFC (chlorofluorocarbon) solvents. X-1P was found to perform well on hard disks during contact start/stop (CSS) and stiction testing with a lubricant thickness of about 0.5 nm [64, 65]. During CSS tests, the friction coefficient increases substantially more for perfluorinated disks than for phosphazene disks. In addition, friction decreases with an increase of relative humidity from 40% to 80%. These results indicate that X-1P lubricant interacts with water from the environment, resulting in a lower surface energy and a lower viscosity/friction.

Material from this chapter is submitted to Intermag conference, 2000 [62].

Perettie et al. [66] also observed that X-1P significantly outperforms ZDOL in CSS testing under hot/wet (30^{o}C/ 80 RH) conditions. One possible explanation for these results is ZDOL decomposition, specifically its lack of stability in the presence of Lewis acid surfaces such as Al_2O_3. It is speculated that X-1P maintains its structural integrity because of lower tribochemical reactivity with the surface.

However, the high viscosity of X-1P is an important issue in ambient conditions, which induces an initial transfer of the lube to the head during the initial increase in the stiction/friction [65]. Thus, it is very important to coat X-1P at less than 6Å if it is used as a single lubricant. The viscosity of X-1P is much higher than that of the AM or ZDOL lubricants at room temperature. To achieve a viscosity for the phosphazene lubricant system corresponding to the viscosity of AM or ZDOL, it may be necessary to mix the X-1P lubricant with these low viscosity PFPE lubricants. This essentially eliminates the need for the ultra thin layer required for X-1P to be used as a single lubricant but enhances the performance of the head-disk interface. There are two issues to be addressed here: (1) does X-1P perform as well in a mixture as it does "neat" and is the lubricating mechanism the same for both, and (2) when used with PFPEs, does X-1P help the performance and why?

In this chapter we study the effect of adding X-1P in PFPE lubricant using an ultra-high vacuum (UHV) tribochamber equipped with a mass spectrometer. The studies consist of drag tests in the UHV tribochamber. The optical surface analyzer (OSA) is also used to observe the lube migration behavior. We observe that X-1P passivates the head and prevents catalytic reaction of the PFPE when used as an additive. In addition, X-1P also increases the PEPE's mobility and, hence, improves the tribological performance at the head-disk interface because a faster lubricant reflow rate into the test track.

7.2 EXPERIMENTAL PROCEDURE AND SET-UP

Drag tests were conducted were initiated with the following parameters: 0.2 m/s drag speed, a load of 25 mN, and a sliding time of 20 minutes. The sliders were 30% (1.2mm by 1mm) negative-pressure Al_2O_3/TiC sliders with and without amorphous diamond like carbon (DLC) films on the air bearing surfaces. The disks were commercial 95mm super smooth thin film disks. The disks were lubricated with ZDOL or AM by a dipping process. We used FTIR to measure the lubricant thickness of these disks before the UHV drag tests. These FTIR thickness measurements were confirmed by ellipsometry and X-ray reflectivity spectroscopy. The resulting thickness of PFPE on the disks in this study was 12Å.

The optical surface analysis (OSA) system was also used to observe the lube migration behavior. The OSA is an *in situ* device, which has approximately 5 micron resolution and 2 MHz of bandwidth [9]. This device can be used to measure less than one Angstrom of carbon wear or lubricant depletion/accumulation. More information about the OSA system has been shown in chapter 2.

7.3Results and Discussions

7.3.1 Results from the AM3001/CNx samples

In this section, we present the results from the UHV drag tests and OSA measurements of the AM3001/CNx samples. The disks were commercial 95mm very smooth thin film disks with a 105Å amorphous nitrogenated carbon overcoat (CNx). The nitrogen content in the CNx film was 14 atomic percent. The disks were lubricated with 12Å AM3001 with different X-1P additive percents. AM and X-1P lubricant are mutually

soluble in CF (chlorofluorocarbon) solvents because they both have the aromatic units in their chemical structure. The chemical formulas of AM3001 and X-1P are given in Appendix I.

Figure 7.1 shows the friction coefficient curves for the 12Å AM3001 lubricated disks without any X-1P additive. For the 70Å DLC-coated Al_2O_3/TiC slider, the friction coefficient started at 0.9 and increased steadily to 1.7 within 65 drag cycles before wear occurred. For the uncoated Al_2O_3/TiC slider, the friction coefficient increased to a peak value of 1.3 immediately and dropped to 0.3 after reaching its peak value. A wear track was observed on the disk just after the friction coefficient dropped. The above results indicate that 12Å AM3001 has little lubricating action against both the uncoated and the DLC-coated Al_2O_3/TiC sliders. The friction coefficient curves for the 12Å AM3001 lubricated disks with two different X-1P additive percentages are similar to Fig. 7.1, and they are shown in Figs. 7.2 and 7.3.

Figure 7.4 shows the OSA data: a plot of lube migration as a function of X-1P percentage. Before the OSA measurements, lubricant was removed from a section of the disk by a solvent, HFE. This method was chosen because it was the least invasive and least likely to change the reflective properties of the carbon layer underneath the lubricant, which could affect the results. Figure 7.4(a) shows the lubricant thickness versus time. This lubricant thickness is defined as the difference between the region where the lubricant was removed and the untreated portion of the disk. The disk was scanned by S and P circularly polarized light every thirty minutes for thirteen hours. Figure 7.4(b) shows the average migration rate of AM3001 lubricant versus X-1P percent. The rate is just the linear slope of

the lubricant thickness versus time in Fig. 7.4(a). We observed that the lube mobility of AM3001 increases with increasing X-1P percent.

Figure 7.5 shows the wear durability of these CNx disks as a function of X-1P percentage. For both the 70Å DLC coated and uncoated Al_2O_3/TiC sliders, the wear durability improved when the X-1P additive percentage increased. These results demonstrate the benefits of using X-1P additive to increase the mobility of AM3001 lubricant - more material reflowed into the wear track to protect the carbon overcoat surface for a longer duration against sliding. We believed that X-1P molecules preferably occupied the bonding sites on the carbon surface. Therefore, less ZDOL molecules could be bonded to the carbon surface resulting in the faster mobility. Mate [67] reported that X-1P proved to be an underlayer of PFPE (ZDOL) by ESCA measurements, resulting in a faster lube recovery. This may be the reason that X-1P has been shown to be so effective as a lubricant additive in providing excellent wear and corrosion protection during operation.

Figure 7.6 shows the integrated mass spectra of AM3001 fragments produced at the head-disk interface. The four primary peaks are from mass fragments CFO (47), CF_2O (66), CF_3 (69), and C_2F_5 (119). The degradation intensities of four major AM3001 fragments during UHV drag tests on CNx disks with different percentages of X-1P. The degradation intensities of the major AM3001 fragments increased as the X-1P percent increased for both the uncoated and coated slider cases. We believe the role of the mobile AM3001 layer is to replenish the lube displaced during dragging. With a larger X-1P percent more AM lubricant reflows into the test track due to its faster migration rate. Thus, more material is decomposed, resulting in the stronger degradation intensity as shown in Fig. 7.5.

7.3.2 Results from the ZDOL2000/CHx samples

In this section, we present the results from the UHV drag tests of the ZDOL2000/CHx samples. The disks were commercial 95mm very smooth thin film disks with a 105Å amorphous hydrogenated carbon overcoat (CHx). The hydrogen content in the CHx film was 30 atomic percent. The disks were lubricated with 12Å ZDOL by a dipping process with/without 6% X-1P additive. X-1P and ZDOL are mutually insoluble, requiring tight processing controls to optimize performance.

Figure 7.7 shows the wear durability of these CHx disks as a function of X-1P additive percentage. For both the DLC coated and uncoated sliders, the wear durability was significantly improved by adding X-1P into ZDOL. The enhanced wear durability may be attributed to two mechanisms: (1) X-1P improves PFPE's mobility as described in section A; (2) X-1P passivates the catalytic decomposition of PFPE. We will address the second mechanism here. Figure 9 shows the degradation intensities of four major ZDOL fragments during UHV drag tests of CHx disks with different X-1P percents. The degradation intensities of the major ZDOL fragments decreased with the addition of X-1P into ZDOL for both the uncoated and coated slider cases, most notably, the catalytic reaction associated with the uncoated slider has been prevented by using the X-1P additive. Kasai [60] also observed that X-1P passivates the catalytic activity of Al_2O_3 – the activity centers of Lewis acids Al_2O_3 are passivated by the nucleophilic (Lewis base) attack of the X-1P phosphazene ring. The usefulness of X-1P as an additive results from its ability to cover the catalytically active Al_2O_3 surface on the slider, thus preventing the disproportionation reaction [68].

Waltman et al. [69] also used a computer code to identify the reactive sites on the X-1P molecule. Their theoretical studies indicate that the strongest binding between X-1P

and AlF_3 occurs with the endocyclic nitrogen and aluminum. The reason for the strong bonding between AlF_3 and the ring nitrogen atom originates from the polar character of the endocyclic P-N bond, which polarizes the nitrogen atom negatively. The binding energy of the P-N bond is of the order of –55 kcal/mole. The addition of X-1P into ZDOL lubricant significantly retards the degradation of ZDOL. Since the binding energies for the perfluorinated ethers are of the order of only –10 kcal/mole, the X-1P imparts protection to ZDOL by preferentially interacting, and therefore passivating the Lewis acid sites. The selective binding is based upon the strong binding energies that develop between X-1P and AlF_3. Without the addition of X-1P into ZDOL, the intensities of the catalytic fragments CF_3 and C_2F_5 increased more than one order with uncoated Al_2O_3 sliders compared to the DLC coated sliders. In addition, more hydrogen evolution occurred with the CHx films as compared to the CNx films, which generates more fragments from the catalytic reactions.

7.4 Conclusion

The UHV tribochamber was used to monitor the gaseous wear products generated at the HDI during dragging. The UHV drag tests and OSA data show that the X-1P additive increases the mobility of AM3001 lubricant – more material reflowed into the wear track to protect the carbon overcoat surface for a longer duration against sliding. We believed that X-1P molecules preferably occupied the bonding sites on the carbon surface. Therefore, less ZDOL molecules could be bonded to the carbon surface resulting in the faster mobility.

In addition, the catalytic reaction associated with uncoated Al_2O_3/TiC sliders has been prevented by using X-1P as an additive in ZDOL. X-1P passivates the catalytic activity of Al_2O_3 – the activity centers (Lewis acid) of Al_2O_3 are passivated by the nucleophilic

(Lewis base) attack of the X-1P phosphazene ring. The usefulness of X-1P as an additive in ZDOL results from its ability to cover the catalytically active Al_2O_3 surface on the head, thus preventing the catalytic decomposition of ZDOL lubricants.

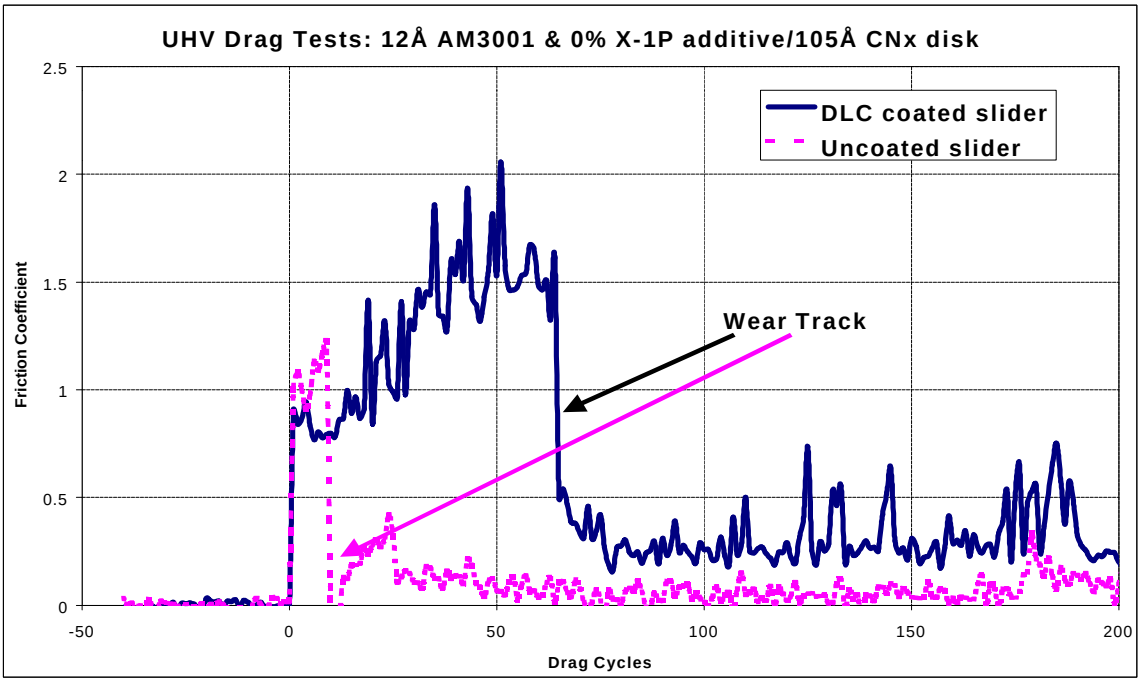

Figure 7.1 Friction coefficient of 12Å pure AM3001 lubricated CNx disk in UHV drag tests.

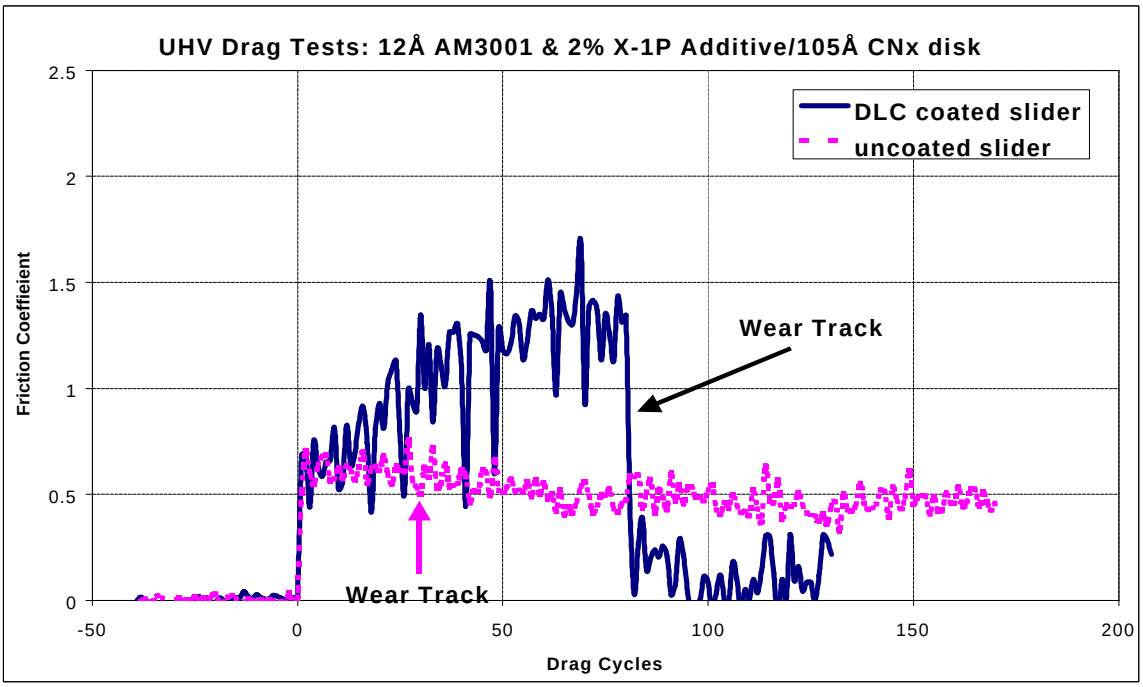

Figure 7.2 Friction coefficient of 12Å AM3001/2% X-1P lubricated CNx disk in UHV drag tests.

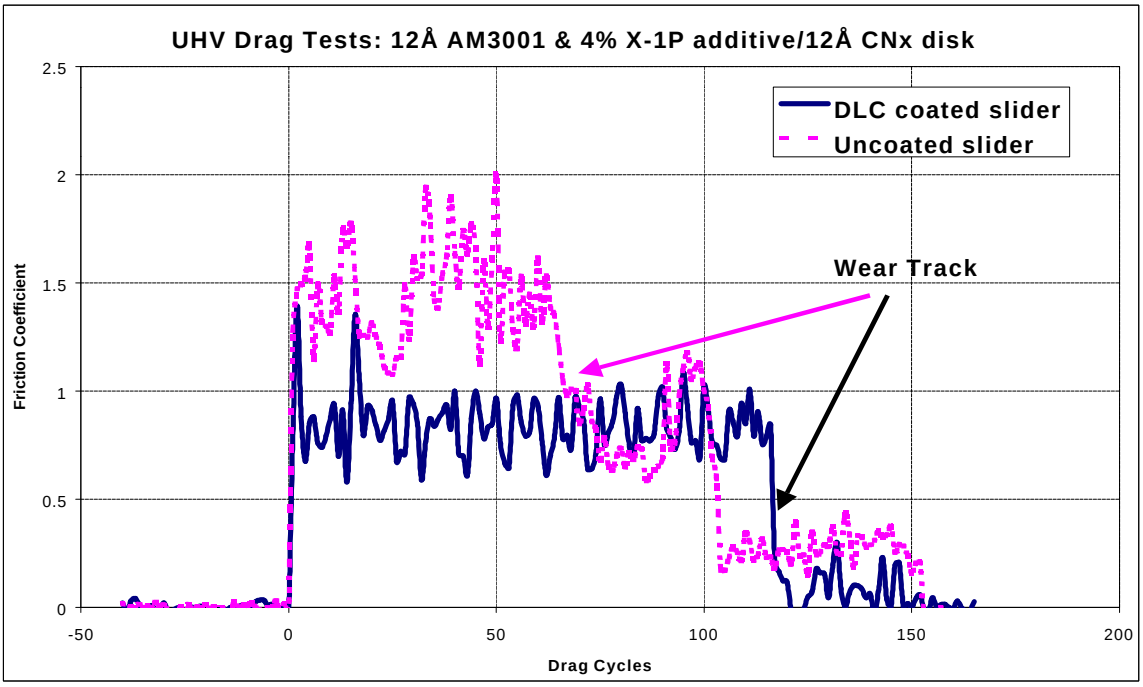

Figure 7.3 Friction coefficient of 12Å AM3001/4% X-1P lubricated CNx disk in UHV drag test.

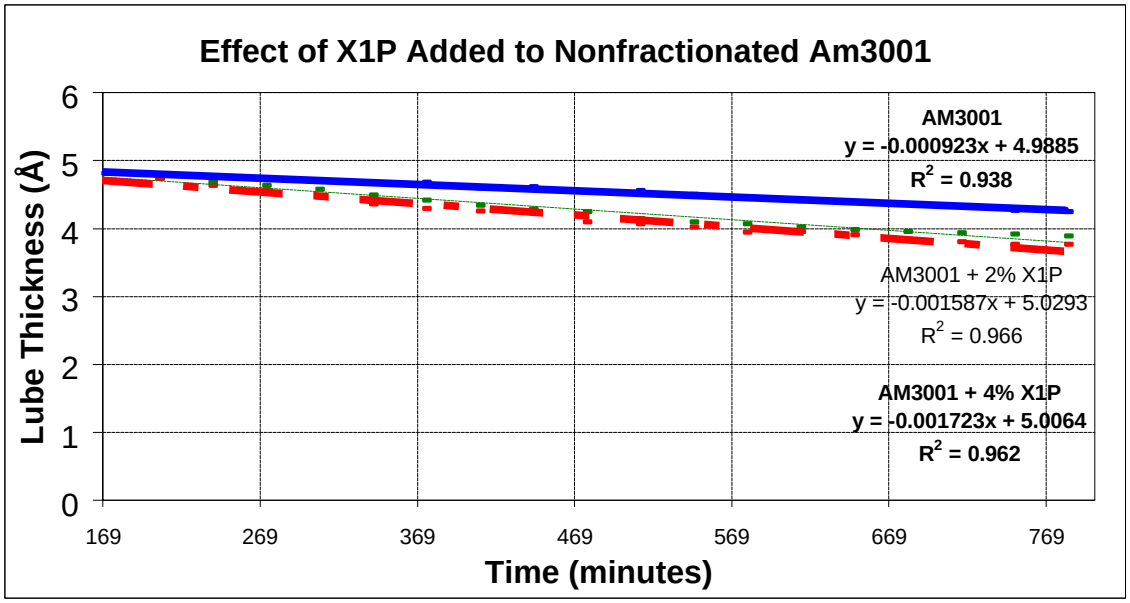

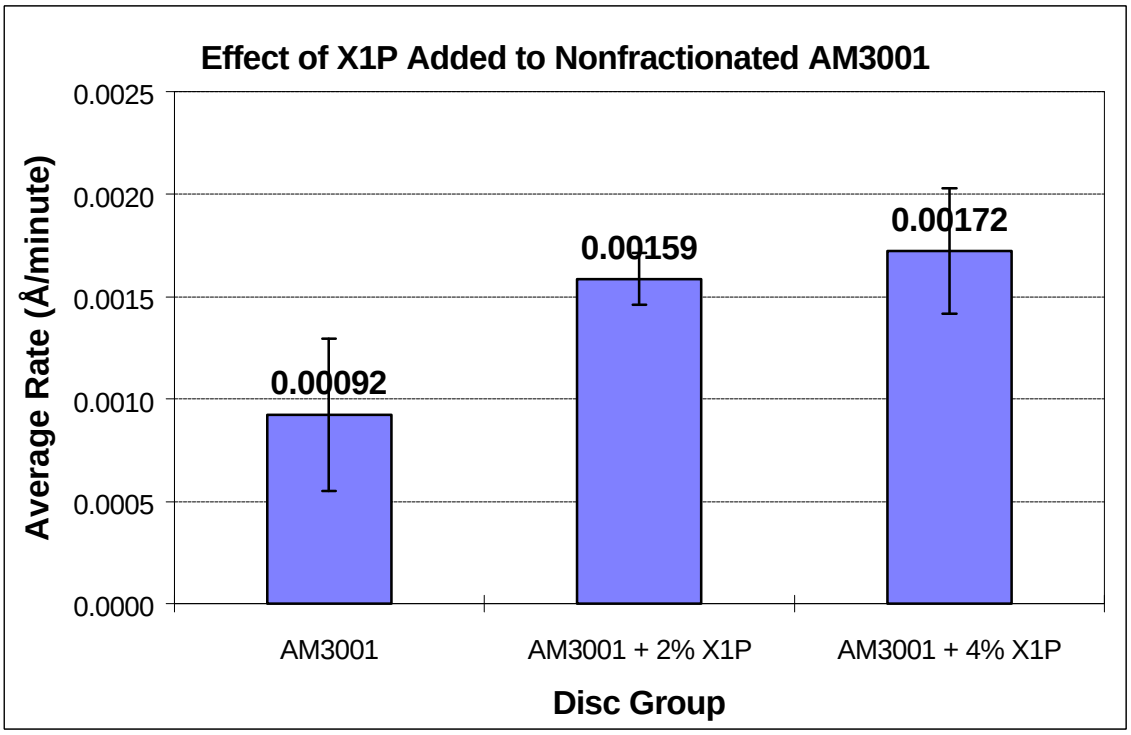

Figure 7.4 (a) lubricant thickness versus time graphs from OSA data; (b) the AM3001 lube migration rate versus X-1P additive %.

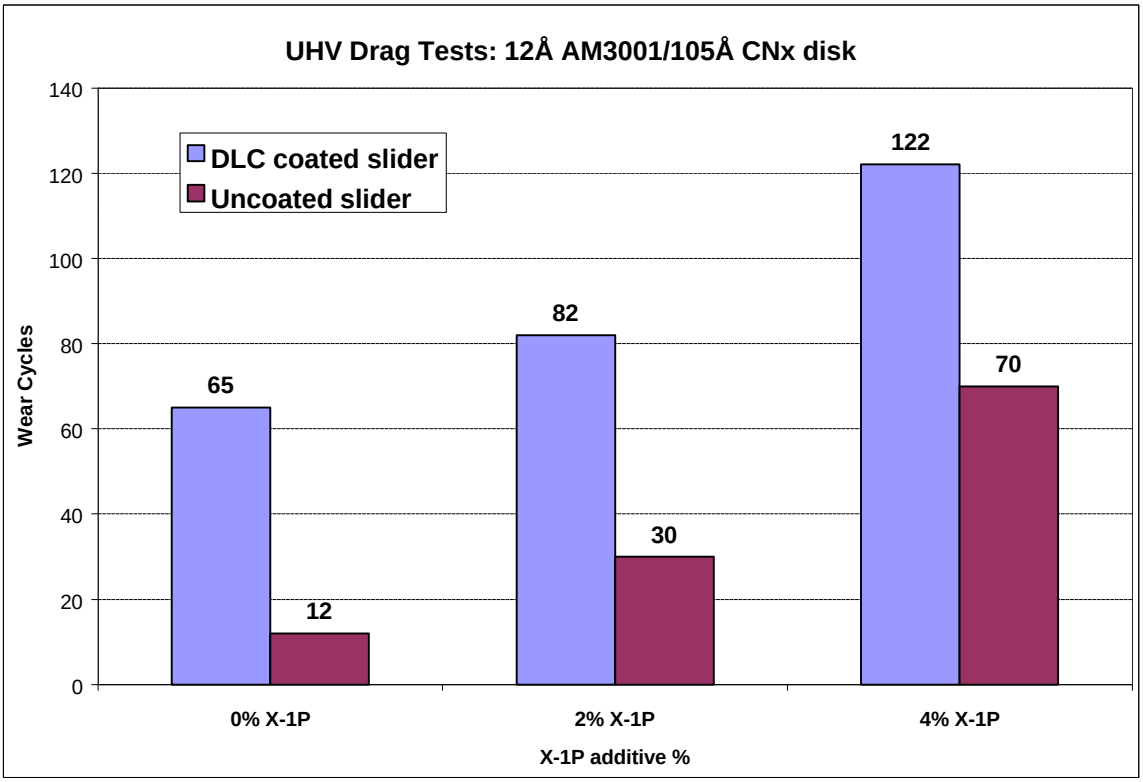

Figure 7.5 Wear durability of CNx disks with different X-1P additive % in AM3001 in UHV drag tests.

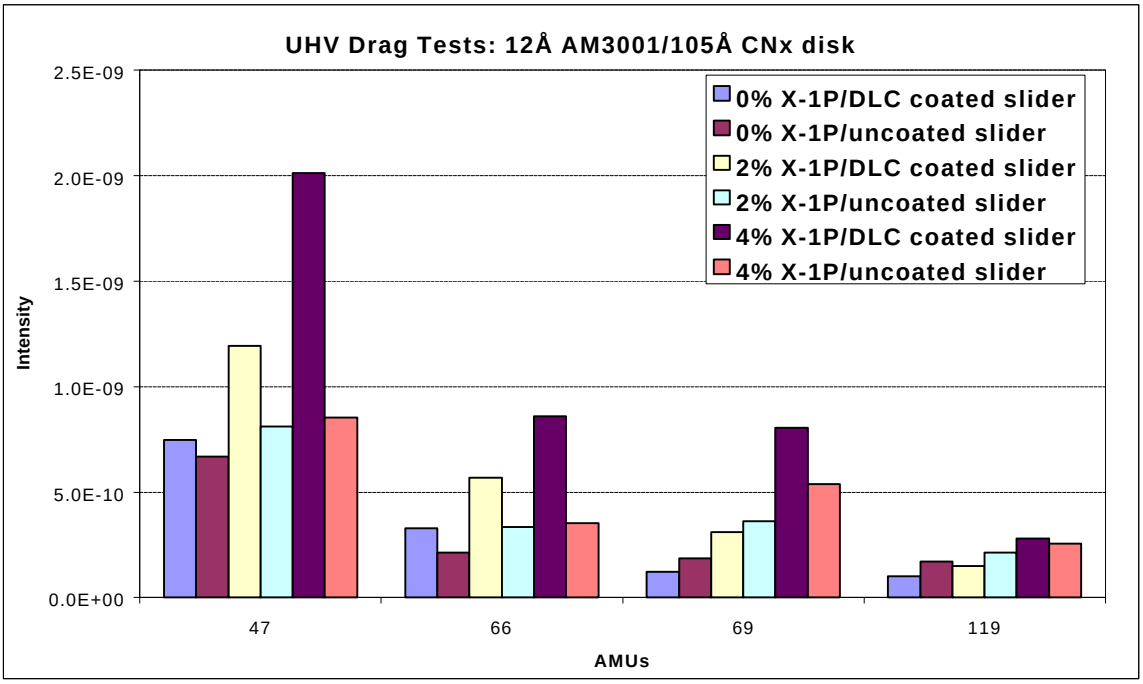

Figure 7.6 Integrated degradation intensities of four major AM fragments during UHV drag tests on CNx disks with different X-1P additive %.

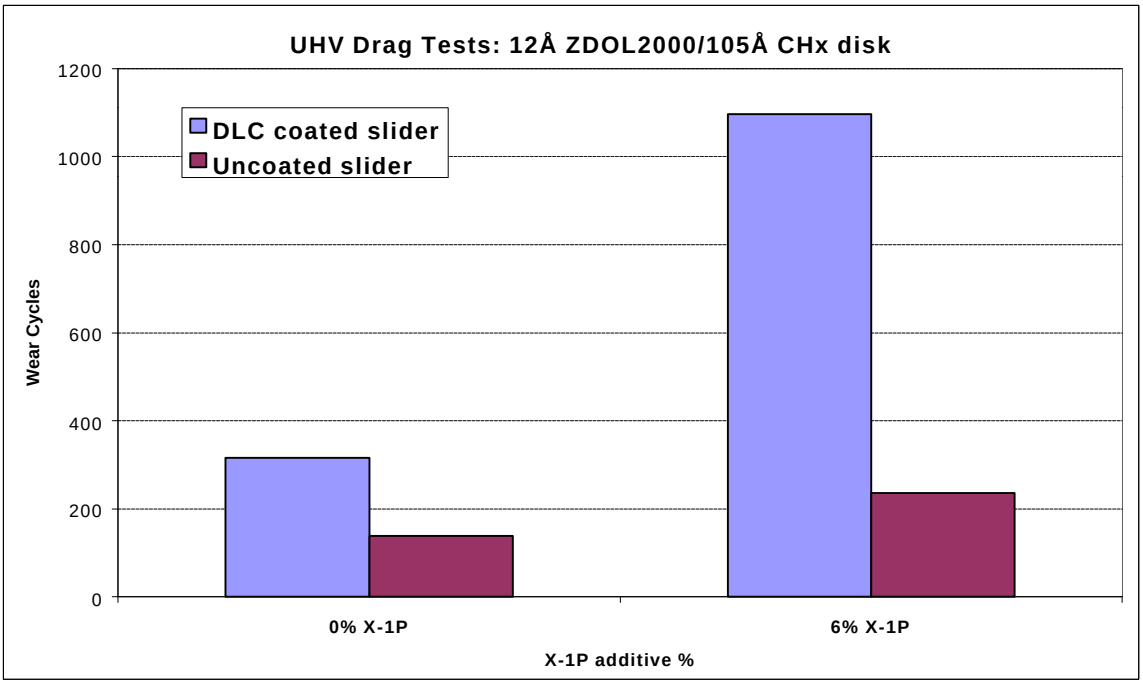

Figure 7.7 Wear durability of ZDOL/CHx disks with X-1P additive in UHV drag tests.

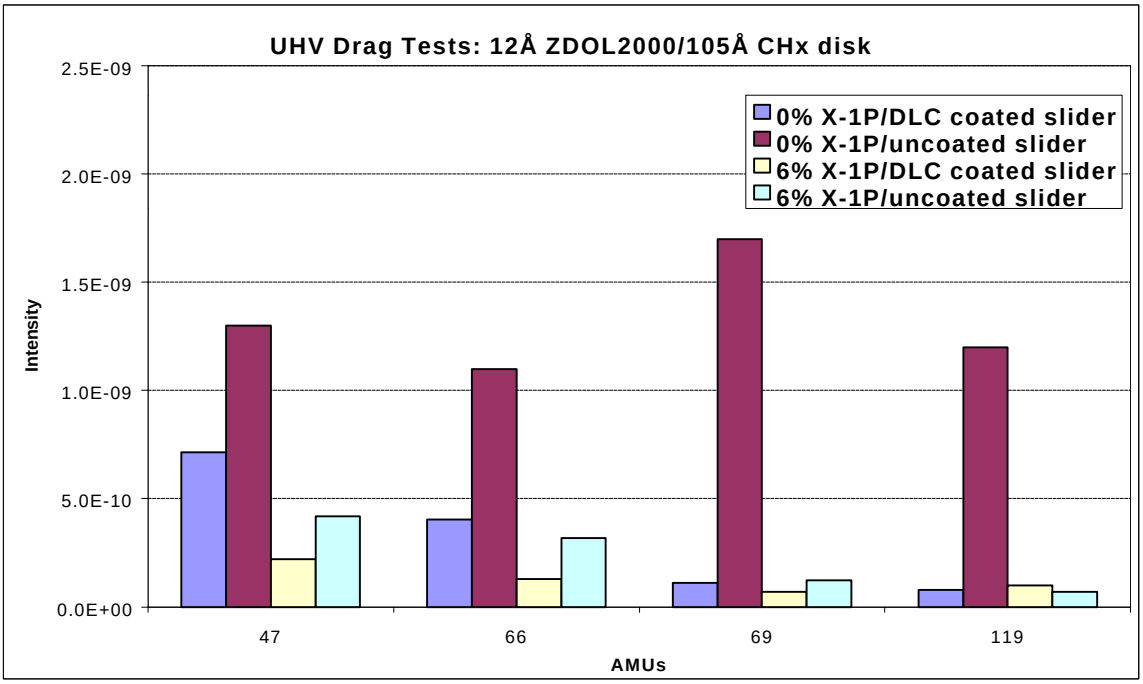

Figure 7.8 Integrated degradation intensities of four major ZDOL fragments generated during UHV drag tests of CHx disks with X-1P additive.

Chapter 8

EFFECT OF LUBRICANT MOLECULAR WEIGHT

8.1 Introduction

An effective lubricant should exhibit slow removal and loss rate, fast recovery, and minimum tribochemistry [72]. Lubricant is also lost by centrifugal flow, or spin-off, and evaporation [73]. Lower molecular weight increases the rate of recovery, and also the rate of loss through spin-off and evaporation. Hence, there is a tradeoff between lubricant loss and recovery by spreading. Waltman and Tyndall [74] showed that the activation energy for lubricant evaporation from the carbon surface increases with increasing molecular weight. They also found that the low activation energies determined for the evaporation and bonding of ZDOL 2000 are attributed to the polydispersity in the ZDOL molecular weight [75].

In this chapter, we study the ZDOL molecular weight effect on carbon films using an ultra-high vacuum (UHV) tribochamber equipped with a mass spectrometer. The studies consist of drag tests in the UHV tribochamber. We illustrate the lubricant molecular weight effect on the tribological performance. Optical surface analysis (OSA) measurements were also used to observe the spreading behavior of PFPE lubricants. The lubricant mobility decreased with increasing molecular weight. Finally, the thermogravimetric analysis (TGA) data shows that the desorption temperature of narrowly dispersed ZDOL increased with increasing molecular weight.

∗ Material from this chapter is submitted to JVST [70, 71].

8.2 Experimental Procedure and Set-up

8.2.1 UHV Drag Tests

Drag tests in the tribochamber were conducted with the following parameters: 0.2 m/s drag speed, a load of 25 mN, and a sliding time of 20 minutes. The sliders were 30% (1.2mm by 1mm) negative-pressure Al_2O_3/TiC sliders with and without amorphous carbon films on the air bearing surfaces. The disks were commercial 95mm thin film disks with a 105Å amorphous carbon overcoat. The disks were lubricated with ZDOL by a dipping process. The resulting thickness of ZDOL on the disks in this study was 24Å. The ZDOL lubricants of different molecular weight were obtained by fractionating the commercially available ZDOL. The lubricants were fractionated by the CO_2 solvent extraction method [67, 76]. Molecular weight distribution (Mw/Mn) determined by gel permeation chromatography (GPC) using a newly developed polyfluoropolyether (PEPFE) calibration curve. The table below lists the narrowly dispersed fractions of ZDOL used in this work.

Lubricant	Number-average molecular weight M_n (g/mole)	Polydispersity (M_w/M_n)
ZDOL-1	4200	1.15
ZDOL-2	7600	1.02
ZDOL-3	8500	1.07

The number-average molecular weight M_n is defined as $M_n = W/N$. Where

W = total sample weight = $\Sigma w_x = \Sigma n_x M_x$,

N = total number of moles in the sample (of all sizes) = Σn_x,

w_x = total weight of x-mer,

M_x = molecular weight of x-mer,

n_x = number of moles of x-mer.

The weight-average molecular weight M_w is defined as $M_w = \Sigma w_x M_x / \Sigma w_x$. It may be shown that $M_w \geq M_n$ (since $w_x \geq n_x$) [76]. These two averages are equal only for a monodisperse (all molecules the same size) polymer. The ratio M_w/M_n is known as the polydisperse index, and is a measure of the breadth of the molecular weight distribution. Polydisperse values range from about 1.02 for carefully fractionated polymers to over 50 for some commercial polymers. In our study the polydispersity of these fractionated ZDOL lubricants are between 1.02 and 1.15, which are much lower than those of non-fractionated ZDOL lubricants (Ausimont typically quotes 1.2~1.5).

8.2.2 Optical Surface Analysis (OSA)

The optical surface analysis (OSA) system was also used to observe the lube migration behavior. The OSA is an *in situ* device, which has approximately 5 micron resolution and 2 MHz of bandwidth [9]. This device can be used to measure less than one Angstrom of carbon wear or lubricant depletion/accumulation. Samples with two lube molecular weights were tested in the OSA measurements: one was MW 4200 and the other was MW 7600.

8.2.3 Thermogravimetric Analysis (TGA)

The thermogravimetric analysis (TGA) is a sensitive measurement to observe the weight change of a sample as a function of temperature. Typical applications include the assessment of thermal stability and decomposition temperature in polymers. The TGA

experiments were carried out in a TGA model 2050 manufactured by TA Instruments Inc., which has a temperature range from liquid nitrogen temperatures to 650^{o}C, and was operated at a mass resolution of 0.3 μg. A typical sample size is on the order of 8 mg. Evaporation rate data was collected during a linear temperature ramp-up, usually 10^{o}C/min, under a dry nitrogen purge. The samples were contained in aluminum pans. Samples with lube molecular weights from 1500 to 7500 were tested in the TGA measurements.

8.3 Results and Discussions

8.3.1 Results from the UHV drag tests

In this section we present the results from the UHV drag tests. Figures 8.1 through 8.3 part (a) show the friction coefficient curves for the ZDOL lubricated CHx disks against an uncoated and a DLC coated Al_2O_3/TiC pico sliders. Figures 8.1 through 8.3 part (b) show the integrated mass spectra of the ZDOL fragments produced from the head-disk interface.

Figure 8.1(a) shows the friction coefficient curves for the 24Å fractionated ZDOL MW4200 lubricated disk. For the 70Å DLC coated Al_2O_3/TiC slider, the friction coefficient started at 1.2 and increased steadily to 1.4 within 1990 drag cycles before wear occurred. For the uncoated Al_2O_3/TiC slider, the friction coefficient started at 1.3 and increased steadily to a peak value of 1.9 within 295 cycles, then dropped to 0.3 after reaching its peak value. A wear track was observed on the disk just after the friction coefficient dropped. These results indicate that 24Å of monodispersed ZDOL MW4200 has good lubricating action against the DLC coated slider, but provides little protection against the uncoated slider. Figure 8.1(b) shows the integrated mass spectra of the major ZDOL decomposed fragments produced from the head-disk interface. The mass spec is similar to those in

previous chapters. The friction curve and mass spectra of higher molecular weight ZDOL are similar to Fig. 8.1 and are shown in Figs. 8.2 & 8.3.

Figure 8.4 shows the degradation intensities of (a) mass 47 (CFO), and (b) mass 69 (CF_3) during UHV drag tests on CHx disks with different lubricant molecular weights. The degradation intensities of the frictional fragments 47 (CFO) and 66 (CF_2O) decrease with both the uncoated sliders and DLC coated sliders as the molecular weight increases. We believed that some polymers start to depolymerize from endgroup weak bonds. In these cases, the rate of initiation decreases with the molecular weight of polymers since the concentration of the endgroup is inversely proportional to the degree of polymerization. Conversely, the above relation is often thought of as proof of chain end initiation. Another possibility is effect of the bonded fraction. The bonded fraction increases with increasing molecular weight [51]. In chapter 10 of the bonded fraction study, we concluded that lube degradation decreased as the bonded fraction decreased for both the uncoated and coated slider cases. Figure 8.4(b) shows a similar result for the catalytic fragments 69 (CF_3) and 119 (C_2F_5). However, the degradation intensities of the catalytic fragments decrease more rapidly than those of the frictional fragments as the molecular weight increases (less endgroup functionals). These results further support that the catalytic reactions occur at the endgroup functionals as discussed in chapter 3.

Figure 8.5(a) shows the wear durability of these CHx disks as a function of ZDOL molecular weight. With DLC coated sliders, the wear durability was improved as lubricant molecular weight increased. This enhanced performance may be due to the slower lubricant decomposition rate. However, the wear durability, with uncoated sliders, was not monotonically improved with increasing molecular weight. More discussion will be

presented on this point later. Figure 8.5(b) shows the friction coefficient of these CHx disks as a function of ZDOL molecular weight. The friction coefficient increased as the molecular weight increased. It is well-established that larger molecules will impede flow more readily than smaller ones and give a higher viscosity. Studies of the intrinsic viscosity of essentially monodisperse polymer fractions indicate a rather simple relation, known as Mark-Houwink-Sakurada (MHS) relation [77]:

$[\eta]_x = K(M_x)^a$, $(0.5 < a < 1)$

where $[\eta]_x$ = viscosity of x-mer, while "K" and "a" are MHS constants.

The measured intrinsic viscosity of a mixture of monodisperse fractions is a weight average:

$[\eta] = \Sigma[\eta]_x \, w_x/\Sigma w_x$.

The viscous component is dominant in liquids, hence their flow properties may be described by a Newtonian dashpot relation [78]:

$\tau = \eta \, d\gamma/dt$

where τ is the applied shear stress, and $d\gamma/dt$ is the rate of strain

With higher molecular weight, the higher viscosity (η) will cause higher friction (τ) during the head-disk sliding.

Table 8.1 lists the normalized mass spectra of the major ZDOL decomposition fragments for DLC coated sliders and uncoated sliders with respect to different molecular weight. The normalized percentage of some fragments increased as molecular weight increased, but it decreased for some other fragments. The number of the endgroup functionals (-CF_2-CH_2-OH) dominates these phenomena. As the molecular weight increases, the number of the endgroup functionals decreases if the lubricant thickness is controlled. Therefore, the normalized degradation intensity of fragments 31 (CF), 50 (CF_2), and 51 (CF_2H) almost scales with the number density of endgroups. These results indicate that these three decomposition fragments are mostly due to the lubricant fragmentation at the active endgroup functional. However, the normalized degradation intensity of mass 66 (CF_2O) increases as the molecular weight increases. This result indicates that the mass 66 (CF_2O) fragment is mostly from the lubricant decomposition within the main body that consists of two backbone groups 66 (CF_2O) and 116 (CF_2CF_2O). In addition, this decomposition is due to the weak-link degradation at the lowest-energy bonds. The normalized degradation intensities of the catalytic reaction fragments 69 (CF_3) and 119 (C_2F_5) decrease as molecular weight increases. These results support our earlier observation that the catalytic reactions occur at the endgroup functionals as shown in reactions (3-8) through (3-12), where the fluorine atom transfer is from the endgroup to the internal sector in the presence of the Al_2O_3 surface. The lower number of endgroup functionals with higher lubricant molecular weight reduces the possibility of the occurrence of the catalytic reactions.

8.3.2 OSA measurements

Figure 8.6 shows the OSA data: a plot of lube migration as a function of molecular weight. Before the OSA measurements, lubricant was removed from a section of the disk by a solvent, HFE-7100. This method was chosen because it was the least invasive and least likely to change the reflective properties of the carbon layer underneath the lubricant, which could affect the results. Figure 8.6(a) shows the lubricant thickness versus time. This lubricant thickness is defined as the difference between the region where the lubricant was removed and the untreated portion of the disk. The disk was scanned by S and P circularly polarized light every thirty minutes for thirteen hours. Figure 8.6(b) shows the average migration rate of ZDOL lubricant versus molecular weight. The rate is just the linear slope of the lubricant thickness versus time in Fig. 8.6(a). We observed that the lube mobility of ZDOL decreased with higher molecular weight.

From the data of the UHV drag tests, there was no such benefit in using higher molecular weight for the uncoated slider cases. Strong catalytic reactions occurred with the uncoated slider and these strong catalytic reactions accelerated the depletion of the lubricant layer. Hence, the reflow rate of mobile ZDOL in the wear track dominates the wear durability against uncoated slider. The wear durability of the ZDOL MW 4200 lubricated disk is better than those of the ZDOL MW 7600 or MW 8500 lubricated disks. The enhanced wear durability with lower molecular weight is due to its better mobility. The mobile ZDOL lubricants reflow in the wear track and improve their wear durability against uncoated sliders. For the DLC coated sliders, the depletion rate of the lubricant layer is much lower than that of the uncoated slider cases. The lubricant mobility is not as crucial as the

lubricant-consuming rate. Hence, the lubricant decomposition rate dominates the wear durability against DLC coated sliders in this case.

8.3.3 Results from TGA measurements

Figure 8.7(a) shows the weight loss of narrowly dispersed ZDOL 2000 vs. temperature during the TGA experiments. The loss in weight was initially recorded in milligrams on the strip-chart recorder, and then converted to the fractional loss. To determine the desorption temperature, a best-fit tangent line was drawn as indicated in Fig. 8.7(a), and the interception point between the tangent line and the curve represents the desorption temperature. Figure 8.7 (b) shows the desorption temperature of fractionated ZDOL vs. molecular weight. The desorption temperature increased with increasing molecular weight. These results indicate that the desorption energy of lubricants increases with increasing molecular weight. It is known that the transition temperatures of polymers depend on three mechanisms: (1) the internal mobility of the chains; (2) the chain length; and (3) the cohesive energy.

From OSA data, we observed that the spreading rate of ZDOL lubricant decreases with increasing molecular weight. As the mobility (freedom to rotate about bonds) of the chains decreases the desorption energy needed to break the lubricants increases, resulting in higher transition temperatures.

The second mechanism can be demonstrated by the Gibbs free energy function as shown below:

$\Delta G_m = \Delta H_m - T_m \Delta S_m$,

where G_m is the Gibbs free energy of melting

H_m is the energy needed to overcome the bonding forces

S_m is the entropy or molecular order

T_m is the melting temperature

At the equilibrium melting point T_m, $\Delta G_m = 0$, so $T_m = \Delta H_m / \Delta S_m$. For a given mass of polymer an increasing chain length results in more random order upon melting and a lower ΔS_m. Thus, the melting point (T_m) increases with increasing chain length (lower ΔS_m). The longer chain will also cause higher degrees of entanglement. The entanglement restricts the chain mobility and causes an increase in the transition temperatures.

The third mechanism is the cohesive energy. Cohesive energy is the total energy necessary to remove a molecule to a position far from its neighbors. With higher molecular weight, the total cohesive energy per molecule becomes greater due to the higher intermolecular attractive forces (Van der Waals forces). With a longer chain, more ethers of the ZDOL lubricants are expected to adsorb to the carbon surface, resulting in higher cohesive energy.

8.4 Conclusions

The ZDOL lubricants of different molecular weight were obtained by fractionating commercially available ZDOL. The UHV drag tests show that less lubricant decomposition occurs when the molecular weight is higher. The corresponding wear durability of ZDOL against the DLC coated sliders improves with increasing molecular weight. This enhanced

performance with heavier ZDOL may be due to the slower lubricant decomposition rate. However, there was no such benefit in using higher molecular weight for the uncoated slider cases. Strong catalytic reactions occurred with the uncoated slider and these strong catalytic reactions speeded up the depletion of the lubricant layer. Hence, the reflow rate of mobile ZDOL in the wear track dominates the wear durability against uncoated sliders. From the OSA data, we observed that the mobility of the PFPE lubricants decreased with increasing molecular weight. These results demonstrate the better wear performance of ZDOL with lower molecular weight in the uncoated slider case.

In addition, the friction coefficient increased as the molecular weight increased. The larger molecules impede flow more than smaller ones and give a higher viscosity. Hence, with higher molecular weight the higher viscosity causes higher friction during the drag tests. From the TGA data, we observed that the transition temperature increased with increasing molecular weight. The transition temperatures of polymers is believed to depend on three mechanisms: (1) the internal mobility of the chains; (2) the chain length; and (3) the cohesive energy.

	31-CF	**47-CFO**	**50-CF2**	**51-CF2H**	**66-CF2O**	**69-CF3**	**119-C2F5**
ZDOL 4200/coated slider	24%	100%	9%	17%	38%	5%	12%
ZDOL 4200/uncoated slider	42%	100%	34%	38%	67%	89%	58%
ZDOL 7600/coated slider	23%	100%	4%	10%	43%	4%	14%
ZDOL 7600/uncoated slider	22%	100%	14%	12%	74%	73%	42%
ZDOL 8500/coated slider	13%	100%	4%	11%	53%	5%	14%
ZDOL 8500/uncoated slider	19%	100%	3%	5%	78%	59%	37%

Table 8.1 Normalized mass spectra of the major ZDOL decomposition fragments during the UHV drag tests with respect to different ZDOL molecular weight.

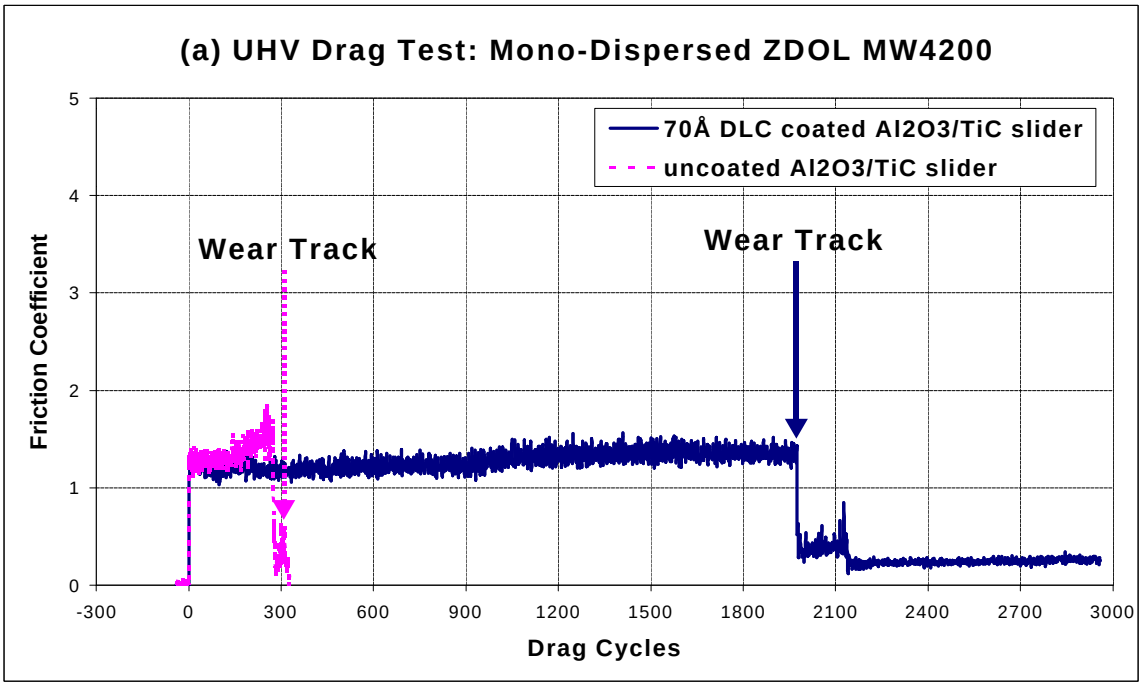

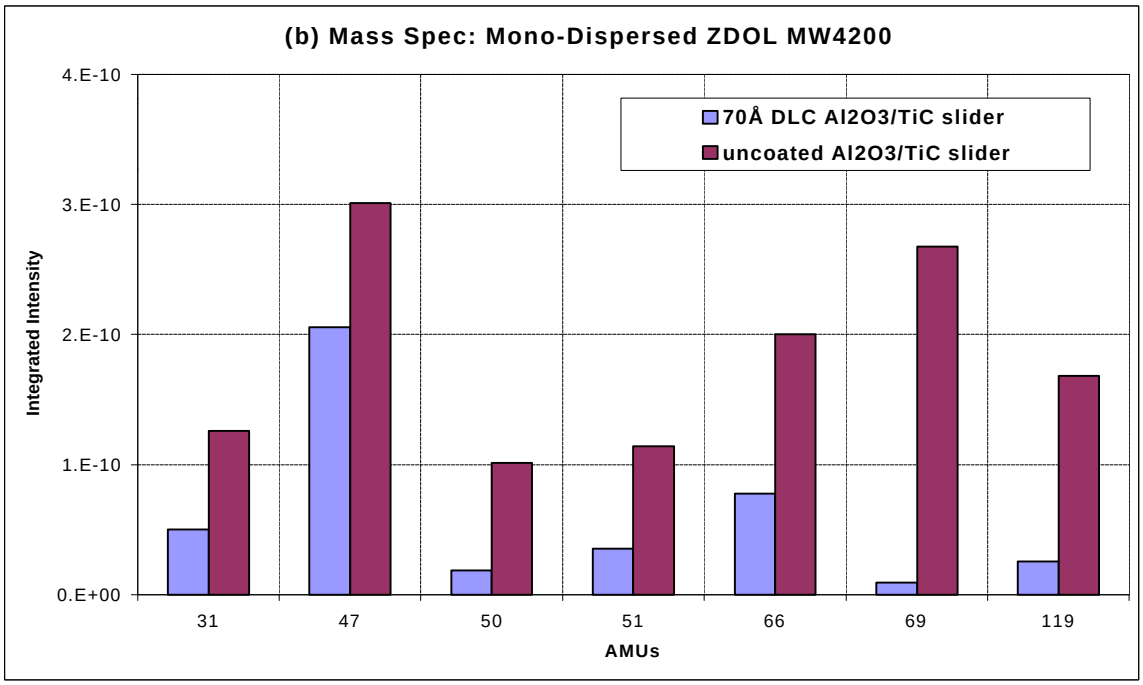

Figure 8.1 (a) friction coefficient of UHV drag test on 24Å mono-dispersed ZDOL MW4200 lubricated disk; (b) mass spectrum of the major ZDOL decomposition fragments.

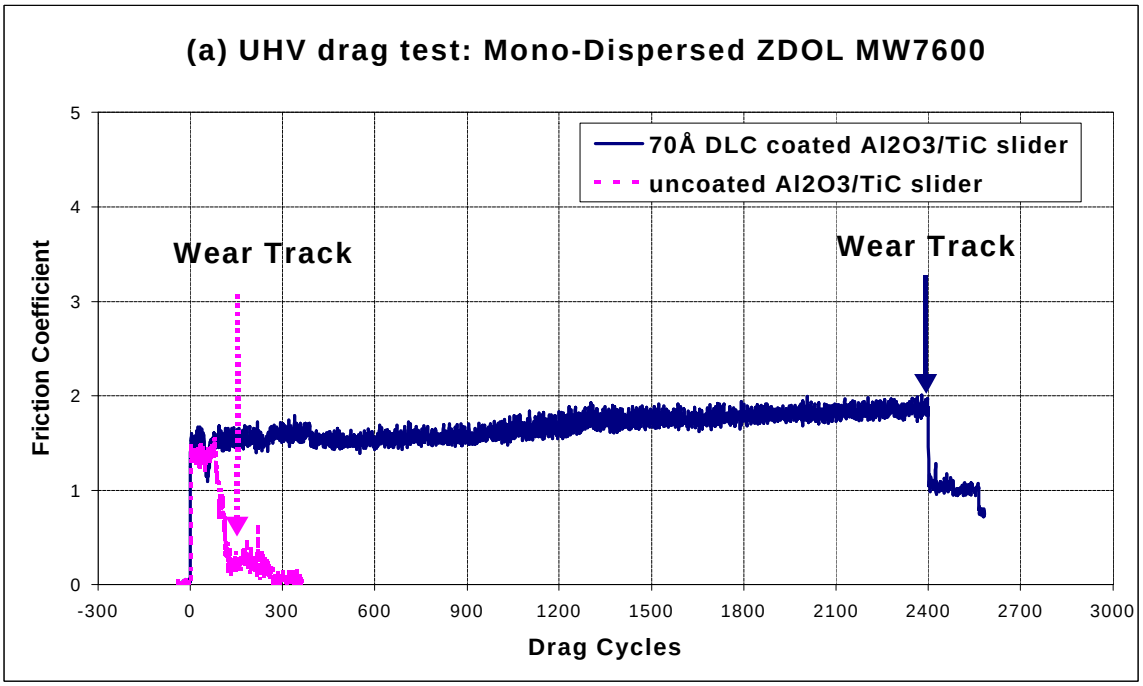

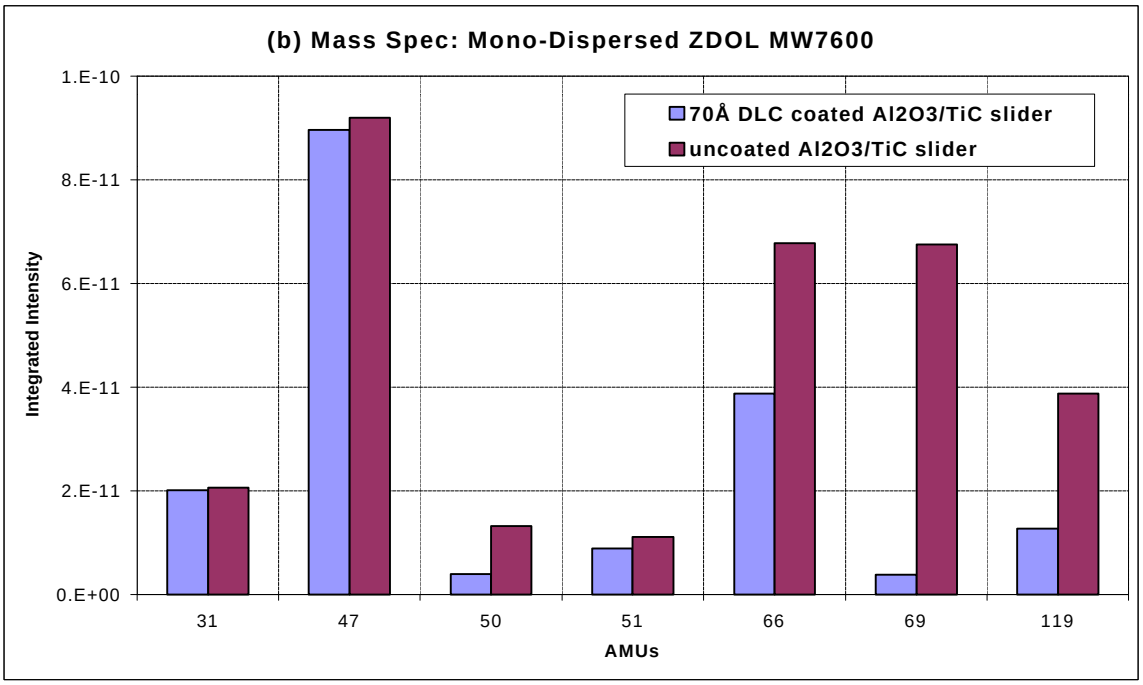

Figure 8.2 (a) friction coefficient of UHV drag test on 24Å mono-dispersed ZDOL MW7600 lubricated disk; (b) mass spectrum of the major ZDOL decomposition fragments.

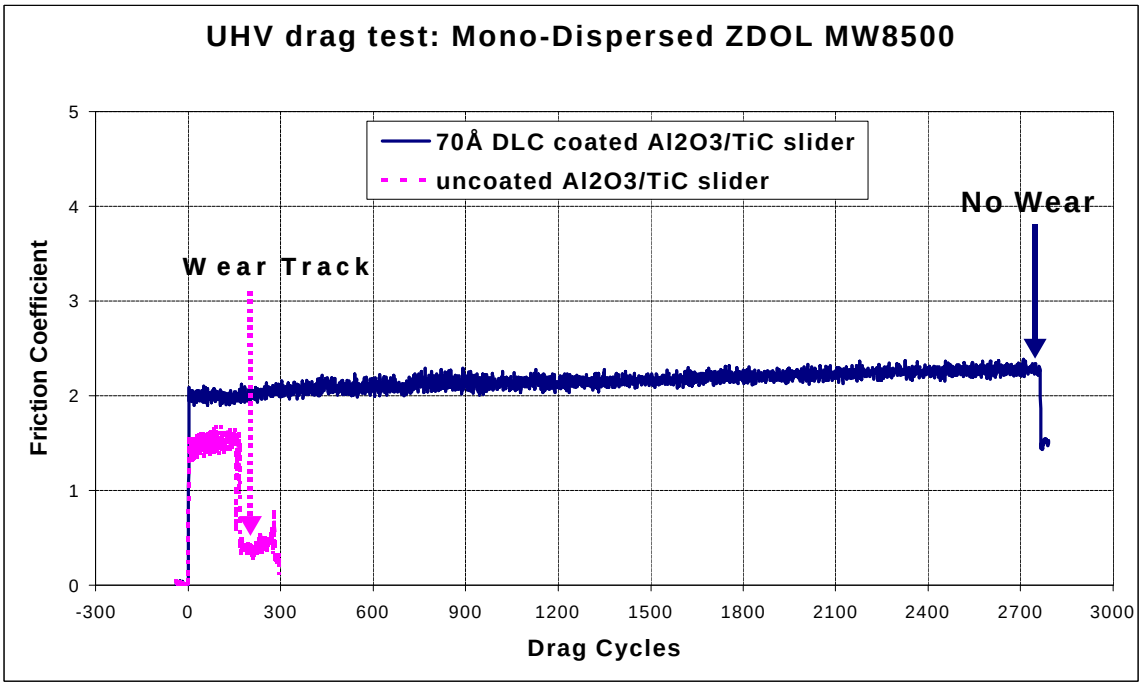

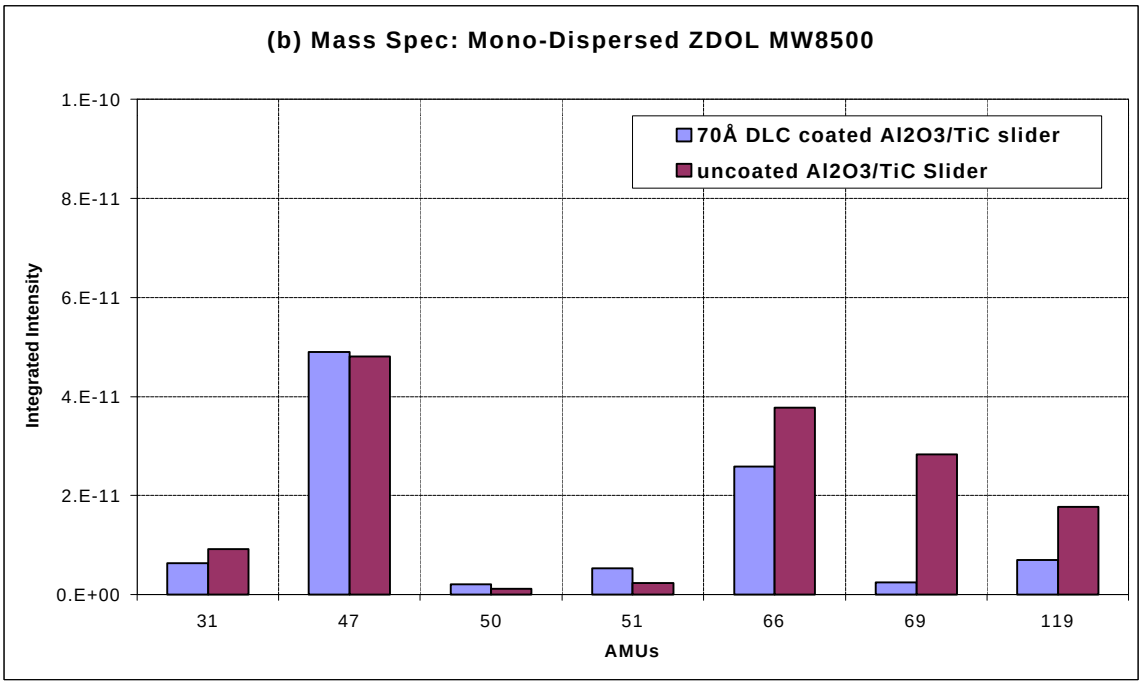

Figure 8.3 (a) friction coefficient of UHV drag test on 24Å mono-dispersed ZDOL MW8500 lubricated disk; (b) mass spectrum of the major ZDOL decomposition fragments.

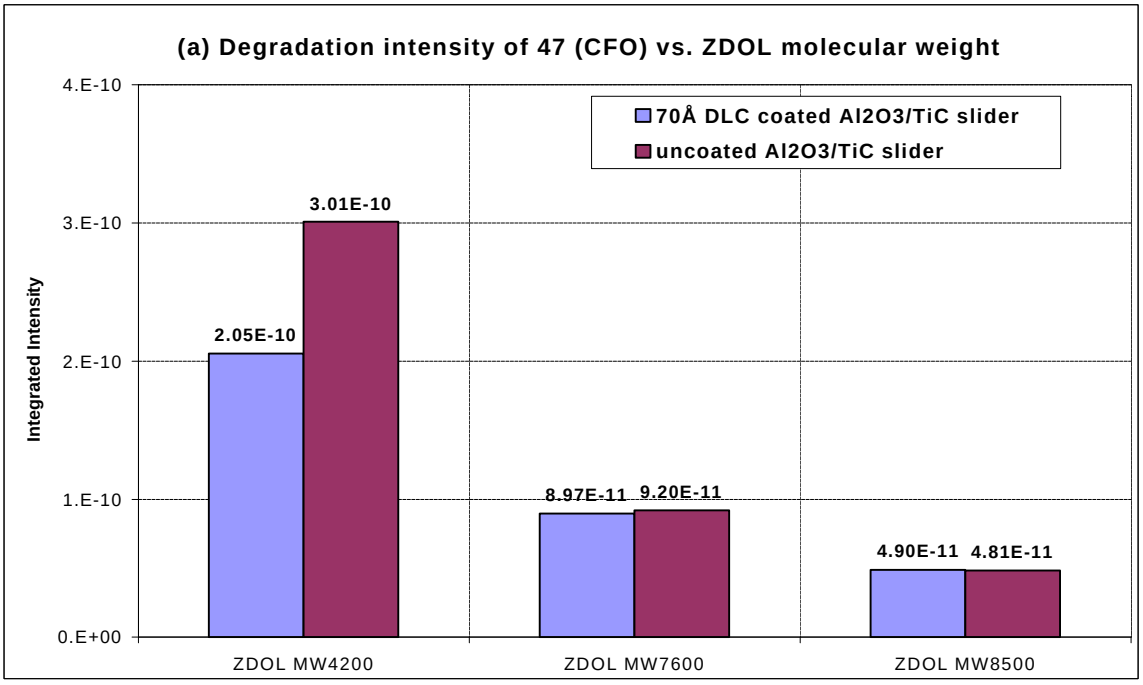

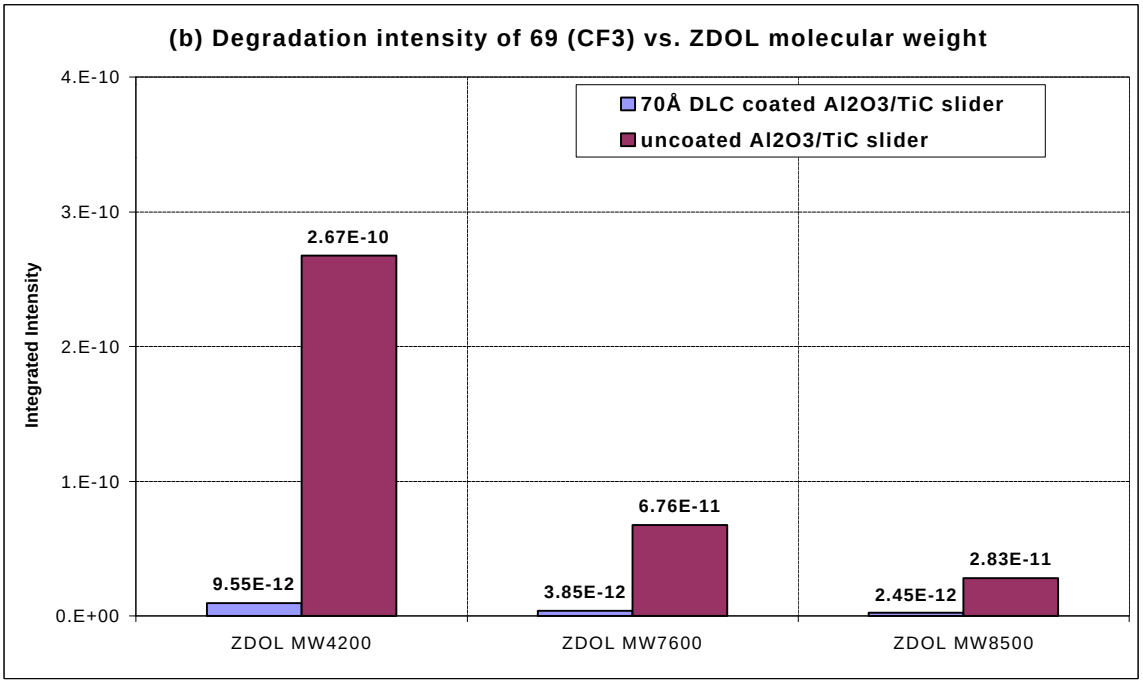

Figure 8.4 Integrated degradation intensity of ZDOL during UHV drag tests on CHx disks with different ZDOL molecular weight. (a) mass 47 (CFO) under frictional action, and (b) mass 69 (CF3) under catalytic reaction.

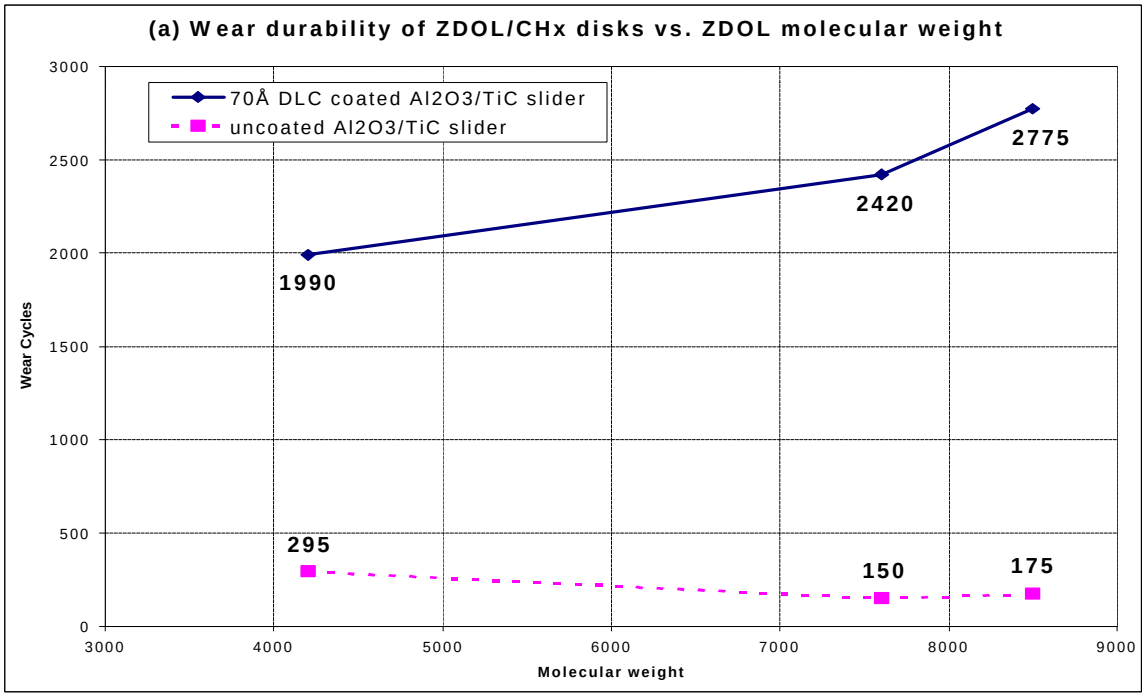

Figure 8.5 (a) wear durability and (b) friction coefficient of CHx disks with different ZDOL molecular weight during UHV drag tests with DLC coated or uncoated Al_2O_3/TiC sliders.

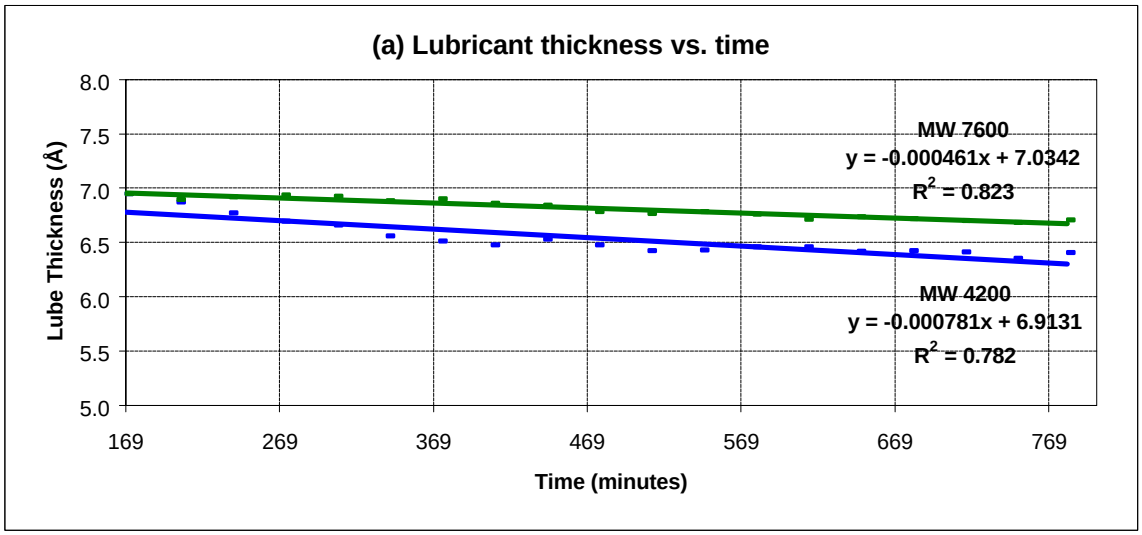

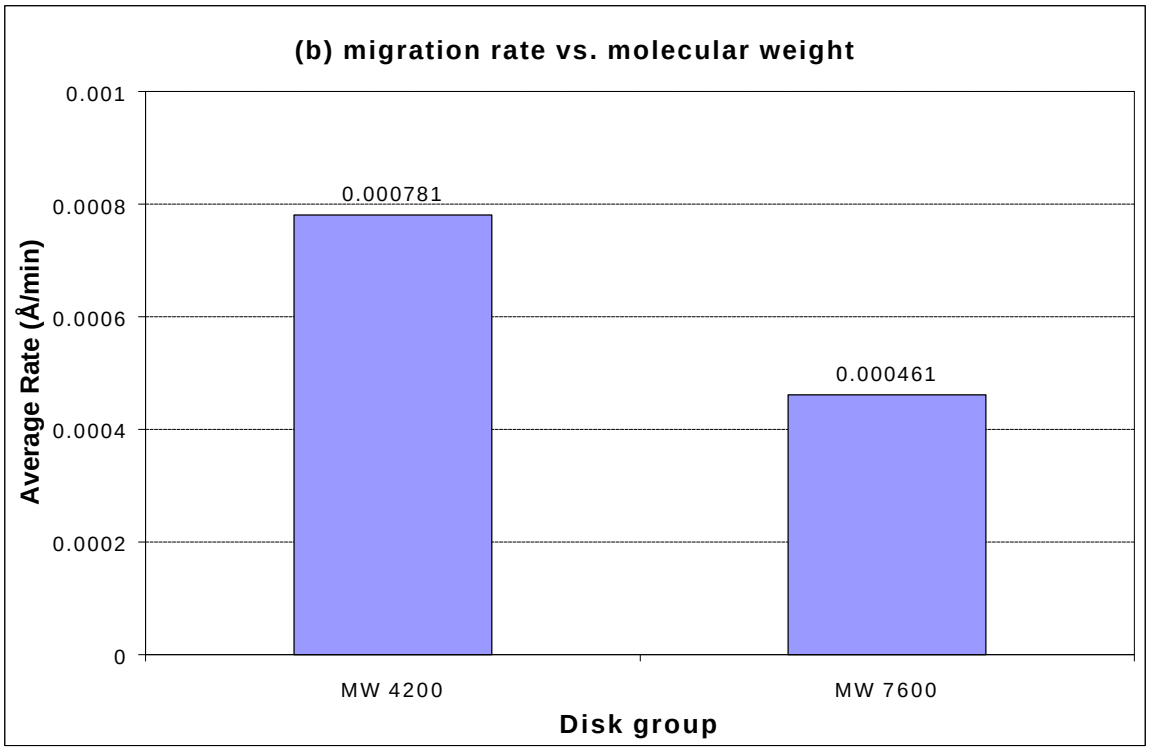

Figure 8.6 (a) the OSA data on the lubricant thickness versus time; (b) the ZDOL lube migration rate versus molecular weight.

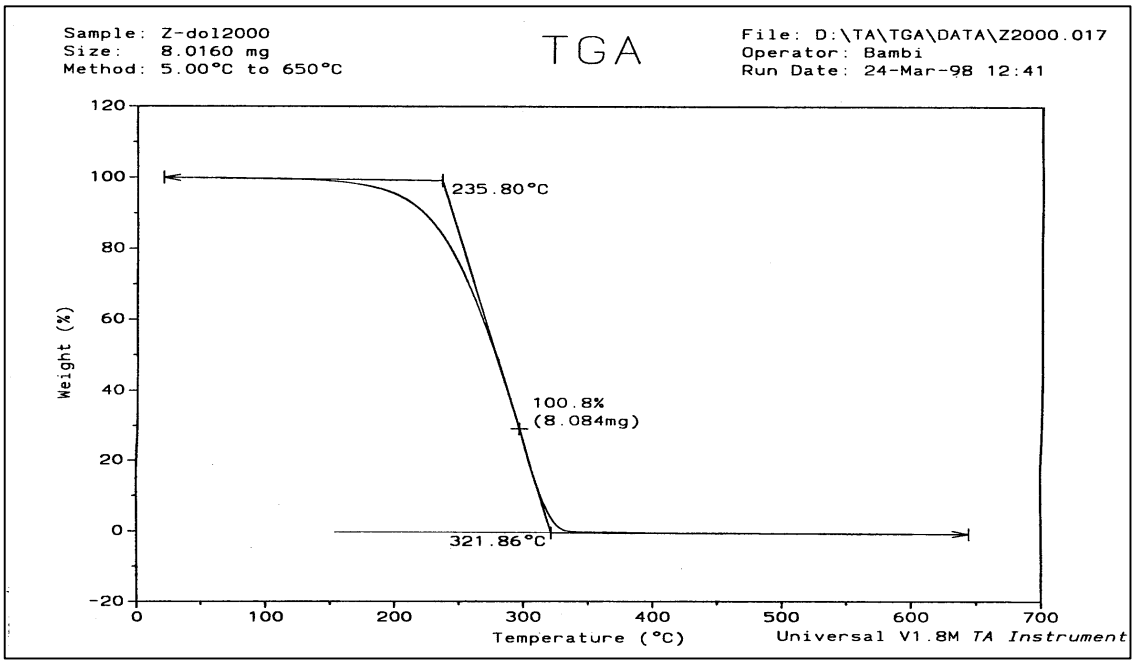

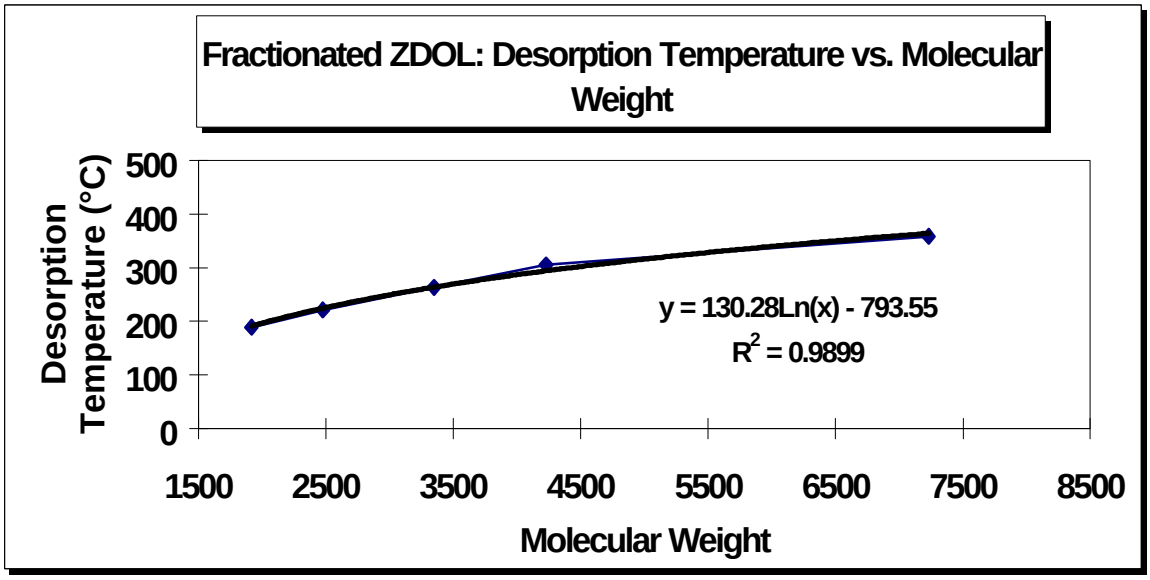

Figure 8.7 (a) the TGA data on the lube weight loss versus temperature; (b) the TGA data on the desorption temperature versus molecular weight.

Chapter 9

LUBRICANT THICKNESS EFFECT

9.1 Introduction

The thickness of the PFPE lubricant layer must be chosen carefully to provide maximum wear protection and acceptable life performance of the head-disk drive. If the lubricant film is too thick, excessive stiction is observed upon start up of the drive. On the other hand, if the lubricant film is too thin, insufficient protection of the head-disk interface is provided, and tribological failure can occur in the early operating period. The trend in the industry in recent years has been to decrease the amount of lubricant used. Lubricant thicknesses of a single layer or less (sub-monolayer) are becoming quite common in disk drives. Therefore, the interactions between the lubricant and the carbon surface may be more important to the tribological performance of the disk drive than the bulk properties of PFPE lubricants.

Tyndall et al. [80] used surface energy measurements to extract information about the PFPE lubricant-carbon interfacial interactions. They measured the dispersive surface energy to determine the lubricant coverage of the carbon surface and yield information on the relative orientation of the lubricant backbone with respect to the carbon surface. They found that the surface energy of PFPE lubricated disks decreases with increasing lubricant thickness.

---

* Materials from this chapter is published in Tribology Letters, Oct. 1999 [79].

Waltman et al. [81] showed that the surface energy of a bonded lubricant is lower than that of a mobile lubricant, reflecting the increased interaction strength that occurs as a result of bonding. In the case of bonded ZDOL, the nonpolar nature of the lubricant/carbon combination indicates that much stronger interactions occur between the hydroxyl end-groups of ZDOL and the carbon surface. Also, Tyndall and Karis et al. [80, 82] showed that the polar component of the surface energy for ZDOL exhibits oscillations as a function of lubricant thickness. As the amount of lubricant applied to the surface increases, the surface energy decreases since the fraction of the higher-energy carbon surface covered by the low surface energy PFPE increases. Neutralization of the surface active sites by the addition of hydroxyl terminated ZDOL results in a decrease in the measured surface energy with increasing ZDOL thickness. A local minimum in the polar surface energy results at the point where the number of lubricant end-groups matches the number of active oxide sites on the carbon surface. Matching of the ZDOL end-group density with active site density on the carbon surface results in the complete coverage of the carbon surface by ZDOL lubricant.

In this chapter, we study the ZDOL thickness effect on hydrogenated carbon films (CHx) using an ultra-high vacuum (UHV) tribochamber equipped with a mass spectrometer. The studies consist of drag tests and thermal desorption experiments in the UHV tribochamber. We illustrate the lubricant thickness effect on the tribological performance as well as the strength of the bonding between the lubricant and the carbon surface.

9.2 Experimental Procedure and Set-up

Drag tests were conducted in the UHV with the following parameters: 0.2 m/s drag speed, a load of 30 mN, and a sliding time of 20 minutes. The sliders were 30% (1.2mm by 1mm) negative-pressure Al_2O_3/TiC sliders with and without amorphous diamond like carbon (DLC) films on the air bearing surfaces. The disks were commercial 95mm smooth thin film disks with a 75Å amorphous hydrogenated carbon overcoat (CHx). The hydrogen content in the CHx film was 30 atomic percent. The disks were lubricated with ZDOL by a dipping process. The resulting thickness of ZDOL on the disks in this study were 4.5Å, 6.2Å, 9Å, 12.5Å, and 15.4Å. We used FTIR to measure the lubricant thickness of these disks before the UHV drag tests. The molecular weight of polydisperse ZDOL is 2000 AMU.

For the thermal desorption tests in the tribochamber, a CHx/ZDOL disk was cut into 2 cm x 2 cm squares. The lubricated samples were mounted on the heater and the temperature was measured by a thermocouple in contact with the heater near the heated sample. A typical experiment consisted of heating a sample at a rate of 0.2 K/sec starting at room temperature and stopping before 550 K. A mass spectrum was collected on a computer every two seconds during the heating.

9.3 Results and Discussions

9.3.1Results from the UHV drag tests

In this section, we present the results from the UHV drag tests. Figure 9.1(a) shows the friction coefficient curves for the **4.5Å ZDOL** 2000 (polydisperse) lubricated disk. The friction coefficient curves for the thicker ZDOL lubricated disks are similar to Fig. 9.1(a) and will not be shown here. We will note, however, that the onset of the wear track

formation is displaced to larger number of drag cycles with increasing lubricant thickness, as will be discussed in more detail below. For the 100Å DLC coated Al_2O_3/TiC slider, the friction coefficient started at 0.3 and became very unstable immediately. A wear track was observed on the disk after just 10 drag cycles. For the uncoated Al_2O_3/TiC slider, the friction coefficient increased to a peak value of 1.3 immediately and dropped to 0.3 after reaching its peak value. A wear track was observed on the disk just after the friction coefficient dropped. The above results indicate that ZDOL of 4.5Å thickness has little lubricating action against both the uncoated and the DLC coated Al_2O_3/TiC sliders.

Figure 9.1(b) shows the integrated mass spectra of four major ZDOL decomposed fragments produced from the 4.5Å ZDOL lubricated disk. Once again, the mass spectra for the thicker ZDOL lubricated disks are similar to Fig. 9.1(b) and will not be shown here. The four primary peaks are for mass fragments CFO (47), CF_2O (66), CF_3 (69), and C_2F_5 (119). For the 100Å DLC coated Al_2O_3/TiC slider, the primary decomposition peaks are masses 47 (CFO) and 66 (CF_2O) due to frictional heat action [12]. For the uncoated Al_2O_3/TiC slider, the mass intensities of the four major ZDOL fragments are almost one order higher than those in the DLC coated slider case. For the uncoated slider, catalytic reactions control the ZDOL decomposition and the catalytic reactions lead to the generation of masses 69 (CF_3) and 119 (C_2F_5). In figure 9.1(b), mass 69 (CF_3) is the highest peak in the uncoated slider case as shown in figure 9.1(b).

Figure 9.2 shows the degradation intensities of (a) mass 47 (CFO) and (b) mass 66 (CF_2O) during UHV drag tests on CHx disks with different ZDOL thicknesses. The degradation intensities of the frictional fragments 47 (CFO) and 66 (CF_2O) increased one

order of magnitude with uncoated sliders when the thickness of ZDOL exceeded 12Å. However, no such increase was noted with disks tested against DLC coated sliders.

Figure 9.3 shows similar result for the catalytic fragments 69 (CF_3) and 119 (C_2F_5). However, the intensities of masses 69 and 119 are significantly higher than those of masses 47 and 66 for the uncoated slider case when the lubricant thickness exceeds 12Å. These results indicate that strong catalytic reactions occur with the uncoated slider when the lubricant thickness exceeds 12Å.

Figure 9.4 shows the wear durability of these CHx disks as a function of ZDOL thickness. With DLC coated sliders, the wear durability was significantly improved when the lubricant thickness exceeded 12Å. These results explain the better wear durability of using thicker ZDOL – a thicker layer of ZDOL provides more lubricant to be decomposed so the carbon overcoat surface is protected for a longer duration against sliding. The enhanced wear durability could also be attributed to the better coverage of the carbon surface by the thicker ZDOL layers. However, there was no benefit in using thicker lubricant for the uncoated slider cases. Strong catalytic reactions occurred with the uncoated slider when the ZDOL thickness exceeded 12Å. These catalytic reactions counteract the benefits of using thicker ZDOL, so 15.4Å of ZDOL performs as poorly as thinner ZDOL with an uncoated slider.

With DLC coated sliders, the wear durability of disks lubricated with ZDOL significantly improves when the lubricant thickness exceeds 12Å. This enhanced performance with thicker ZDOL may be due to two mechanisms: (1) full coverage of the carbon surface with ZDOL, and (2) a thicker layer of mobile ZDOL to reflow into the wear track. Using surface energy (dispersive & polar) of ZDOL on carbon-coated disks, Karis et

al. [82] showed that complete coverage of the disk surface occurs at 10Å for ZDOL 1600 and 15Å for ZDOL 3100. Tyndall et al. [80] also measured the surface energy for ZDOL on carbon-coated disks and found that complete coverage of the carbon surface occurs at 14 ± 2Å for ZDOL 2000. These results support the first mechanism we cited for improvement in wear durability – at 12Å, the surface is completely covered.

The second mechanism for improved wear durability may be attributed to the refill of the mobile ZDOL layer in the track area. We used FTIR to measure the lubricant thickness of these disks before the UHV drag tests. These FTIR thickness measurements were confirmed by ellipsometry, and X-ray reflectivity. After the thicknesses were measured, the disks were washed sequentially in perfluorohexane and 2,3-dihydro-perfluoropentane to remove any soluble lubricant [74, 75], and then the thickness was remeasured. The lubricant that is retained on these disks is defined as the amount "bonded", while the portion removed by the solvent wash process is defined as the "mobile" portion. The results are summarized in the Table 9.1:

Table 9.1

Disks	Bonded Thickness (Å)	Mobile Thickness (Å)
4.5Å ZDOL	**3.3**	**1.2**
6.2Å ZDOL	**4.7**	**1.5**
9Å ZDOL	**5.7**	**3.3**
12.5Å ZDOL	**7.9**	**4.6**
15.4Å ZDOL	**10.4**	**5**

Figure 9.5 is a plot of the wear durability vs. the mobile ZDOL thickness during UHV drag tests. For the disks tested with 70Å DLC coated sliders, the wear durability improves considerably with thicker mobile ZDOL. These results reflect the importance of the mobile ZDOL layer in providing good wear durability. We believe the role of the mobile layer is to

replenish the lube displaced during dragging. As lube thickness increases, the replenishment rate also increases as suggested by O'Connor et al.[83] and Ma et al. [84, 85, 86] in their studies of the spreading behavior of PFPE on silica surfaces. In their paper, Ma suggests that the functional end-groups of ZDOL significantly retard the diffusion process, owing probably to their stronger interactions with the carbon surface. In the context of our study, as the lubricant thickness increases, the end-group effect on the diffusion process decreases, and the diffusion coefficient increases. As a result, faster replenishment of the lubricant occurs on disks with thicker ZDOL on the protective carbon surface, enhancing the wear durability at the interface. In a different study of lubricant bonded fraction (not presented here) using samples with 12Å ZDOL total lubricant but with different mobile fractions, we observed that wear durability improves with an increase in the mobile portion. More information in details will be shown in chapter 10.

9.3.2 Results from UHV thermal desorption tests

In this section, we present and discuss the results from UHV thermal desorption experiments. Figure 9.6 shows the thermal desorption history profiles for masses 47 (CFO) and 66 (CF_2O) of CHx disks with different ZDOL thickness ranging from 4.5Å to 15.4Å at a heating rate of 0.2K/sec. These two fragments are characteristic of friction/mechanical shear actions and electron tribo-chemistry bombardment [40] in drag tests. Figure 9.7 shows the thermal desorption history profiles for masses 69 (CF_3) and 119 (C_2F_5) of CHx disks with different ZDOL thickness ranging from 4.5Å to 15.4Å. These two fragments are used to monitor the catalytic decomposition. Two thermal desorption peaks were found during these experiments: one is between 300K and 375K, and the other is between 375K and 500K. We

used FTIR to measure the lubricant thickness of the samples before and after the thermal desorption experiments. We will describe the procedure for the 9Å ZDOL disk – it is similar for the others. Three samples (labeled A, B, and C) were cut from the same 9Å ZDOL disk and measured. Sample A did not go through the thermal desorption test; sample B was heated just past the first thermal desorption peak (300K to 375K); sample C was tested up to the temperature of 500K (after going through the first and second thermal desorption peaks). The measurements are listed in the Table 9.2:

Table 9.2

	Sample A	Sample B	Sample C
total thickness	8.5Å	6.2Å	0.7Å
bonded thickness	5.2Å	5.8Å	*
mobile thickness	2.3Å	0.4Å	*

* could not measure

From the data, we conclude that most of the mobile lubricant is desorbed during the first thermal desorption period, and the bonded lubricant increased 0.6Å due to the annealing effect at temperatures above 350K. These results are similar to those found by Waltman et al. [74]. They found that the initially applied mobile ZDOL 2000 (polydisperse) is depleted via evaporative loss as well as bonding of the lubricant to active sites on the carbon surface at the elevated temperatures between 40^{o}C (313K) to 60^{o}C (333K), which is the operating temperature of the disk drives. The relative branching into the evaporation and bonding channels is molecular weight dependent, with increasing molecular weight favoring bonding. The activation energy for ZDOL evaporation is highly dependent on molecular weight, decreasing rapidly with decreasing molecular weight. Therefore, the lower molecular weight components present in ZDOL 2000 will preferentially evaporate from the disk surface. In our

current case of ZDOL 2000 (low molecular weight), evaporation is the dominant channel responsible for the depletion of mobile ZDOL 2000, and only 0.6Å mobile ZDOL became bonded on the carbon surface during annealing. Samples C shows that most of the ZDOL lubricant is desorbed by 500K. Thus, we can conclude that only the mobile ZDOL layer is desorbed during the first thermal desorption period and the residual bonded ZDOL layer is desorbed during the second thermal desorption period. This indicates that the desorption energy of bonded ZDOL lubricant is higher than that of mobile ZDOL lubricant. Waltman et al. [81] also showed similar results in that the surface energy of the bonded lubricant is substantially lower than the mobile lubricant, reflecting the increased interaction strength that occurs as a result of bonding.

Figures 9.6 and 9.7 illustrate that CFO (47) and CF_2O (66) are the primary thermal desorption fragments from the first peak, which corresponds to desorption of the mobile ZDOL layer. These results are consistent with those of Lin and Kasai [20, 30]. During the second thermal desorption peak (between 375K and 500K), the bonded ZDOL layer was desorbed and all four primary fragments were observed. When the lubricant thickness is below 9Å (4.5Å and 6.2Å in our study), the generation of fragments associated with friction heat/electron bombardment (CFO and CF_2O) is much higher than that of the catalytic related fragments (CF_3 and C_2F_5). However, when the lubricant thickness reaches 9Å and higher (9Å, 12.5Å, and 15.4Å in our study), the intensity of the catalytic related fragment (CF_3) equals that of the friction heat/electron bombardment associated fragments (CFO and CF_2O). The generation of fragment CF_3 may be a consequence of the desorption of bonded lubricant from the CHx surface [40].

Moreover, the ZDOL desorbed peak temperatures shifted to lower temperatures with increasing lubricant thickness. Figure 9.8 shows the thermal desorption peak temperatures of ZDOL for CHx disks with ZDOL thickness ranging from 4.5Å to 15.4Å. The temperature at the first peak, which is attributed to the desorption of the mobile ZDOL layer, remains almost constant as a function of ZDOL thickness. This result indicates that the desorption energy of the mobile ZDOL layer is independent of the lubricant thickness.

However, the temperature at the second peak, corresponding to the desorption of bonded ZDOL, shifts to a lower temperature with increasing ZDOL thickness as shown in Fig. 9.7. This result indicates that the desorption energy of bonded lubricant decreases with increasing lubricant thickness. One possible explanation is that the surface of the amorphous carbon is populated with sites of different interaction strengths, where stronger bond sites are associated with higher binding energy [32]. When ZDOL molecules adsorb on the surface, they first occupy the stronger sites (sites with higher desorption energy). As more ZDOL molecules (thicker lubricant) are adsorbed, weaker sites (sites of lower desorption energy) are occupied. Thus, at thinner ZDOL the second peak temperature is higher, and it is lower for thicker ZDOL. Earlier UHV drag tests show that strong catalytic reaction occurs for the uncoated slider case when the lubricant is thicker. With thicker ZDOL, the thermal desorption energy of bonded lubricant decreases, so the decomposition of ZDOL is easier as well as the catalytic reaction.

Figure 9.9 shows the integrated thermal desorption intensity of CFO (47) versus (a) mobile ZDOL thickness during the first desorption peak, and (b) bonded ZDOL thickness during the second desorption peak. The integrated intensity of the fragment CFO during the first desorption peak increases as thicker mobile ZDOL layer is desorbed. However, the

intensity - thickness curve does not have a linear relationship as shown in Fig. 9.9(a). In the result shown in the Table II, we found that, at the first desorption peak, evaporation is the dominant mechanism for the depletion of mobile ZDOL 2000, but a small portion of it became bonded on the carbon surface due to the annealing effect. Thus, the integrated desorption intensity of CFO is not exactly proportional to the original mobile ZDOL thickness at the first desorption peak. The desorption intensity of this fragment is, however, almost proportional to the bonded ZDOL thickness at the second desorption peak, as shown in Fig. 9.9(b). The small fraction of bonded ZDOL originating from the mobile ZDOL will not affect the linearity of the intensity thickness curve shown in Fig. 9.9(b). These results further support the assertion that the bonded ZDOL layer was desorbed during the second peak.

9.4 Conclusions

UHV drag tests show that the lubricant interaction with the carbon overcoat varies as a function of lubricant thickness. Wear durability of ZDOL against DLC coated sliders improves considerably when the carbon overcoat surface is fully covered by one layer of ZDOL. This enhanced performance with thicker ZDOL can be due to two mechanisms: (1) full coverage of the carbon surface with ZDOL, and (2) a thicker layer of mobile ZDOL to reflow into the wear track. However, there was no benefit in using thicker lubricant for the uncoated slider cases. Strong catalytic reactions occurred with the uncoated slider when the ZDOL thickness exceeded 12Å. These catalytic reactions counteract the benefits of using thicker ZDOL.

Based on the thermal desorption experiments, only mobile ZDOL lubricant was desorbed at the first thermal desorption peak (between 300K and 375K), and the residual bounded ZDOL lubricant was desorbed at the second thermal desorption peak (between 375K and 500K). In the sub-monolayer regime, adhesion of lubricant to the carbon overcoat is much stronger because it requires a much higher temperature to desorb the lubricant molecule. When the lubricant thickness is around or above a monolayer, cohesion among the lubricant molecules plays a greater role and a much lower temperature is needed for lubricant desorption.

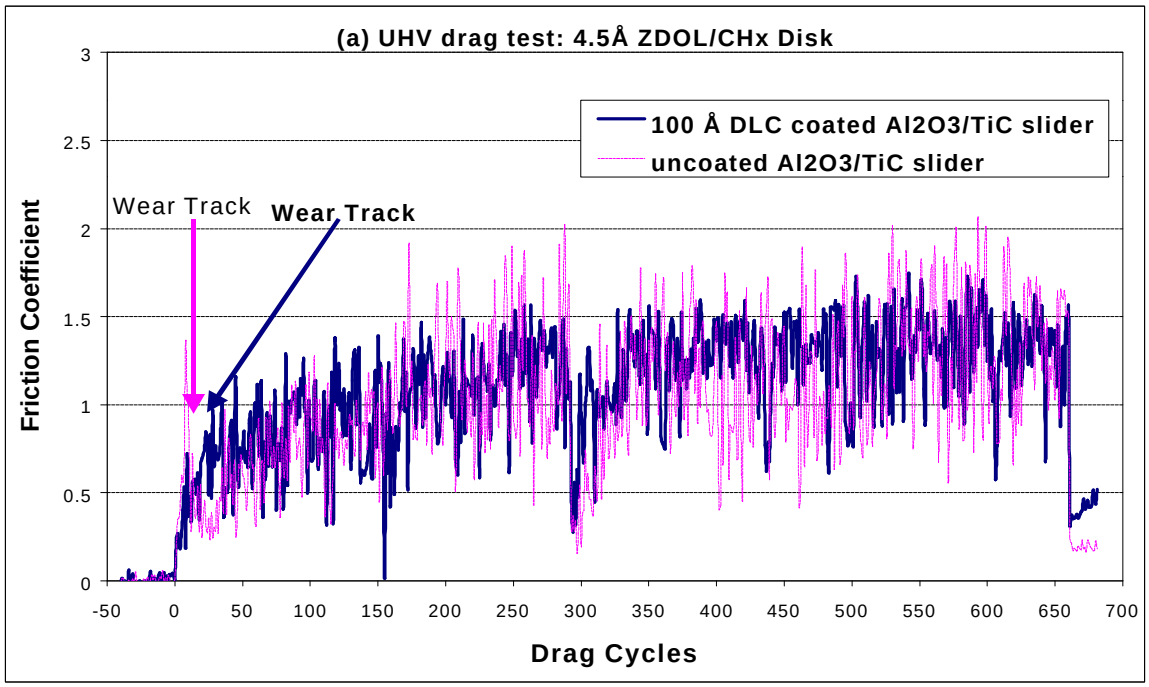

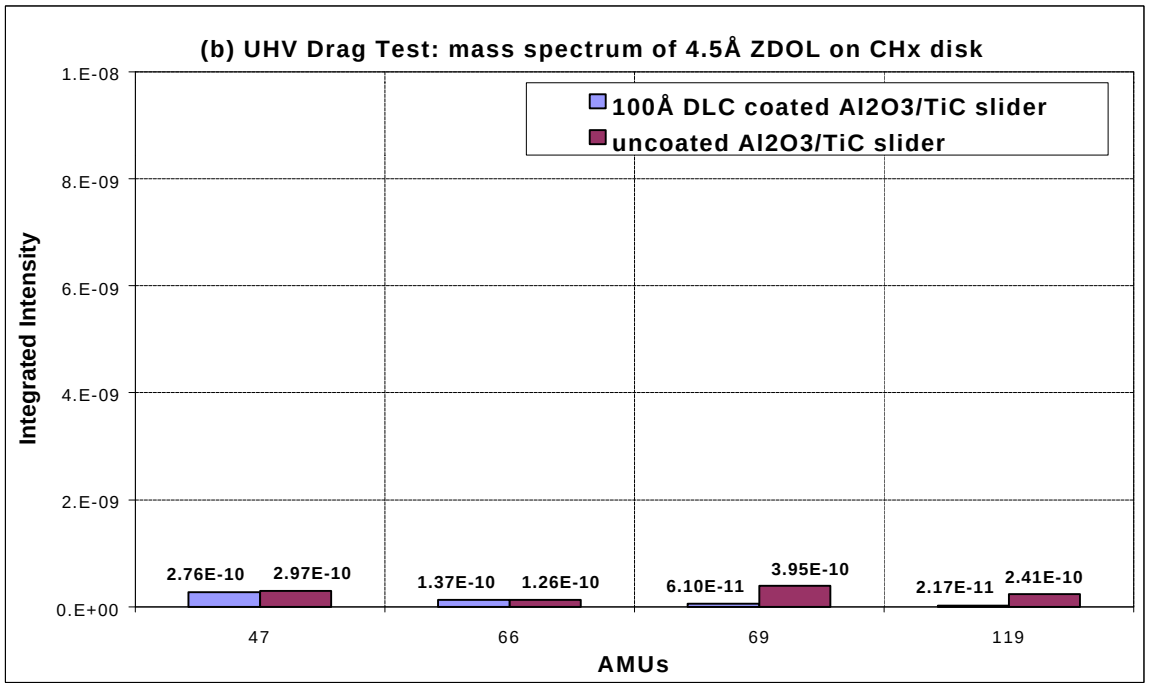

Figure 9.1 (a) friction coefficient of UHV drag test on 4.5Å ZDOL lubricated disk; (b) mass spectrum of four major ZDOL decomposed fragments.

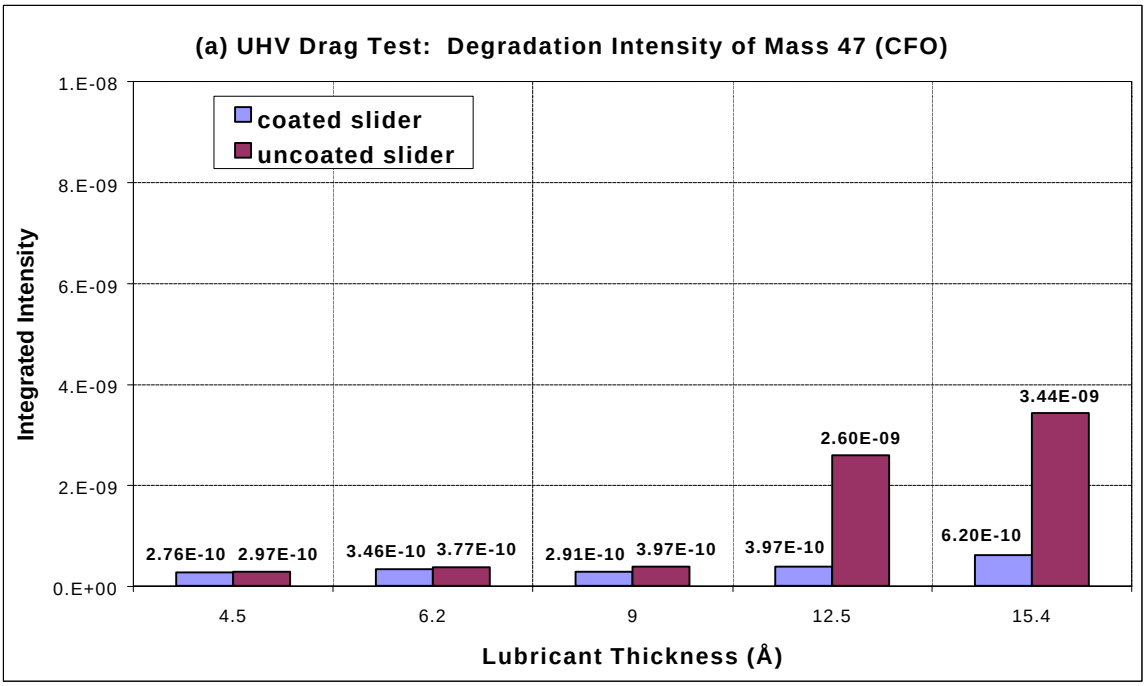

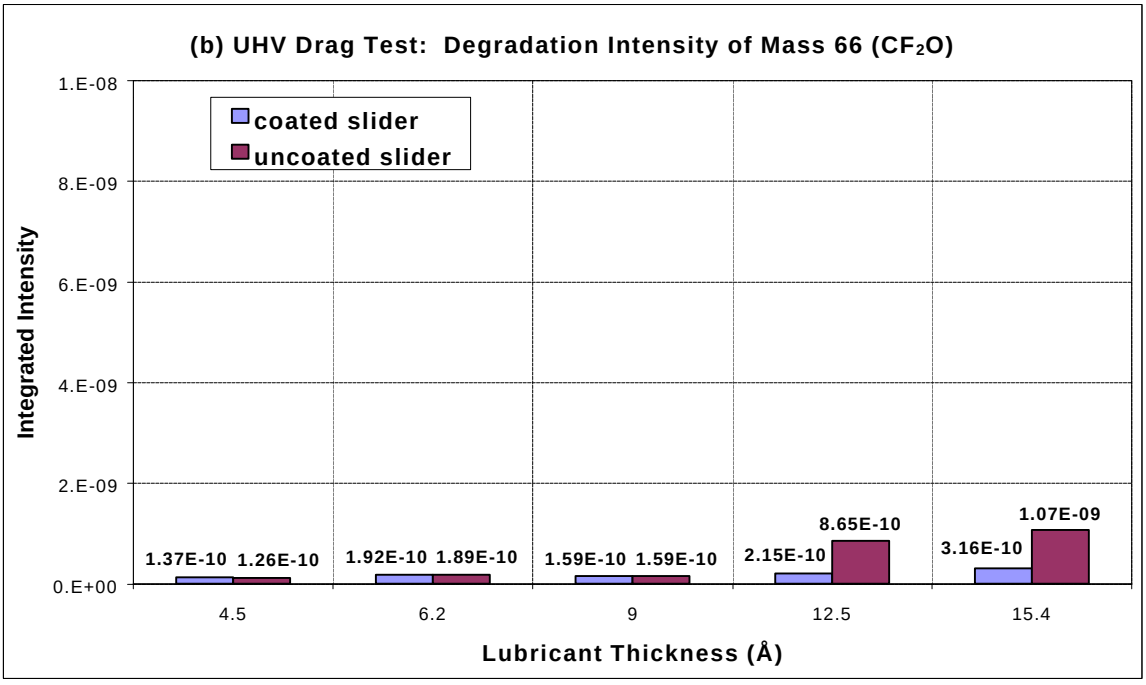

Figure 9.2 Integrated degradation intensity of ZDOL during UHV drag tests on CHx disks with different ZDOL thickness. Two major decomposition fragments occur under frictional action: (a) mass 47 (CFO), and (b) mass 66 (CF_2O).

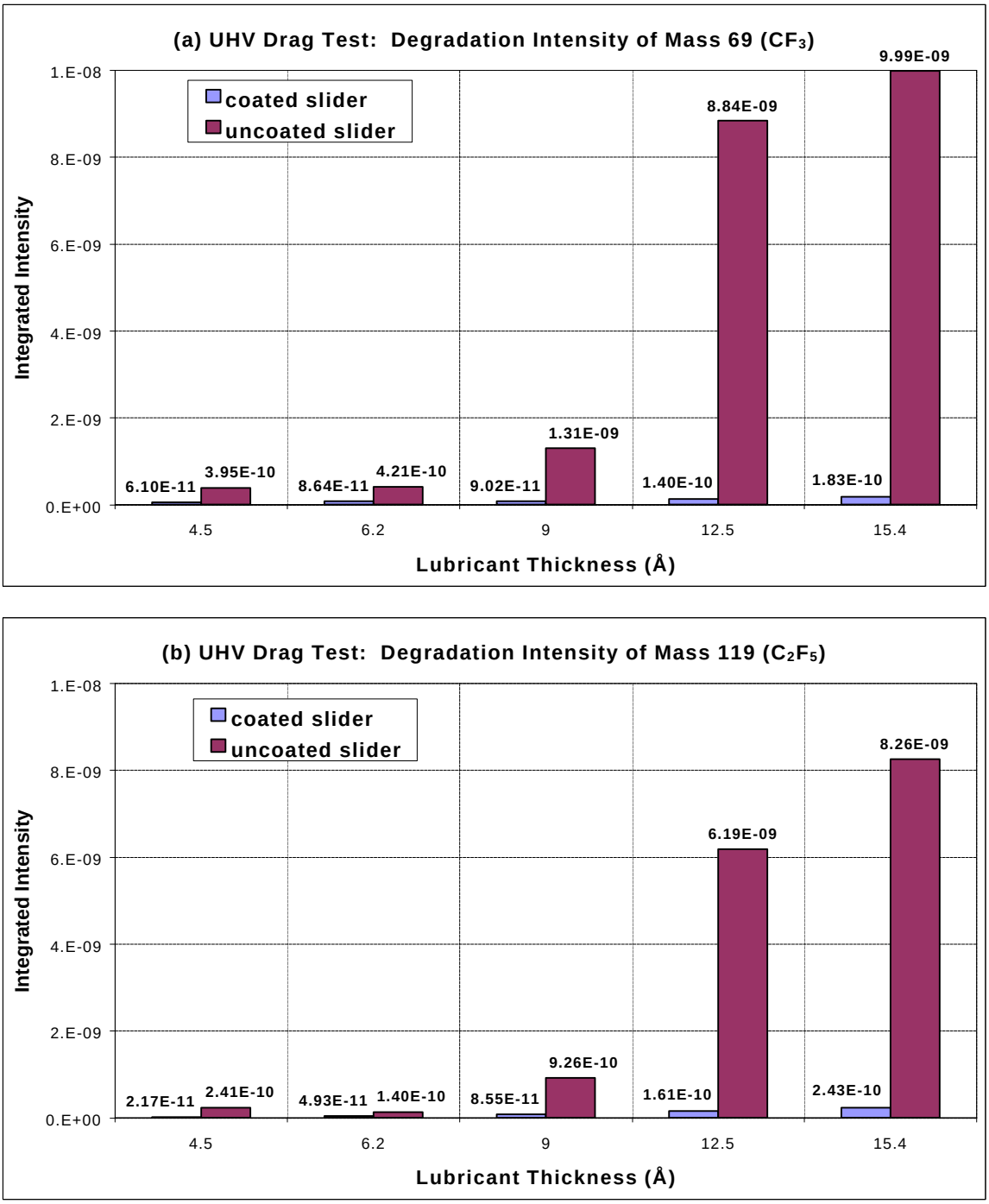

Figure 9.3 Integrated degradation intensity of ZDOL during UHV drag tests on CHx disks with different ZDOL thickness. Two major decomposition fragments occur under catalytic reaction: (a) mass 69 (CF_3), and (b) mass 119 (C_2F_5).

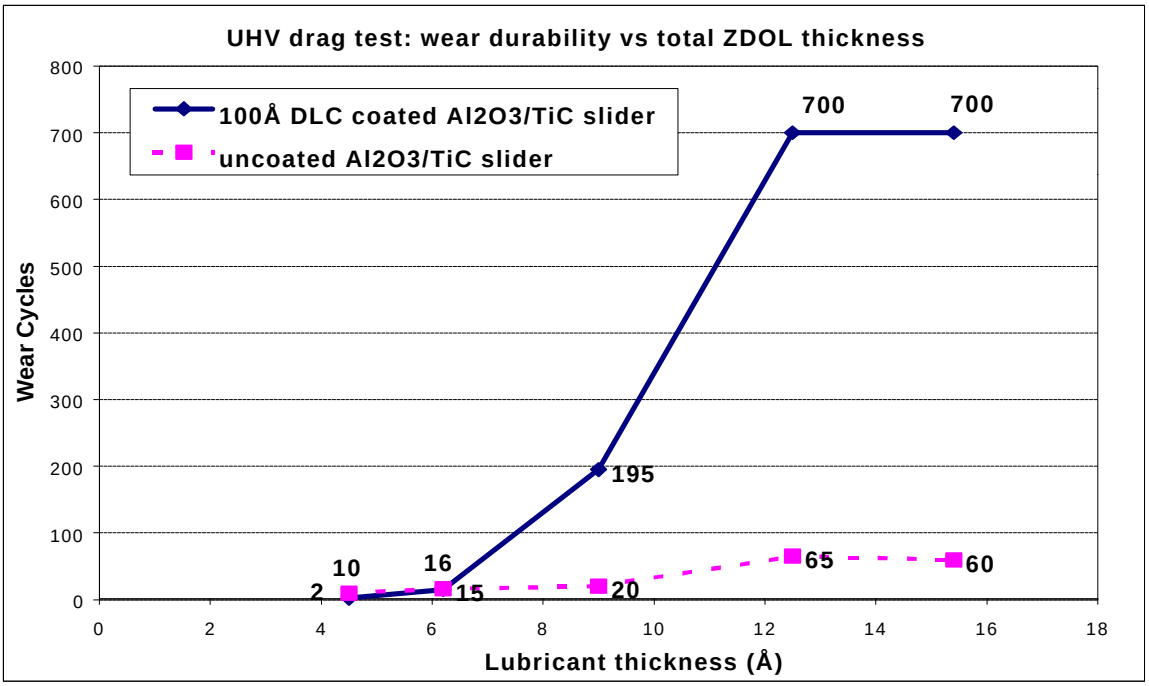

Figure 9.4 Wear durability of CHx disks with different ZDOL thickness during UHV drag tests with DLC coated or uncoated Al_2O_3/TiC sliders.

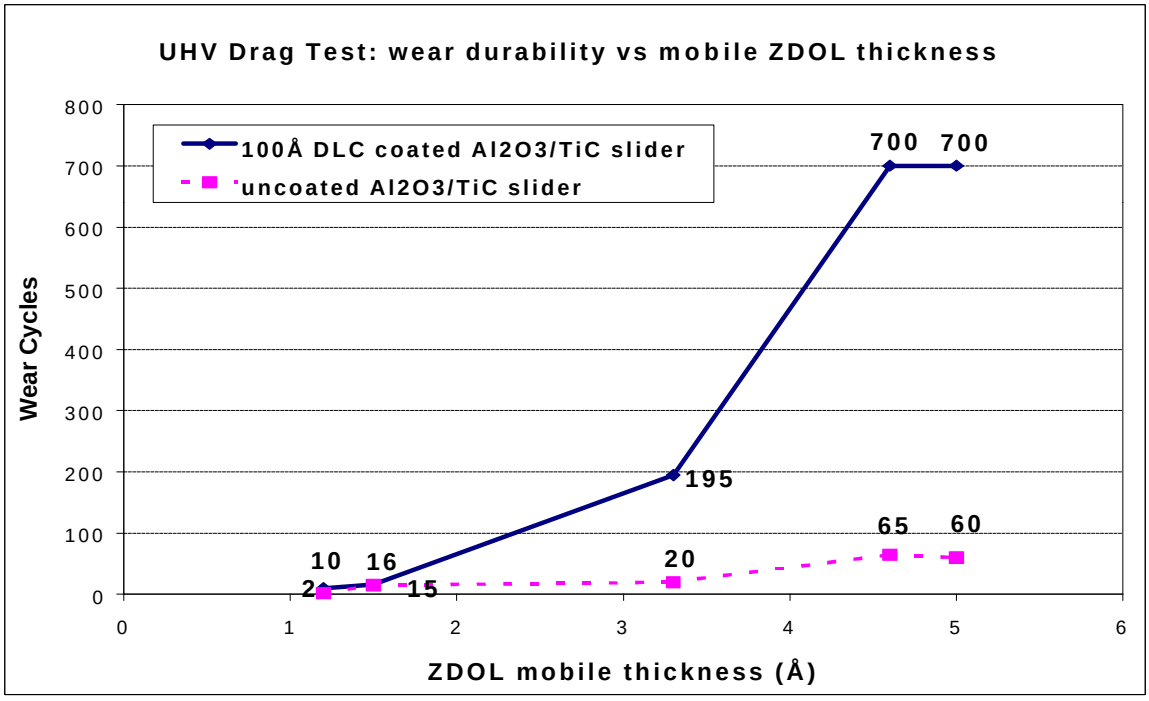

Figure 9.5 Wear durability of CHx disks with different mobile ZDOL thickness during UHV drag tests against DLC coated or uncoated Al_2O_3/TiC sliders.

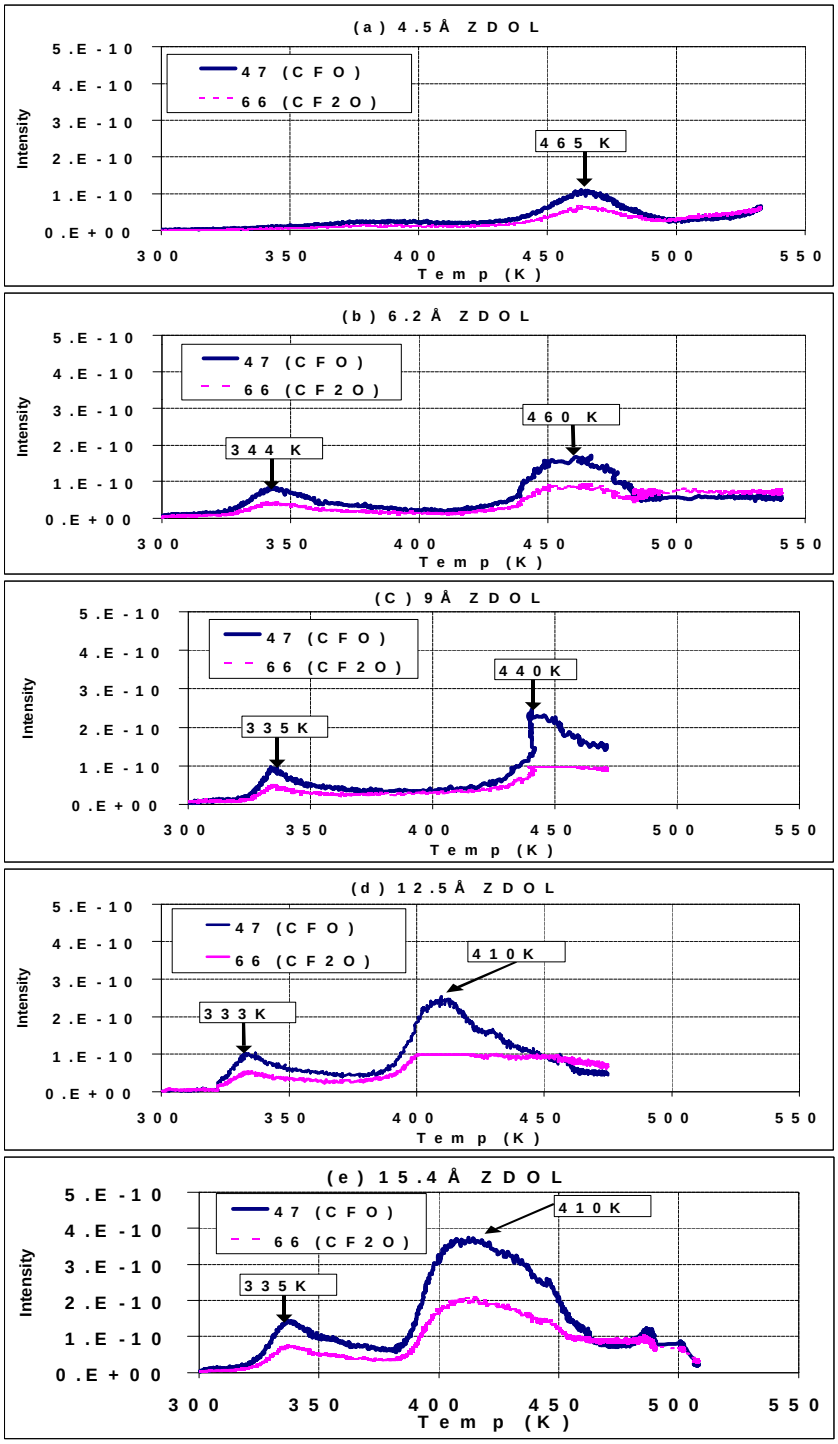

Figure 9.6 History profiles of mass 47 (CFO), and mass 66 (CF_2O) during the thermal desorption tests of CHx disks with ZDOL thickness ranging from 4.5Å to 15.4Å.

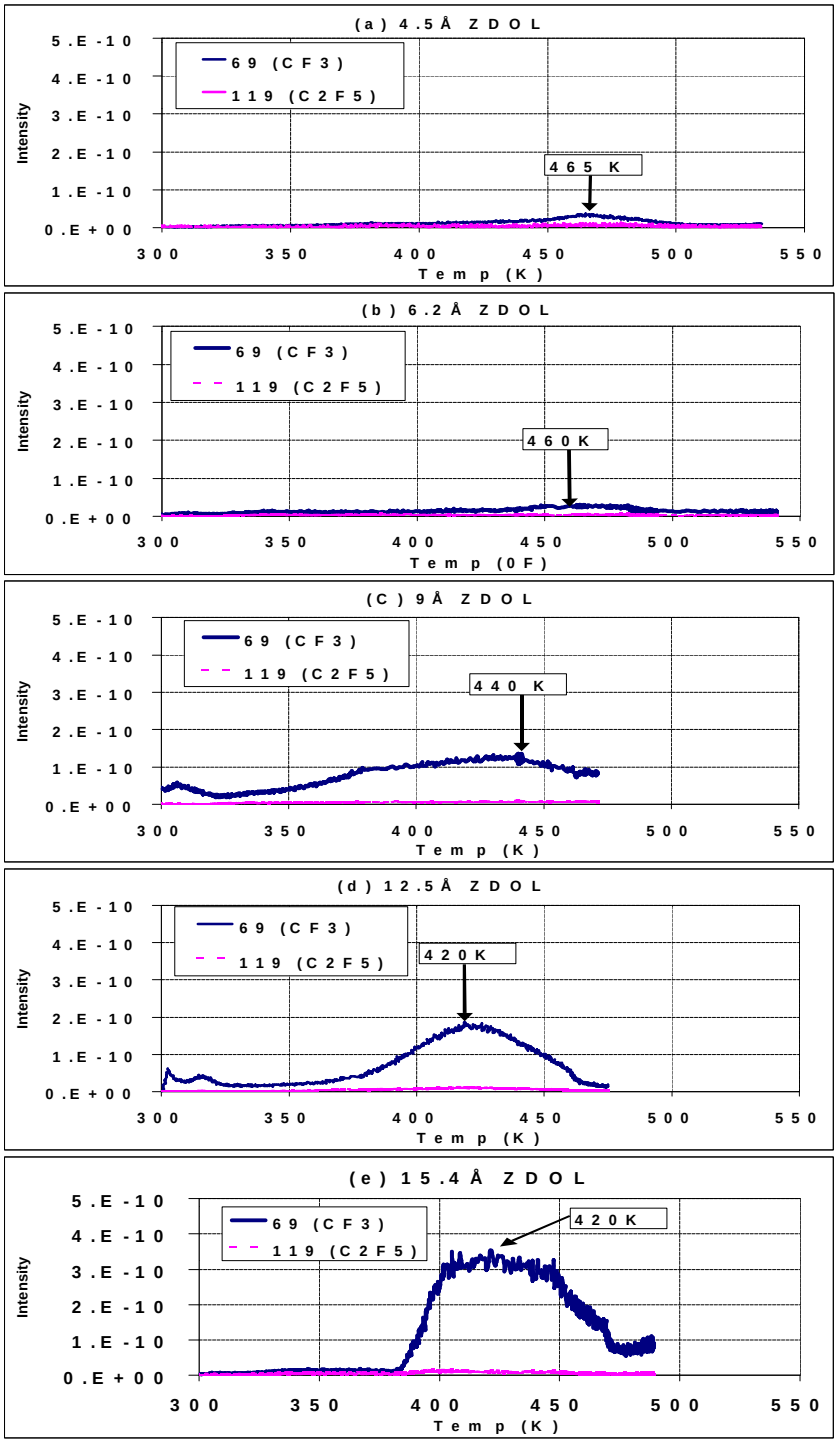

Figure 9.7 History profiles of mass 69 (CF_3), and mass 119 (C_2F_5) during the thermal desorption tests of CHx disks with ZDOL thickness ranging from 4.5Å to 15.4Å.

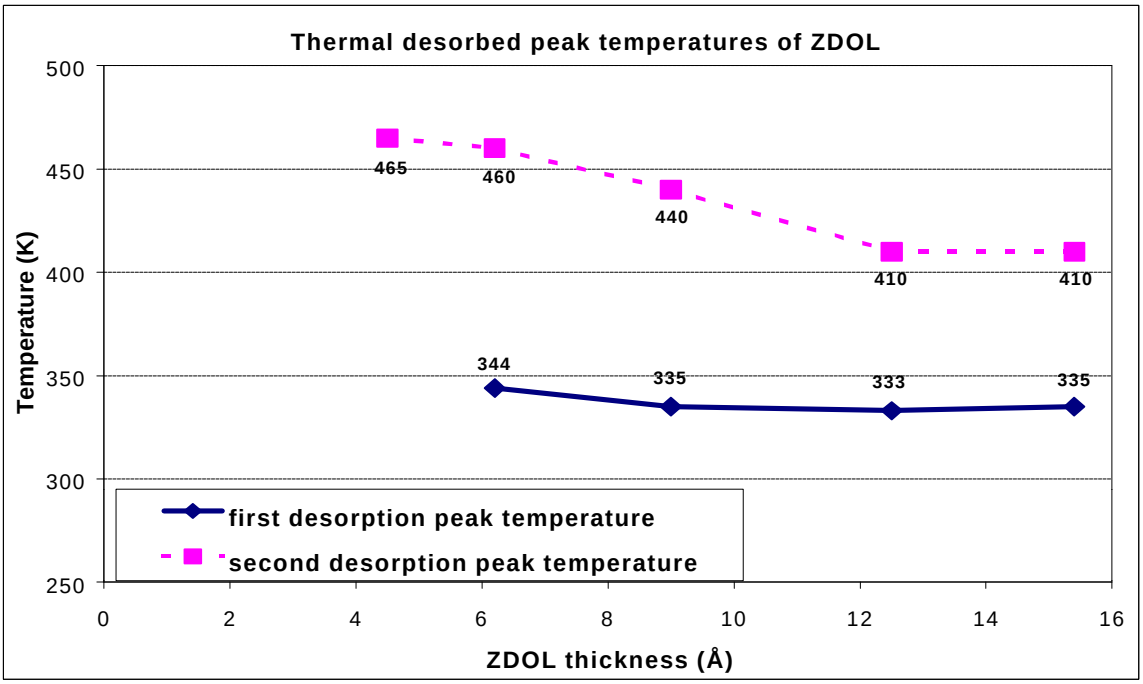

Figure 9.8 Thermal desorption peak temperatures of ZDOL for CHx disks with ZDOL thickness ranging from 4.5Å to 15.4Å.

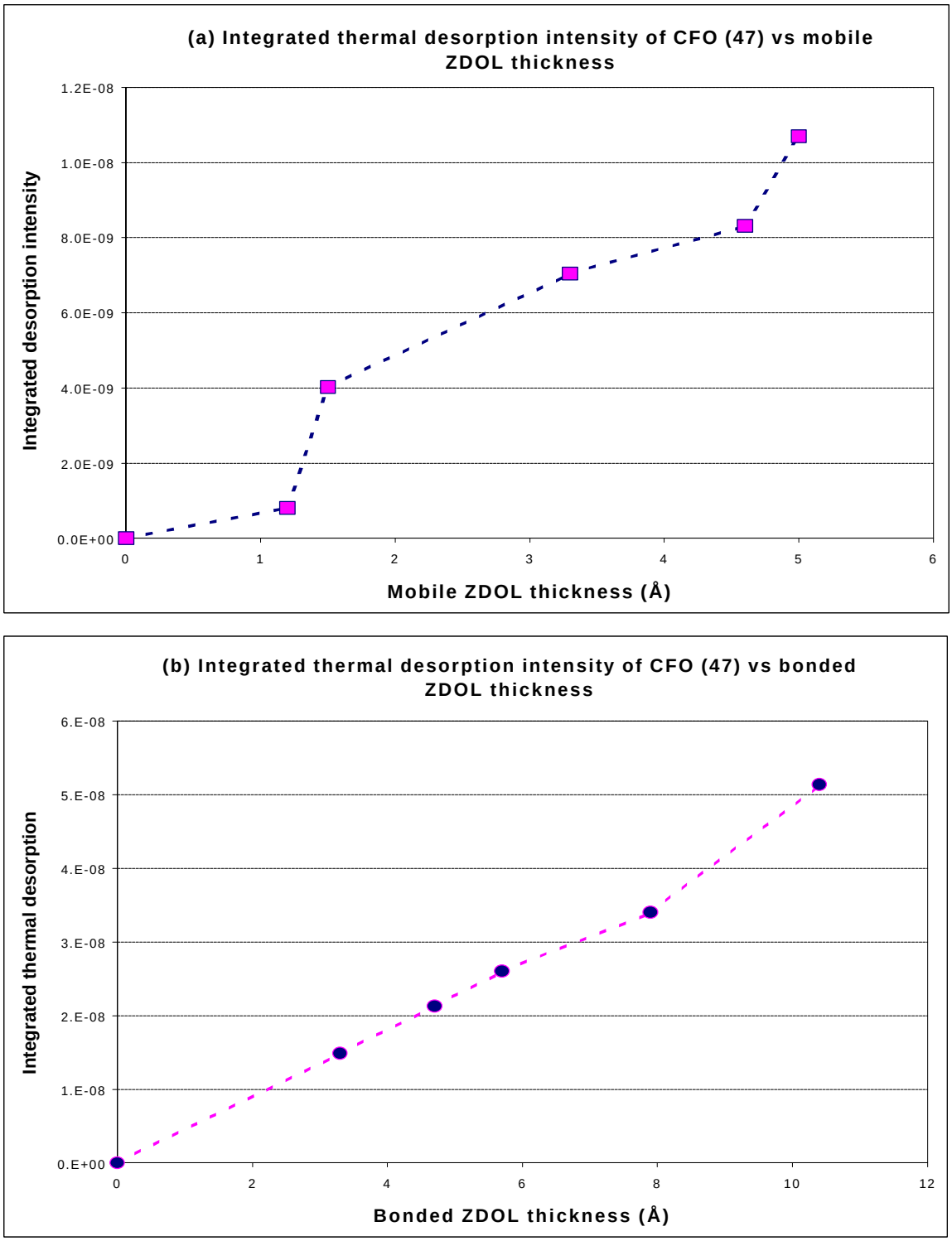

Figure 9.9 Integrated thermal desorption intensity of CFO (47) versus (a) **mobile** ZDOL thickness during the first desorption peak, and (b) **bonded** ZDOL thickness during the second desorption peak.

Chapter 10

EFFECT OF LUBRICANT BONDING FRACTIONS

10.1 Introduction

In chapter 9 we studied the ZDOL thickness effect on the tribological performance of ZDOL on hydrogenated carbon films (CHx). We observed that the wear durability of ZDOL against DLC coated sliders improves considerably when the carbon overcoat surface is fully covered with one layer of ZDOL as compared to less lubricant. This enhanced performance with thicker ZDOL can be attributed to a thicker layer of mobile ZDOL to reflow into the wear track and replenish the lube displaced during dragging. These results illustrate the importance of the mobile ZDOL layer in providing good wear durability. However, the bonded ZDOL layer also interacts strongly with the carbon surface, resulting in a lower removal rate of ZDOL molecules from the carbon surface. Thus, an optimized composition (mobile/bonded) of ZDOL lubricant should provide the best tribological performance at the head-disk interface.

In this chapter, we study the effect of ZDOL bonding on hydrogenated carbon films (CHx) using the ultra-high vacuum (UHV) tribochamber described in Chapter 2. The studies consist of drag tests and thermal desorption experiments in the UHV tribochamber. Samples with a total of 12Å ZDOL lubricant but different mobile fractions were used in this study. We observed that wear durability in slow speed drag tests improves with an increase in the

---

∗ Parts of this chapter have been submitted to J. Chem. Phys [90].

mobile portion.

10.2 Experimental Procedure and Set-up

Drag tests in the UHV tribochamber were conducted with the following parameters: 0.2 m/s drag speed, a load of 30 mN, and a sliding time of 20 minutes. The sliders used were 30% (1.2mm by 1mm) negative-pressure Al_2O_3/TiC sliders with and without amorphous diamond like carbon (DLC) films on the air bearing surfaces. The disks were commercial 95mm super smooth thin film disks with a 75Å amorphous hydrogenated carbon overcoat (CHx). The hydrogen content in the CHx film was 30 atomic percent. The disks were lubricated with ZDOL by a dipping process. FTIR was used by IBM to measure the lubricant thickness of these disks before the UHV drag tests. These FTIR thickness measurements were confirmed by ellipsometry and X-ray reflectivity spectroscopy. After the thicknesses were measured, the disks were washed sequentially in perfluorohexane and 2,3-dihydro-perfluoropentane to remove any soluble lubricant, and then the thickness was remeasured. The lubricant that was retained on these disks is defined as the “bonded” portion, while that removed by the solvent wash process is defined as the “mobile” portion. The resulting thickness of ZDOL on the disks in this study were 12Å but with four different mobile portions (0%, 33%, 67%, and 100%). The molecular weight of the polydisperse ZDOL is 2000 AMU.

For the thermal desorption tests in the tribochamber, a CHx/ZDOL disk was cut into 2 cm x 2 cm squares. The lubricated samples were mounted onto the heater and the temperature was measured by a thermocouple in contact with the heater near the sample. A typical experiment consisted of heating a sample at a rate of 0.2 K/sec starting at room

temperature and stopping before 550 K. A mass spectrum was collected on a computer every two seconds during the heating.

10.3 Results and Discussions

10.3.1 Results from the UHV drag tests

Figure 10.1(a) shows the friction coefficient curves for the 12Å of all bonded ZDOL lubricant. The friction coefficient curves for the 12Å ZDOL disks with different bonded fractions are similar to those in Fig. 10.1(a) and will not be shown here. For the 70Å DLC-coated Al_2O_3/TiC slider, the friction coefficient started at 1 and increased steadily to 1.2 within 40 drag cycles before wear occurred. For the uncoated Al_2O_3/TiC slider, the friction coefficient increased to a peak value of 1.8 immediately and then dropped to 0.5. A wear track was observed on the disk just after the friction coefficient dropped. The above results indicate that 12Å of all bonded ZDOL has little lubricating action against both the uncoated and the DLC-coated Al_2O_3/TiC sliders.

Figure 10.1(b) shows the integrated mass spectra of ZDOL fragments produced at the head-disk interface. The four primary peaks are from mass fragments CFO (47), CF_2O (66), CF_3 (69), and C_2F_5 (119). Again, masses 47 (CFO) and 66 (CF_2O) are the highest peaks in the coated slider case, while masses 69 (CF_3) and 119 (C_2F_5) are the highest peaks in the uncoated slider case.

Figure 10.2 shows the degradation intensity of mass 47 (CFO) during UHV drag tests on CHx disks with different ZDOL bonded fractions. The degradation intensity of the frictional fragment 47 (CFO) increased as the bonded fraction decreased for both the uncoated and coated slider cases. This suggests that an important role of the mobile ZDOL

layer is to replenish the lube displaced during dragging. With a larger mobile portion, more lubricant reflows into the test track. Thus, more material is decomposed, resulting in the stronger degradation intensity.

Figure 10.3 shows the wear durability of these CHx disks as a function of ZDOL bonded fraction. With DLC coated sliders, the wear durability significantly improved when the lubricant mobile fraction increased. These results demonstrate the benefits of using more mobile ZDOL - a reflow of the lubricant into the wear track provides more material to be decomposed so the carbon overcoat surface is protected for a longer duration against sliding. As the mobile portion increases, the replenishment rate also increases. As a result, faster replenishment of the lubricant occurs on disks with more mobile ZDOL on the protective carbon surface which enhances the wear durability of the interface. However, there was no benefit in using more mobile lubricant for the uncoated slider cases. Strong catalytic reactions occurred with the uncoated slider during dragging, resulting in the very poor tribological performance for every case.

10.3.2 Results from UHV thermal desorption tests

In this section, we present and discuss the results from UHV thermal desorption experiments. Figure 10.4 shows the thermal desorption profiles for mass 47 (CFO) of CHx disks with different ZDOL bonded fractions at a heating rate of 0.2 K/sec. Two thermal desorption peaks were found during these experiments: one is between 350 K and 400 K, and the other is between 425 K and 500 K. In chapter 9, we concluded that most of the mobile lubricant is desorbed at the first thermal desorption peak, while the bonded lubricant portion increased due to the annealing effect of temperature during the first period. These results are

similar to those found by Waltman et al. [46, 84]. They found that the initially applied mobile ZDOL is depleted via evaporative loss as well as bonding of the lubricant to active sites on the carbon surface at elevated temperatures above 320 K. The initially applied lubricant is thermodynamically unstable during the thermal desorption process. As a result of the intramolecular motion within the ZDOL polymer on the surface, the free hydroxyl endgroups of the mobile lubricant pass through orientations favorable for bonding. Since transitions from the mobile state to the bonded state are thermodynamically driven by the decrease in the free energy associated with this transition, the bonded lubricant present on the surface increases with increasing temperature during the first desorption period. In Fig. 10.4 we also observed that more mobile lubricant was desorbed during the first period with an increasing mobile portion, while more bonded lubricant was desorbed during the second period as the bonded portion increased. In addition, for the pure mobile ZDOL case, some mobile lubricant became bonded lubricant during the first period and then desorbed during the second period. For the pure bonded ZDOL case, very little was desorbed during the first period. Thus, we can conclude that only the mobile ZDOL layer is desorbed during the first thermal desorption period and the residual bonded ZDOL layer is desorbed during the second thermal desorption period.

Moreover, the temperature at the first peak, which is attributed to the desorption of the mobile ZDOL layer, remains almost constant as a function of ZDOL thickness. This result indicates that the desorption energy of the mobile ZDOL layer is independent of the lubricant thickness. However, the temperature of the second peak, corresponding to the desorption of bonded ZDOL, shifts to a lower temperature with increasing ZDOL bonded portion as shown in Fig. 10.5. This result indicates that the desorption energy of bonded

lubricant decreases with increasing bonded lubricant thickness. One possible explanation is that the surface of the amorphous carbon is populated with sites of different interaction strengths, where stronger bonding sites are associated with higher binding energy [30]. When ZDOL molecules adsorb on the surface, they first occupy the stronger sites (sites with higher desorption energy). As more ZDOL molecules (thicker lubricant) are adsorbed, weaker sites (sites of lower desorption energy) are occupied. Thus, for samples with lower bonded portions the second peak temperature is higher, and it is lower for higher bonded fractions. These results are similar to those of the lubricant thickness study in chapter 9. We observed that the second peak temperature is lower for thicker lubricant due to thicker bonded lubricant.

10.4 Conclusion

The UHV drag tests show that the lubricant interaction with the carbon overcoat varies as a function of the fraction of bonded lubricant. The wear durability of disks with DLC-coated sliders improves with increased mobile lube fraction because the lubricant provides a reservoir to constantly replenish the ZDOL displaced in the wear track during the drag tests. However, there was no benefit found by using a larger mobile portion for the uncoated slider cases. Strong catalytic reactions occurred with the uncoated sliders and these catalytic reactions counteracted the benefits of using a larger mobile fraction.

Based on the results from the thermal desorption experiments, we conclude that only the mobile ZDOL lubricant was desorbed at the first thermal desorption peak (between 350 K and 400 K), and the residual bonded ZDOL lubricant was desorbed at the second thermal desorption peak (between 425 K and 500 K). Moreover, the temperature of the second peak,

corresponding to the desorption of the bonded ZDOL, shifts to a lower temperature with increasing bonded ZDOL thickness.

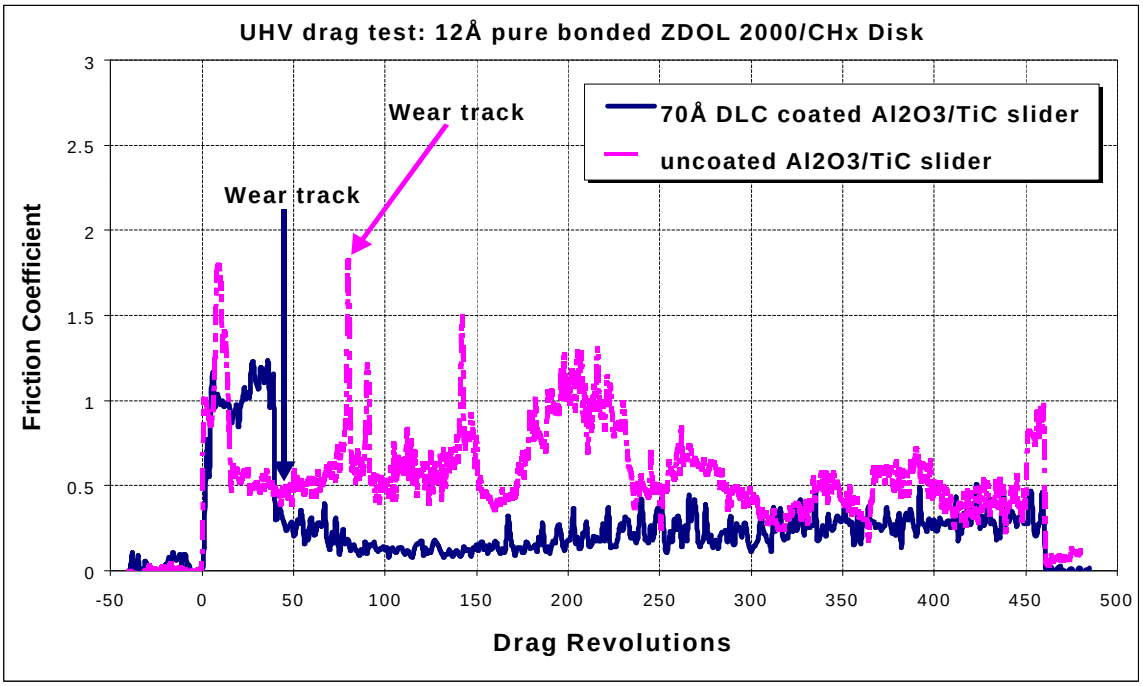

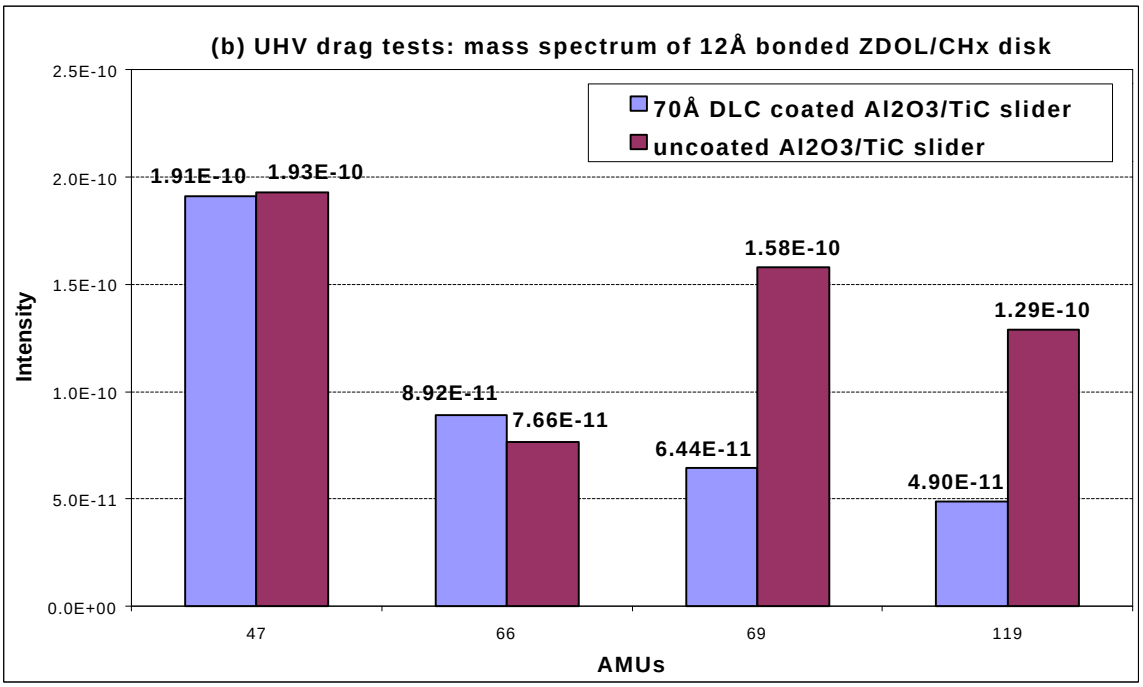

Figure 10.1 (a) friction coefficient of UHV drag test with 12Å pure bonded ZDOL lubricated disk; (b) mass spectrum of four major ZDOL decomposition fragments.

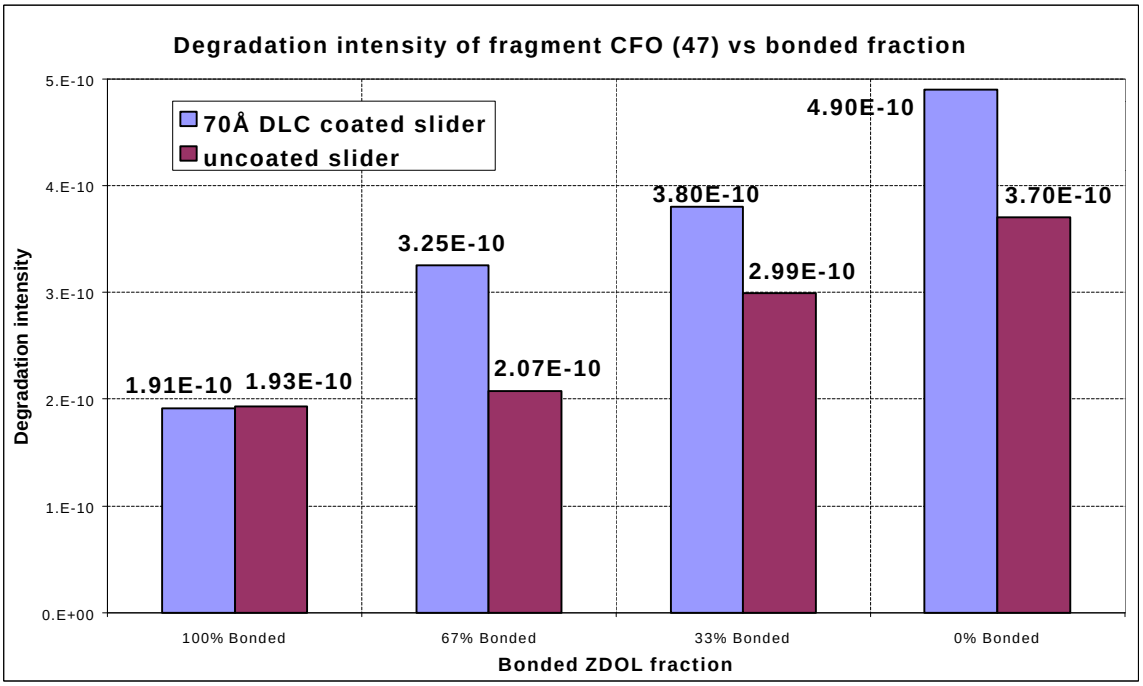

Figure 10.2 Integrated degradation intensity of ZDOL fragment CFO (47) during UHV drag tests on CHx disks with different ZDOL bonded fractions.

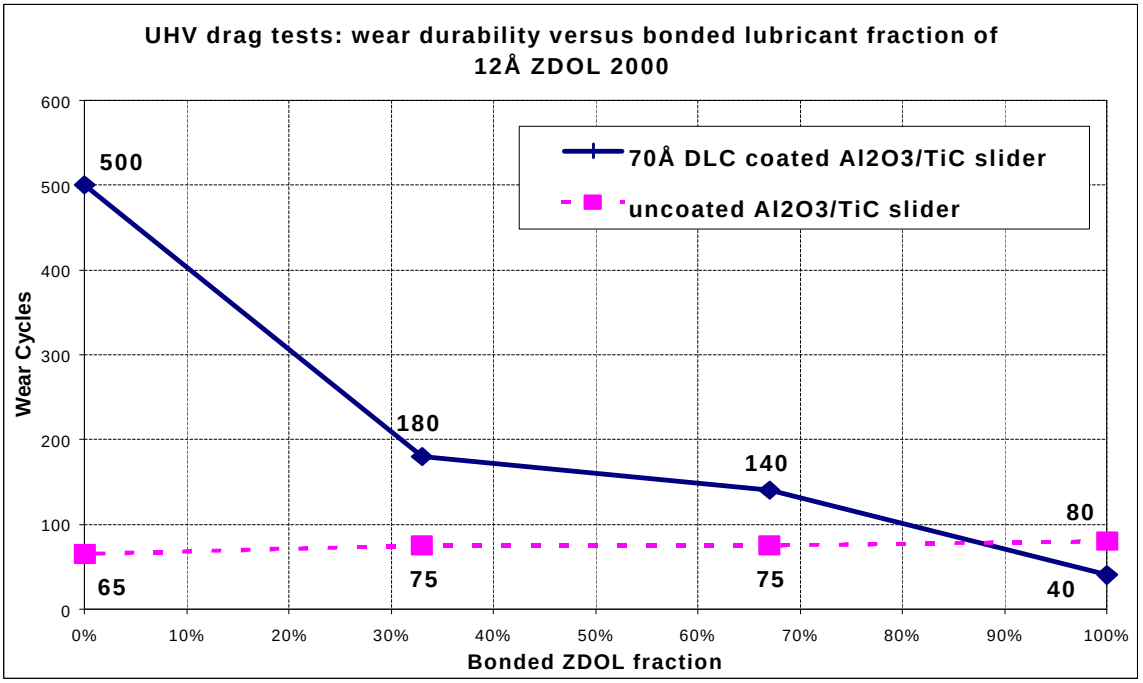

Figure 10.3 Wear durability of CHx disks with different ZDOL bonded fractions during UHV drag tests against coated and uncoated Al_2O_3/TiC sliders.

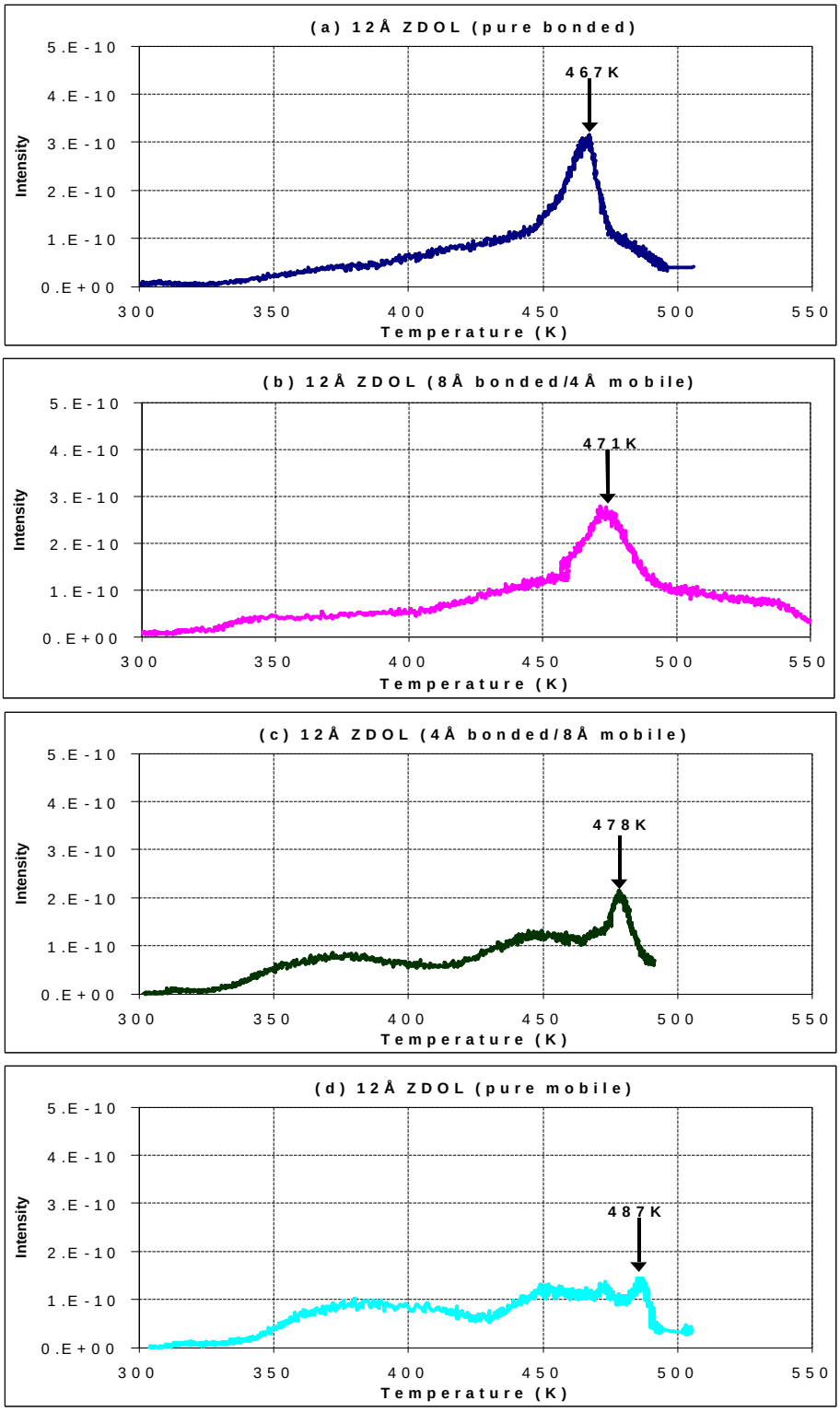

Figure 10.4 Thermal desorption history profiles of mass 47 (CFO) during thermal desorption tests on CHx disks with different ZDOL bonded fractions.

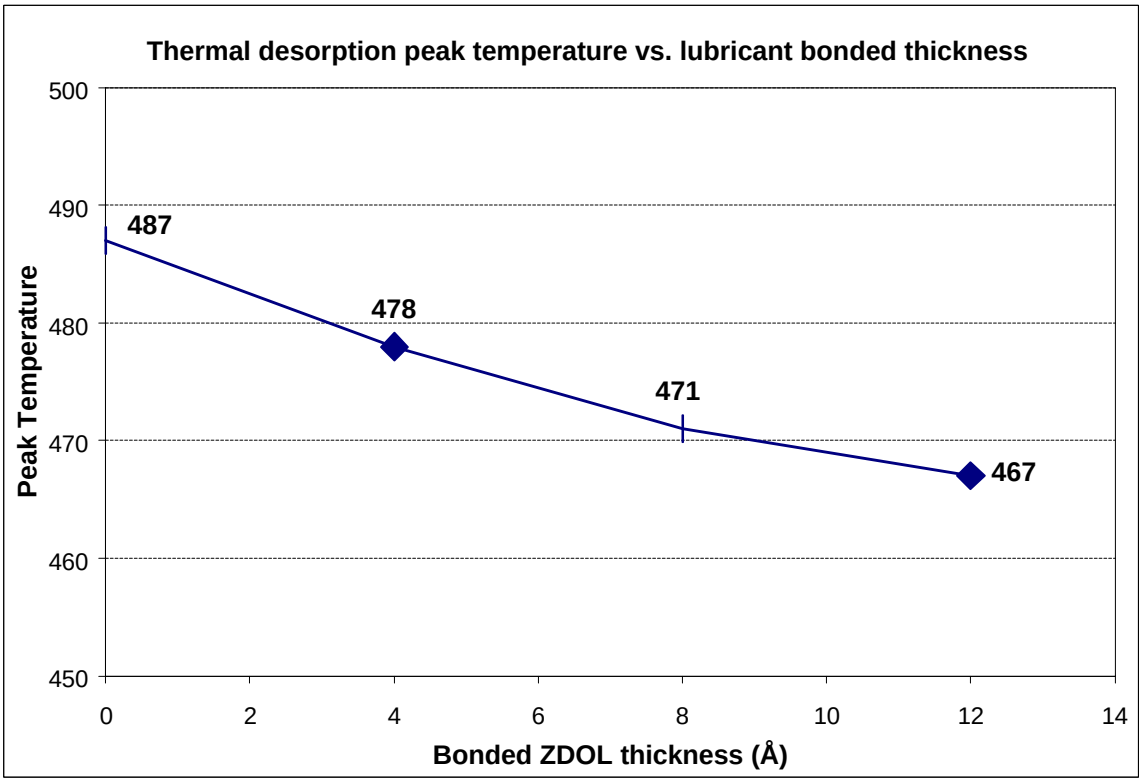

Figure 10.5 Thermal desorption peak temperatures of ZDOL for CHx disks with different ZDOL bonded fractions.

Chapter 11

Conclusions

For higher recording density systems where the spacing between the head and the disk will be closer, it is important to control the tribological properties such as friction, wear and adhesion. These tribological phenomena are caused by contact of microscopic asperities and can be improved by lubrication. In such a system, the lubricant film tends to thin out so the lubricant plays an important role in sustaining durability at the head-disk interface. Therefore, in order to control the tribological properties, it is essential to know the lube decomposition mechanisms and lube interactions with the carbon surface during contact sliding.

In this dissertation, the research focus is on the decomposition mechanisms of the PFPE lubricants in order to improve the wear durability of disks and sliders during their contact. The interactions of the PFPE lubricant with the carbon overcoats are investigated in terms of overcoat content, lube backbone, lube endgroup, lube additive, lube molecular weight, lube thickness, and lube bonded fraction.

Two decomposition mechanisms of PFPE lubricants are studied: one is frictional scission/thermal action, and the other is the catalytic reaction. Carbon coatings on the slider air bearing surfaces significantly improve the wear durability by preventing the catalytic reactions at the head-disk interface. The absence of a carbon coating led to a more complex catalytic decomposition mechanisms of ZDOL: (1) initial friction decomposition of ZDOL and degradation of CH_x to form gaseous products such as CF_2O and H_2; (2) reaction of these

products with H_2 to produce HF and CF_2H; (3) production of AlF_3 when CF_2O and HF react with Al_2O_3, followed by rapidly decomposition of ZDOL.

The thermal stability of PFPE lubricants and their thermal desorption mechanisms are also studied. It is found that the mass spectrum of mobile ZDOL is very similar to the mass spectrum obtained from sliding at the carbon-coated slider/CHx disk interface. These results illustrate that frictional heating is the primary decomposition mechanism of ZDOL in the carbon-coated slider/CHx disk case.

The hydrogen evolution from the CHx overcoat initiates lubricant catalytic decomposition with an uncoated Al_2O_3/TiC slider, forming CF_3 (69) and C_2F_5 (119). The generation of hydroflouric acid (HF) during the thermal desorption experiments provides the formation mechanism of Lewis acid, which is the necessary component for catalytic reaction causing ZDOL lube degradation. On the other hand, for CNx films, catalytic reactions were prevented with an uncoated slider due to less hydrogen evolution from the CNx overcoat, resulting in a better tribological performance for the CNx film as compared to the CHx film.

A good lubricant should have one active endgroup and one non-active endgroup. The active one enhances lubricant's adsorption onto the carbon surface and reduces the removal rate of the lubricants during the contact sliding. In the other hand, the non-active one prevents the catalytic decomposition in the presence of the Al_2O_3 surface of the uncoated slider.

The studies also demonstrate that the catalytic degradation process of ZDOL in the presence of Lewis acid occurs most readily at the acetal units (-O-CF_2-O) within the internal backbones (CF_2O and CF_2CF_2O) instead of the endgroup functionals. Therefore, Demnum,

without any acetal units, experiences less catalytic degradation with the uncoated Al_2O_3/TiC sliders as compared to ZDOL.

X-1P additive increases the mobility of AM3001 lubricant – more material reflowed into the wear track to protect the carbon overcoat surface for a longer duration against sliding. It is believed that X-1P molecules preferentially occupied the bonding sites on the carbon surface. Therefore, less ZDOL molecules could be bonded to the carbon surface, resulting in the faster mobility. In addition, the catalytic reaction associated with uncoated Al_2O_3/TiC sliders is prevented by using X-1P as an additive in ZDOL. X-1P passivates the catalytic activity of Al_2O_3 – the activity centers (Lewis acid) of Al_2O_3 are passivated by the nucleophilic (Lewis base) attack of the X-1P phosphazene ring. The usefulness of X-1P as an additive in ZDOL results from its ability to cover the catalytically active Al_2O_3 surface on the head, thus preventing the catalytic decomposition of ZDOL lubricants.

Studies are carried out to investigate the lubricant molecular weight effect on the tribological performance by testing fractionated ZDOL. With higher molecular weight, the poor mobility causes higher viscosity and higher friction. However, the degradation rate is slower with higher molecular weight. In addition, the thermal desorption temperatures increase with increasing molecular weight. The desorption temperatures of polymers are believed to depend on three mechanisms: (1) the internal mobility of the chains; (2) the chain length; and (3) the cohesive energy.

The wear durability of ZDOL against DLC coated sliders improves considerably when the carbon overcoat surface is fully covered by at least one layer of ZDOL. This enhanced performance with thicker ZDOL can be due to two mechanisms: (1) full coverage of the carbon surface with ZDOL, and (2) a thicker layer of mobile ZDOL to reflow into the

wear track. In the sub-monolayer regime, adhesion of the lubricant to the carbon overcoat is much stronger since it requires a much higher temperature to desorb the lubricant molecule. When the lubricant thickness is around or above a monolayer, cohesion among the lubricant molecules plays a greater role and a much lower temperature is needed for lubricant desorption.

The wear durability of disks with DLC-coated sliders improves with increased mobile lube fraction because the lubricant provides a reservoir to constantly replenish the ZDOL displaced in the wear track during the drag tests. Based on the results from the thermal desorption experiments, we conclude that only the mobile ZDOL lubricant was desorbed at the first thermal desorption peak (between 350 K and 400 K), and the residual bonded ZDOL lubricant was desorbed at the second thermal desorption peak (between 425 K and 500 K). Moreover, the temperature of the second peak, corresponding to the desorption of the bonded ZDOL, shifts to a lower temperature with increasing bonded ZDOL thickness.

Based on the above studies, the conclusion can be made that the tribochemistry at the head-disk interface plays a very important role in affecting the friction and wear at the interface. In order to understand the tribological issues at the head-disk interface, combined studies from both mechanical and chemical aspects should be carried out.

REFERENCES

[1] Petroff N.P., "Friction in Mechines and the Effect of the Lubricant", Eng. Journ. St. Petersburg, Vol. 1, pp71-140; Vol. 2, pp227-279; Vol. 3, pp377-436; Vol. 4, pp435-464, (1883).

[2] Tower, B., "First Report in Friction Experiments", Proc. Inst. Mech. Eng., pp623-666, (1883); "Second Report", pp58-70, (1885).

[3] Reynolds, O., "On the Theory of Lubrication and its Application to Mr. Beauchamp Tower's Experiments Including an Experimental Determination of the Viscosity of Olive Oil", Phil. Trans., Vol. 177 91), pp157-234, (1886).

[4] Kingsbury, A., "Experiments with Air Lubricated Bearing", Journ. Of Amer. Soc. Of Naval Engrs., Vol. 9, (1897).

[5] Harrison, W.J., "The Hydrodynamic Theory of Lubrication with Special Reference to Air as a Lubricant", Trans. Camb. Phil. Soc., Vol. 22, No. 3, pp39, (1913).

[6] Reyleigh, Lord, "Notes on the Theory of Lubrication", Phil. Mag., Vol. 35, No. 1, (1918).

[7] C. Mathew Mate, "Quantifying How Lubricants Are Pushed arounf on Disk Surfaces", 10th Annual Symposium on Information Storage and Processing Systems, (1999).

[8] Murat U. Guruz, Y.-H. Yu, V.P. Dravid, Y.-W. Chung, M. Lacerda, and C.S. Bhatia, "Synthesis and Corrosion Performance of Ultrathin Carbon Nitride Overcoats", Procedings of the Symposium on Interface Technology towards 100 Gbit/in^2, (1999).

[9] Steven W. Meeks, Walter E. Weresin, and Hal J. Rosen, “Optical Surface Analysis of the Head-Disk-Interface of Thin Film Disks” ASME Tribology Trans., Vol. 117, pp112-118, (1995).

[10] Fred W. Billmeyer, “Textbook of Polymer Science”, John Wiley & Sons, Inc., pp122-124, (1971).

[11] Jen Chiu, “Applications of Thermogravimetry to the Study of High Polymers”, Appl. Poly. Symp. 2, pp25-43, (1966).

[12] Gerald W. Miller, “The Thermal Characterization of Polymers”, Appl. Poly. Symp. 10, pp35-72, (1969).

[13] M.J. Stirniman, S.J. Falcone, and B.J. Marchon, “Volatility of Perfluoropolyether Lubricants Measured by Thermogravimetric Analysis”, Tribology Letters 6, pp199-205, (1999).

[14] Pacansky J. and Waltmann R. J., “Electron Beam Irradiation of Polyperfluoroethers: Experimental Analysis of Main-chain Degradation”, Chem.Mater. 5, pp486-494, (1993).

[15] Vurens G., Zehringer R. and Saperstein D., “The Decomposition Mechanisms of Perfluoropolyether Lubricants during Wear”, Surface Science Investigations in Tribology, Chung Y.W., Homola A. M. and street B., Eds, Washington, D. C.: American Chemical Society, pp169-180, (1992).

[16] M.J. Zehe and O. O. Faut, “Acid Attack of Perfluorinated Alkyl Ether Lubricant Molecules by Metal Oxide Surfaces”, Tribology Trans., 33, pp634-640, (1990).

[17] P.H. Kasai, “Degradation of Perfluoropolythers Catalyzed by Lewis Acids”, Adv. Info. Storage Syst. 4., pp291-314, (1992).

[18] A. Steritwieser, and C. H. Heathcock, “Introduction to Organic Chemistry”, Macmillan Publishing Co., Inc., New York, (1976).

[19] D. Sianesi, V. Zamboni, R. Fontanelli, and M. Binaghi, “Perfluoropolythers: Their Physical Properties and Behavior at High and Low Temperatures”, Wear, 18, pp85-100, (1971).

[20] Jong-Liang Lin, C. Singh Bhatia, and John T. Yates, Jr., “Thermal and Electron-simulated Chemistry of Fomblin-ZDOL Lubricant on a Magnetic Disk”, J. Vac. Sci. Technol. A 13(2), pp163-168, (1995).

[21] J.L. Vossen and W. Kern, “Thin Film Process”, Academic Press, pp416-417, (1978).

[22] P.J. John and J. Liang, “Initial Metal Fluoride Formation at Metal/Fluorocarbon Interfaces”, J. Vac. Sci. Technol. A, Vol. 12, pp199-203, (1994).

[23] R.J. Berry, J.N. Cutler, B.E. Ream, J.W. Bozzelli, and R.J. Waltman, “An AB Initio Investment of the Unimolecular and AlF_3 Catalyzed Decomposition of Perfluorodimethyl Ether”, submitted to J. Phys. Chem., 1998.

[24] J. Pacansky and R.J. Waltman, “The Effect of Lewis Acid Catalysis on the Decomposition of CF_3OCF_3 to COF_2 and CF_4”, J. Fluorine Chemistry, Vol.83, pp41-45, (1997).

[25] R.J. Waltman, “A Computer Modeling Study on the Interaction of –(CF2CF2O)-Polyperfluorinated Ethers with Lewis Acid Sites: Perfluorodiethyl Ether”, J. Fluorine Chemistry, Vol. 90, pp9-16, (1998).

[26] B. D. Strom and D. B. Bogy, “Gaseous wear products from perfluoropolyether lubricant films”, Wear, 168, pp31-36, (1993).

[27] W.R. Jones, Jr., K. J. L. Paciorek, T.I. Ito, and R. H. Kratzer, Industrial and Engineering Chemistry Production Research, pp166, (1983).

[28] L.S. Helmick and W.R. Jones, Jr., "NASA Tech. Mem. 102", p493, (1990).

[29] M.J. Zehe and O. D. Faut, "NASA Tech. Mem. 101", p962 (1989).

[30] P.H. Kasai, W.T. Tang and P. Wheeler, "Degradation of Perfluopolyethers Catalyzed by Alumina Oxide", Appl. Surf. Sci. 51, pp201-211, (1991).

[31] G. H. Vurens and C. M. Mate, "The Thermal Stability of Perfluoropolythers on Carbon Surfaces", Applied Surface Science, 59, pp281-287, (1992).

[32] Laura Cornaglia and Andrew J. Gellman, "Fluoroether Bonding to Carbon Overcoats", J. Vac. Sci. Technol. A 15(5), pp2755-2765, (1997).

[33] Scott S. Perry, Philip B. Merrill and Hyun I. Kim, "Comparative Studies of Perfluorinated Lubricants Adsorbed on Hydrogenated Amorphous Carbon and Amorphous Carbon Nitride", Tribology Letters 2, pp393-404, (1996).

[34] C.M. McC. Ettles, "Possible Flash Temperatures in Slider and Recording Disk Transient Contact", ASLE Transactions, Vol. 29, pp321-328, (1986).

[35] Shouji Suzuki, and Francis E. Kennedy, Jr., "Friction and Temperature at Head-Disk Interface in Contact Start/Stop Tests", Tribology and Mechanics of Magnetic Storage Systems, Vol. V, pp30-36, (1990).

[36] T.E. Karis, V.J. Novotny, and R.D. Johnson, "Mechanical Scission of Perfluoropolyethers", J. Applied Polymer Science, Vol. 50, pp1357-1368, (1993).

[37] X. H. Yun, D. B. Bogy, and C. S. Bhatia, "Tribochemical Study of Hydrogenated Carbon Coatings with Different Hydrogen Content Levels in Ultra High Vacuum", J. Tribology, 119, pp437-443, (1997).

[38] R. Wang, S. W. Meeks, R.L. White, and W.E. Weresin, “The Effect of Hydrogen in Carbon Overcoats on the Tribology of the Head-Disk Interface”, IEEE Trans. Magn. 31, pp2919-2921, (1995).

[39] Jianjun Wei, Walton Fong, D. B. Bogy and C. S. Bhatia, “The Decomposition Mechanisms of a Perfluoropolyether at the Head/Disk Interface of Hard Disk Drives”, Tribology Letters, Vol. 5, pp203-209, (1998).

[40] Chao-Yuan Chen, Jianjun Wei, Walton Fong, D.B. Bogy, and C. Singh Bhatia, “The Decomposition Mechanisms and Thermal Stability of ZDOL Lubricant on Hydrogenated Carbon Overcoats”, CML Technical Report No. 98-016, Journal of Tribology, in press.

[41] Chao-Yuan Chen, Walton Fong, D.B. Bogy, and C. Singh Bhatia, “Initiation of Lubricant Decomposition by Hydrogen Evolution from Contact Sliding on CHx Overcoats”, CML Technical Report No. 99-011, submitted to Tribology Letters.

[42] D. B. Bogy, X. H. Yun, and B. J. Knapp, “ Enhancement of Head-Disk Interface Durability by Use of DLC Overcoats on the Slider’s Rails”, IEEE Trans on Magnetics, Vol. 30, No.5, pp369-373, (1994).

[43] E. Cutiongco, D. Li, Y.W. Chung, and C. S. Bhatia, “Tribological Behavior of Amorphous Carbon Nitride Overcoats for Magnetic Thin-Film Rigid Disks”, ASME J. Tribology, Vol. 118, pp543-552, (1996).

[44] D. Li, Y-W Chung, M-S Wong, and W.D. Sproul, “Mechanical Properties of Amorphous Carbon Nitride Thin Films Prepared by Reactive Magnetron Sputter-Deposition”, Tribology Letters, Vol.1, pp87-93, (1995).

[45] X. Yun, R. C. Hsiao, and D. B. Bogy, “Hardness and Tribochemical Evaluation of Ultra-Thin CHx and CNx Overcoats”, IEEE Trans. Magn., Vol.33, pp938-943, (1997).

[46] G.W. Tyndall, R.J. Waltman, and D.J. Pocker, “Concerning the Interactions between ZDOL Perfluoropolyether Lubricant and an Amorphous-Nitrogenated Carbon Surface”, Langmuir, Vol.14, pp7527-7536, (1998).

[47] White, R.L., “RF-Sputtered Amorphous CNx for Contact Recording Applications”, J. Tribology, Vol. 6, (1996).

[48] G. H. Vurens and C. M. Mate, “The Thermal Stability of Perfluoropolythers on Carbon Surfaces”, Applied Surface Science, 59, pp281-287, (1992).

[49] Waltman, R.J., Tyndall, G.W., Pacansky, “Computer-Modeling Study of the Interactions of ZDOL with Amorphous Carbon Surfaces”, J., Langmuir, Vol. 15, (1999).

[50] S.C. Bhatia, W. Fong, Chao-Yuan Chen, J.Wei, D. Bogy, S. Anders, T.Stammler, and J. Stohr, "Tribochemistry at the head/disk interface", published in IEEE Transactions on Magnetics, Vol. 35, No. 2, pp910-915, March 1999

[51] Waltman, R.J., Zhang, H., Khurshudov, A., Pocker, D., Karplus, M., York, B., Xiao, Q.-F., Zadoori, H., Thiele, J.-U., and Tyndall, G.W., “The Effect of Carbon Overcoat Thickness on the ZDOL Boundary Lubrication Film”, proceedings of the symposium on Interface Technology towards 100 Gbit/in^2, (1999).

[52] Chao-Yuan Chen, Walton Fong, David Bogy, C.S. bhatia, P. Kasai, “Effects of Backbone and Endgroup on the Decomposition Mechanisms of PFPE Lubricants and their Tribological Performance at the Head-Disk Interface”, CML Technical Report 99-023, ready for submission.

[53] Chao-Yuan Chen, Walton Fong, David Bogy, and C. Singh

of Monodispersed ZDOL with Hydrogenated Carbon Overcoats", CML Technical

[54] D. Sianesi, A. Fontanelli, G.C. Bernardi, and G.

"Perfluoropolyethers by Fluoroolefins", La Chim. E.

pp208-221, (1973).

[55] Y. Perfluorinated

Polyethers",

[56] Ping Li, Elisa Munro, and Lily M. Ng, "Adsorption and Reaction

Mechanism of $_2O$, TiO_2 $_2$ surfaces: Implications for

[57] S. Mori and W. Morales, "Tribological Reactions of Polyether Oils

with Stainless Steel under Ultra High Vacuum Conditions at Room Temperature", Wear

[58] P.H. Kasai and P. Wheeler, "Degradation of Perfluoropolyethers Catalyzed by

Appl. Surf. Sci. 52, pp91-106, (1991).

Perfluoropolyethers: Intramolecular Disproportionation",

[60] P.H. Kasai, "Degradation of Perfluoropoly(ethers) and Role of X-1P Additives in

Proc. Syst., Vol. 1, pp23-31, (1999).

R.J. Waltman, G.W. Pacansky, and R.J. Berry, "Impact of Polymer

Hydrogenated Carbon", submitted to Tribology Letters, March 1999.

[62] Chao-Yuan Chen, Walton Fong, David B. Bogy, Tai Cheng, Jim Chao, C.S. Bhatia, “Effect of the Additive X-1P on the Tribological Performance and Migration Behavior of PFPE Lubricant at the Head-Disk Interface”, CML Technical Report 99-019, submitted to Intermag, 2000.

[63] Bassam S. Nader, Kishore K. Kar, Ted A. Morgan, Chester E. Pawloski, and Wendell L. Dilling, "Development and Tribological Properties of New Cyclotriphosphazene High Temperature Lubricants for Aircraft Gas Turbine Engines”, STLE Tribology Transactions, Vol. 35, No.1, pp37-44, (1992).

[64] M. Yang, F.E. Talke, D.J. Perettie, T.A. Morgan, K.K. Kar, B. Dekoven, and G.E. Potter, “Cyclotriphosphazenes as New Lubricants for Rigid Magnetic Recording Media”, STLE Tribology Transactions, Vol. 38, pp636-642, (1995).

[65] M. Yang and F.E. Talke, “Environmental Effects on Phosphazene Lubricated Computer Hard Disks”, IEEE Trans on Magnetics, Vol.30, No.6, pp4143-4145, (1994).

[66] D.J. Perettie, W.D. Johnson, T.A. Morgan, K.K. Kar, G.E. Potter, B.M. Dekoven, J. Chao, Y.C. Lee, C.Gao, M.Russak, “Cyclic Phosphazenes as Advanced Lubricants for Thin Film Magnetic Media”, ISPS, Vol.1, Book No. H01016-1995, pp117-121, (1995).

[67] Tai Cheng, Brooke Zhao, Peter Lei, and Jim Chao, “Determination of the Lubricant Migration Rate from the Hard Disk Surface”, submitted to Intermag, 2000.

[68] D.J. Perettie, T.A. Morgan, and K.K. Kar, “X-1P as a Dual Purpose Lubricant for Pseudo-contact Recording”, Insight 9, pp3-6, (1996).

[69] R.J. Waltman, B. Lengsfield, and J. Pacansky, “Lubricants for Rigid Magnetic Media Based upon Cyclotriphosphazenes: Interactions with Lewis Acid Sites”, Chem. Mater., Vol. 9, pp2185-2196, (1997).

[70] Chao-Yuan Chen, Walton Fong, David Bogy, and C.S. Bhatia, “Tribochemistry of Monodispersed ZDOL with Hydrogenated Carbon Overcoats”, CML Technical Report 99-008, submitted to JVST.

[71] Chao-Yuan Chen, Walton Fong, David Bogy, Tai Cheng, Jim Chao, and C.S. Bhatia, “Tribochemistry of Monodispersed ZDOL Lubricants Measured by Opitcal Surface Analysis and Thermogravimetric Analysis”, CML Technical Report 99-022, ready for submission.

[72] Novotny, V.J., and Baldwinson, M.A., “Lubricant Dynamics in Sliding and Flying”, J. Appl. Phys., 70, 10, pp5647-5652, (1991).

[73] Forcada, M.L., and Mate, C.M., “The Flow of Thin Viscous Liquid Films on Rotating Disks”, J. Coll. Int. Sci., 160, pp218-225, (1993).

[74] R.J. Waltman, and G.W. Tyndall, “The evaporation and bonding of ZDOL polyperfluorinated Ether lubricants on CHx carbon overcoated rigid magnetic media. 1. Effect of Molecular Weight.”, submitted to J. Phys. Chem.

[75] R.J. Waltman, and G.W. Tyndall, “The evaporation and bonding of ZDOL polyperfluorinated Ether lubricants on CHx carbon overcoated rigid magnetic media. 2. Effect of Polydispersity in the Molecular Weight”, submitted to J. Phys. Chem.

[76] Seymour R.B., and Carraher C.E. Jr., “Polymer Chemistry- an Introduction”, 2nd ed., pp93-98, (1987).

[77] Fred W. Billmeyer, “Textbook of Polymer Science”, John Wiley & Sons, Inc., pp122-124, (1971).

[78] Seymour R.B., and Carraher C.E. Jr., “Polymer Chemistry- an Introduction”, 2nd ed., pp59-61, (1987).

[79] Chao-Yuan Chen, W. Fong, D. Bogy, and S. C. Bhatia, "Lubricant thickness effect on tribological performance of ZDOL lubricated disks with hydrogenated overcoats", CML Technical Report No. 99-007, 1999, Tribology Letters, in press, 1999.

[80] G.W. Tyndall, P.B. Leezenberg, R.J. Waltman, and J. Castenada, “Interfacial interactions of Perfluoropolyether lubricants with magnetic recording media”, Tribology Letters 4, pp103-108, (1998).

[81] R.J. Waltman, D.J. Pocker, and G.W. Tyndall, “Studies on the interactions between ZDOL Perfluoropolyether lubricant and the carbon overcoat of rigid magnetic media”, Tribology Letters 4, pp267-275 (1998).

[82] T.E. Karis, G.W. Tyndall, and M.S. Jhon, “Spreading profiles of molecularly thin Perfluoropolyether films”, submitted to Tribology Trans., March 1998.

[83] T.M. O’Connor, M.S. Jhon, C.L. Bauer, B.G. Min, D.Y. Yoon, and T.E. Karis, “Surface diffusion and flow activation energies of perfluoropolyaklether”, Tribology Letters 1, pp219-223, (1995).

[84] X. Ma, J. GUI, L.Smoliar, K. Grannen, B. Marchon, M.S. Jhon, and C.L. Bauer, “Spreading of perfluoropolyalkyether films on amorphous carbon surfaces”, J. of Chemical Physics, vol. 110, no. 6, pp3129-3137, (1999).

[85] X. Ma, J. Gui, K. Grannen, L.Smoliar B. Marchon, M.S. Jhon, and C.L. Bauer, “Spreading of PFPE lubricants on carbon surfaces: effect of hydrogen and nitrogen content”, Tribology Letters, 6, pp9-14, (1999).

[86] X. Ma, J. Gui, L.Smoliar, K. Grannen, B. Marchon, M.S. Jhon, and C.L. Bauer, “Complex terraced spreading of perfluoropolyalkyether films on carbon surfaces”, Physical Review E, vol. 59, no. 1, pp722-727, (1999).

[87] Bhatia, “Effect of Lubricant Bonding on the Tribological Performance of ZDOL on Hydrogenated Overcoats”, CML

Appendix I:
Lubricant Chemical Structures

ZDOL

$HOCH_2\text{-}CF_2O\text{-}(CF_2O)_m\text{-}(CF_2CF_2O)_n\text{-}CF_2\text{-}CH_2OH$

AM

$CH_2O_2\text{-}C_6H_3\text{-}CH_2OCH_2\text{-}(CF_2O)_m\text{-}(CF_2CF_2O)_n\text{-}$
$CH_2OCH_2\text{-}C_6H_3\text{-}O_2CH_2$

Demnum SA

$CF_3\text{-}(CF_2CF_2CF_2O)_m\text{-}CF_2\text{-}\ CF_2\text{-}CH_2OH$

X-1P